NASA/TM–2016-219337 Volume I

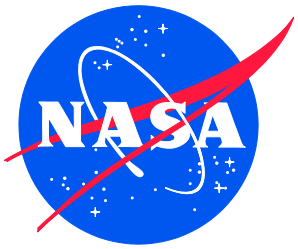

Crew Exploration Vehicle (CEV) (Orion) Occupant Protection

Nancy J. Currie-Gregg/NESC
Langley Research Center, Hampton, Virginia

Michael L. Gernhardt
Johnson Space Center, Houston, Texas

Charles Lawrence
Glenn Research Center, Cleveland, Ohio

Jeffrey T. Somers
KBRwyle, Houston, Texas

September 2016

NASA STI Program . . . in Profile

Since its founding, NASA has been dedicated to the advancement of aeronautics and space science. The NASA scientific and technical information (STI) program plays a key part in helping NASA maintain this important role.

The NASA STI program operates under the auspices of the Agency Chief Information Officer. It collects, organizes, provides for archiving, and disseminates NASA's STI. The NASA STI program provides access to the NTRS Registered and its public interface, the NASA Technical Reports Server, thus providing one of the largest collections of aeronautical and space science STI in the world. Results are published in both non-NASA channels and by NASA in the NASA STI Report Series, which includes the following report types:

- TECHNICAL PUBLICATION. Reports of completed research or a major significant phase of research that present the results of NASA Programs and include extensive data or theoretical analysis. Includes compilations of significant scientific and technical data and information deemed to be of continuing reference value. NASA counter-part of peer-reviewed formal professional papers but has less stringent limitations on manuscript length and extent of graphic presentations.

- TECHNICAL MEMORANDUM. Scientific and technical findings that are preliminary or of specialized interest, e.g., quick release reports, working papers, and bibliographies that contain minimal annotation. Does not contain extensive analysis.

- CONTRACTOR REPORT. Scientific and technical findings by NASA-sponsored contractors and grantees.

- CONFERENCE PUBLICATION. Collected papers from scientific and technical conferences, symposia, seminars, or other meetings sponsored or co-sponsored by NASA.

- SPECIAL PUBLICATION. Scientific, technical, or historical information from NASA programs, projects, and missions, often concerned with subjects having substantial public interest.

- TECHNICAL TRANSLATION. English-language translations of foreign scientific and technical material pertinent to NASA's mission.

Specialized services also include organizing and publishing research results, distributing specialized research announcements and feeds, providing information desk and personal search support, and enabling data exchange services.

For more information about the NASA STI program, see the following:

- Access the NASA STI program home page at http://www,sti.nasa.gov.

- E-mail your question to help@sti.nasa.gov

- Phone the NASA STI Information Desk at 757-864-9658

- Write to:

NASA STI Information Desk
Mail Stop 148
NASA Langley Research Center
Hampton, VA 23681-2199

NASA/TM–2016-219337 Volume I

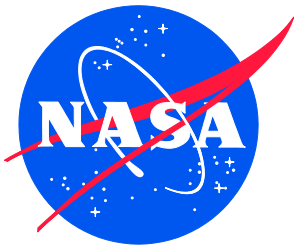

Crew Exploration Vehicle (CEV) (Orion) Occupant Protection

Nancy J. Currie-Gregg/NESC
Langley Research Center, Hampton, Virginia

Michael L. Gernhardt
Johnson Space Center, Houston, Texas

Charles Lawrence
Glenn Research Center, Cleveland, Ohio

Jeffrey T. Somers
KBRwyle, Houston, Texas

National Aeronautics and
Space Administration

Langley Research Center
Hampton, Virginia 23681-2199

September 2016

Acknowledgments

The NESC team would like to acknowledge the following individuals who contributed to this report. Ms. Jennifer Jadwick, Ms. Jennifer Tuxhorn, Ms. Lesley Lee, and Mr. Nick Skytland contributed to the success of this effort as part of the Extravehicular Activity Physiology, Systems and Performance Project at JSC. In addition, the team would like to thank Dr. Jeff Jones, who contributed countless hours of support and was instrumental in the investigation during the first 2 years.

The authors would like to acknowledge the support of the HRP at JSC for their support and funding for this investigation.

Available from:

NASA Center for AeroSpace Information
7115 Standard Drive
Hanover, MD 21076-1320
443-757-5802

Table of Contents

List of Figures

List of Tables

List of Equations

List of Appendices (stand alone volume parts 1 and 2)

Volume II Part 1

Volume II Part 2

Nomenclature

AFB	Air Force Base
AFRL	Air Force Research Library
AIS	Abbreviated Injury Scale
ANSI	American National Standards Institute
ASCII	American Standard Code for Information Interchange
ATD	Anthropomorphic Test Devices
ATK	Alliant Techsystems
ATLS	Advanced Trauma Life Support
BDR	Brinkley Dynamic Response
BMD	Bone Mineral Density
CAD	Computer-Aided Design
CCD	Crew Cursor Device
CCIP	Constellation Crew Injury Prediction [ATD]
CEV	Crew Exploration Vehicle
CFC	Channel Frequency Class
CM	Crew Module
CPU	Central Processing Unit
CSDM	Cumulative Strain Damage Measure
CSSS	Constellation Space Suit System
CxP	Constellation Program
D	Dimensional
DAC	Design Analysis Cycle
DoD	Department of Defense
DOF	Degree of Freedom
DRI	Dynamic Response Index
DR_x	X-axis Dynamic Response
DR_y	Y-axis Dynamic Response
DSS	Decelerator System Simulation
DU	Display Unit
DXA	Dual-energy X-ray Absorbance
EFA	Exploratory Factor Analysis

EOM	End of Mission
EuroSID	European Side-Impact Dummy
EVA	Extravehicular Activity
F/B	Fighter/Bomber
FAA	Federal Aviation Administration
FACB	Flight Activities Control Board
FE	Finite Element
FEM	Finite Element Model
FMVSS	Federal Motor Vehicle Safety Standard
FR	Front Right
FS	Flight Status
FTSS	First Technologies Safety Systems
G	Gravitational constant
GM	General Motors
GRC	Glenn Research Center
GSI	Gadd Severity Index
HANS®	Head and Neck Support®
HIA	Horizontal Impact Accelerator
HIC	Head Injury Criteria
HRP	Human Research Program
HSIR	Human-Systems Integration Requirements
IARV	Injury Assessment Reference Values
IRC	Injury Reference Criteria
IRL	Indy Racing League
IS	Injury Severity
IWE	Independent Witness® Encrypted Format File
IWI	Independent Witness® Unencrypted Binary File
JSC	Johnson Space Center
LaRC	Langley Research Center
lb	pound
LM	Lockheed Martin
LOC	Loss of Consciousness
LS-DYNA®	Finite Element Analysis Software by Livermore Software Technology Corporation
LSTC	Livermore Software Technology Corporation
MADYMO	MAthematical DYnamic Modeling
MATLAB®	MATrix LABoratory data analysis program from The Mathworks
mm	millimeter
MOB	Medical Operations Board
mph	miles per hour
msec	millisecond
MTSO	Management and Technical Support Office
N	Newton
NASA	National Aeronautics and Space Administration
NASCAR	National Association for Stock Car Auto Racing
NESC	NASA Engineering and Safety Center

NFS	Not Further Specified
NHTSA	National Highway Traffic Safety Administration
Nm	Newton meter
NRB	NESC Review Board
OOB	Out-of-Board
OPRA	Order Probit Regression Analysis
ORIS	Operationally Relevant Injury Scale
OSU	Ohio State University
PMHS	Post-Mortem Human Subject
PRA	Probabilistic Risk Assessment
S&G	Sprague-Geers
SAA	Space Act Agreement
SAE	Society of Automotive Engineering
SAR	Search and Rescue
SC	Suit Connector
SE	Self-Egress
SID	Side-Impact ATD
SIMon	Simulated Injury Monitor
SMCCB	Space Medicine Configuration Control Board
SME	Subject Matter Expert
SRD	System Requirement Document
SSP	Space Shuttle Program
STD-DEV	Standard Deviation
TASS	TNO Automotive Safety Solutions
TBI	Traumatic Brain Injury
THUMS	Total HUman Model for Safety
TMA	Transport Modified Anthropometric
US	United States
USAF	United States Air Force
USN	United States Navy
USRA	Universities Space Research Association
VDT	Vertical Drop Tower
WP	Wright Patterson
WPAFB	Wright-Patterson Air Force Base
WSTC	Wayne State Tolerance Curve

Abstract

Dr. Nancy J. Currie, of the NASA Engineering and Safety Center (NESC), Chief Engineer at Johnson Space Center (JSC), requested an assessment of the Crew Exploration Vehicle (CEV) occupant protection as a result of issues identified by the Constellation Program and Orion Project. The NESC, in collaboration with the Human Research Program (HRP), investigated new methods associated with occupant protection for the Crew Exploration Vehicle (CEV), known as Orion. The primary objective of this assessment was to investigate new methods associated with occupant protection for the CEV, known as Orion, that would ensure the design provided minimal risk to the crew during nominal and contingency landings in an acceptable set of environmental and spacecraft failure conditions. This documents contains the outcome of the NESC assessment. NASA/TM-2013-217380, "Application of the Brinkley Dynamic Response Criterion to Spacecraft Transient Dynamic Events." supercedes this document.

1.0 Executive Summary

The NASA Engineering and Safety Center (NESC), in collaboration with the Human Research Program (HRP), investigated new methods associated with occupant protection for the Crew Exploration Vehicle (CEV), known as Orion.

Reliable injury predictive tools and injury criteria are required to ensure that human-rated spacecraft (e.g., Orion or a commercial space venture) be designed with the appropriate level of occupant protection [ref. 1]. It is important the occupants be protected from injury and the vehicle is not designed with excessive protection that leads to unnecessary vehicle weight and/or complexity. While conventional tools used in the aerospace community have led to safe designs, retirement of the Space Shuttle Program (SSP) and transition to a vehicle whose primary landing mode will probably be water based, with contingency land landings using parachutes, will introduce many new challenges. Approaches to ensure safety, such as those used in the commercial aviation and automotive industries, can provide a foundation for human-rated spaceflight for these new vehicles. However, their application to the Orion Project or a commercial venture requires modification and study.

The NESC, HRP, and the Constellation Program (CxP) developed injury criteria and methods for predicting injury for the Orion crew module (CM) and for future commercial space programs. This working relationship was somewhat different from the independent way in which the NESC normally operates. However, due to the complexity of problems and the demand for a strong and diverse skill set, it was determined that a combined effort was required.

The core of the occupant protection criteria is based on the Brinkley Dynamic Response (BDR) model and associated injury criteria limits. These criteria are being used by NASA and the United States (US) military to determine the injury risk or adverse physiological response for vehicle occupants based on seat acceleration. While the BDR is useful for generating an overall estimate of the probability of injury, the criteria have limitations. The BDR model and associated criteria assume a basic seat geometry, restraint, and head protection, and are therefore only an approximation for other seat designs and protection systems. Furthermore, the BDR model cannot

be used to predict risk when improvements are made to the seated environment. Risk can only be lowered by reducing the driving loads into the seat. In addition, the BDR model cannot predict suit-induced injury (e.g., localized blunt trauma and point loading) related to rigid elements or interference with the restraints.

The US Air Force Research Laboratory (AFRL) at the Wright-Patterson Air Force Base (WPAFB) in Dayton, Ohio, evaluates body restraints and support systems using volunteer subjects exposed to anticipated sub-injury impact conditions. These evaluations are conducted by comparison with the baseline BDR body support and restraint systems and evaluation of the likelihood of injury using established biodynamic data. Systems proposed are assessed to reduce the likelihood of injury and to reduce tolerance to impact conditions.

As a result of the present work, additional injury criteria specific to the head, neck, and legs have been incorporated into the Human System Interface Requirements (HSIR) [ref. 1]. These additional injury criteria complement the BDR criteria already incorporated in the requirements. These supplemental injury criteria were developed primarily for the automotive industry and are regularly used to ensure automotive safety. The injury criteria used by the automotive industry are designed for automobile accidents and considerably higher allowable probability of injuries than are acceptable for NASA and manned vehicle landings, so judgment was used to extrapolate the criteria for use for manned spaceflight. The automotive industry criteria provided a better understanding of the location and type of occupant injury and the effect of seating conditions and occupant protection. When used in conjunction with the BDR criteria it can provide a more complete assessment of occupant protection.

Before the National Highway Transportation Safety Administration (NHTSA) for automotive safety and the Federal Aviation Administration (FAA) for commercial aircraft safety implement standards, they anchor their criteria with human test data collected from accidents and laboratory-based human studies. NASA is planning to leverage from these extensive bodies of work. However, NASA should perform human testing specific to the environment and loadings of planned manned vehicles to anchor the occupant protection injury criteria with relevant test data. In the past, NASA deemed this type of testing necessary and performed it for the Apollo Program; similarly, the Russians performed this type of testing for Soyuz. Currently, NASA has no plan to obtain human test data for Orion or other future planned manned vehicles.

In addition to the BDR criteria and occupant protection criteria, body movement requirements were added to the HSIR. These requirements complement the biodynamic injury criteria by establishing requirements that limit relative body motions that could result in injury. Limiting body movement is a sound design practice and will ultimately lead to the necessity for head and torso restraint systems, such as a Head and Neck Support (HANS®), side supports, and at least a partially conformal seat design. Furthermore, the BDR criteria were developed based on data collected for specific seat configurations that provided lateral support and body movement constraints. For the BDR criteria to be applicable to manned spacecraft, body movement requirements are a necessity to provide a similar seated configuration as was used to develop the BDR criteria. A similar seat configuration would be one that provides the same level of body constraint as is provided by the seat used during the development of the BDR model and associated injury criteria.

Implementation of the occupant protection and body movement criteria requires the use of physical and numerical anthropomorphic test devices (ATD) to extract the occupant response in realistic seated environments and loading conditions. Numerical models of the Hybrid III ATDs were

evaluated for assessing potential crew injuries through extensive sled testing at AFRL and numerical modeling. The First Technology Safety Systems (FTSS) model of the Hybrid III was recommended for use by NASA and the Orion Project since this model performed best among the models assessed. However, the FTSS model did not consistently produce correlation results to within the desired 20 percent of the test data. Overall, the FTSS Hybrid III model performed best among the three ATD numerical models. It is recommended that before a numerical model is used to perform a final assessment of occupant injury, the model should be validated through physical testing. This testing should be performed in a similar physical environment, including similar or identical seat, harness, helmet, and suit and loading conditions, comparable to the loading conditions that will ultimately be used for the occupant protection assessments.

2.0 Problem Description

2.1 Background

The CxP plans to replace the SSP with a CEV CM named "Orion." Orion is similar to Apollo, but larger, and will carry a crew of four to six members while Apollo was designed for a crew of three. The Orion CM will descend to Earth with a three-parachute recovery system in the event of an emergency escape during the launch phase or during the final phase of the CM's return to Earth. The CM is designed to be capable of a primary water landing and contingency land landings. Landing systems must be designed for multi-terrain impacts. Earth terrain is highly variable at the proposed landing sites; soil at Edwards Air Force Base (AFB) in California is typically hard, and soil at Carson Sink in Nevada is often soft. During an emergency escape from the launch pad, the CM will be lifted from the launch vehicle by a launch abort system with a trajectory designed for a water landing. Landing and recovery, and crew protection during water or land landings are a design challenge, and despite years of successful space missions cannot be considered routine. To keep the size of parachute systems reasonable and to optimize the weight of the landing system, the terminal velocity of the Orion CM parachute recovery systems was designed to provide a descent velocity at landing of approximately 24 ft/sec nominal to 33 ft/sec contingency (16 to 22.5 mph, 7.3 to 10.1 m/s). In addition to the terminal descent (vertical) velocity, the parachutes and CM will move horizontally depending on the horizontal wind velocity. The CM touchdown velocity is typical of crash impact velocities of small aircraft and helicopters. Thus, the CM's impact velocity may produce injuries without some type of mitigation for impacts onto land. With proper pitch attitude into low sea states, water landings do not require additional mitigation for nominal landings since the water acts as a natural impact attenuator. The Apollo capsule was designed to impact the water with a parachute hang angle of 27 degrees. Since the Apollo entered the water pitched at an angle, the acceleration experienced was nominally 10 G or less for a 30-ft/sec (9.1-m/s) impact [ref. 2]. The Apollo spacecraft had crushable ribs and a crew seat pallet with stroking energy absorbers to alleviate contingency impacts. However, a land landing of Apollo in an abort condition or a flat 0-degree attitude water impact with one parachute fully opened was expected to result in occupant injuries. Since the probability of a pad abort with a land impact was considered low, the CxP accepted those risks.

Under ideal nominal conditions, a land landing with retro-rockets or impact-attenuating airbags, or a water landing will result in tolerable accelerations to the crew if the seats and restraint systems are properly designed. For contingency landing conditions, a stroking crew seat pallet similar to the Apollo design is planned for the Orion CM to reduce the impact accelerations to conditions that are tolerable to the crew and that will prevent injury. However, some mitigation for more

severe contingency impacts can be designed with little weight penalty if a systems approach is taken early in the design phase.

The primary purpose of this assessment was to assess the use of finite element (FE) seat and occupant simulations for assessing injury risk for Orion. These FE seat and crash ATD models allow for varying the occupant restraint systems, cushion materials, side constraints, flailing of limbs, and detailed seat/occupant interactions. Also included in this assessment is a discussion of impact injury criteria used by the automotive industry to assess crash ATD response and how these criteria can be used for Orion occupant protection. With properly designed seats (side supports and restraints), relatively high accelerations can be tolerated with no or minimal injury, especially for impacts with the crew lying on their backs in a seat oriented as shown in Figure 2.1-1. The local inertial axis system has the +X-axis forward, the +Z-axis pointed toward the head, and the +Y-axis to the left. For accelerations along the +X-axis, which would occur for a flat impact, the inertial response to a spine-to-chest acceleration is called 'eyeballs in.' An inertial response to an acceleration along the –X-axis (chest-to-spine) is called 'eyeballs out.' An inertial response to an acceleration along the +Z-axis (seat) is called 'eyeballs down', and an inertial response to an acceleration pointing in the –Z-axis is called 'eyeballs up.' The seat coordinate system is a local system and is a non-inertial axis system. Hence, angular rotations with respect to an inertial system must be considered.

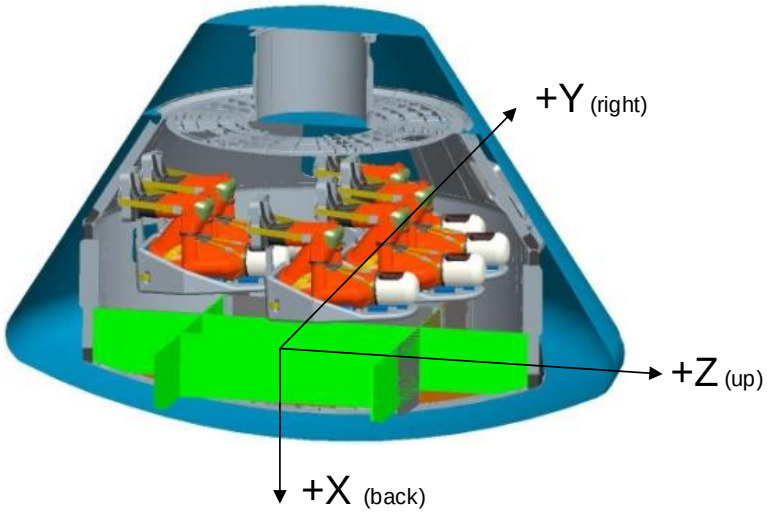

Figure 2.1-1. Six-crew Configuration and Local X-, Y-, and Z-axes

2.2 Current Requirements and the Need for Additional Crew Protection Metrics

The CxP HSIR document [ref. 1] includes provisions for protecting the crew during dynamic phases of flight, including linear and rotational acceleration limits and BDR acceleration exposure limits. Although these requirements add a level of crew protection, it became apparent to the Orion Project Office that additional requirements may be necessary. In addition, the automotive and car racing industry has shown considerable improvements in occupant protection over the last 10 years. In an attempt to leverage this expertise to improve crew protection during Orion launch and landings, a tiger team consisting of NESC and CxP personnel was formed to further investigate occupant protection principles and their applicability to the spaceflight environment.

2.3 Charter

In 2007, the Orion Project was in the early stages of design analysis cycle (DAC) #2 and was challenged with evaluating the 606C vehicle design capability for nominal water landings and contingency land landings. To integrate this technical effort, an Orion Landing Strategy Tiger Team was established per Orion Project Guidance Memo ZV-07-034 (see Appendix A). Additionally, an Occupant Protection Industry Day was held in July 2007 to bring together experts in occupant protection principles, research, and analysis from leading industry, research institutions, and government Agencies.

In the subsequent months, a steering committee (Table 2.3-1) was assembled to oversee the design and analysis activities being performed for the landing event during DAC #2. These activities included:

- assessing current vehicle design for water landing and contingency land landing events,
- assessing the vehicle design susceptibility to roll control and tip over,
- reviewing methods for assessing occupant injury during ascent/aborts/landings,
- developing an alternate seat/attenuation design solution, which improves occupant protection and operability, and
- testing the seat/attenuation system designs to ensure valid results.

Table 2.3-1. Steering Committee Members

Chair	Irene Piatek
Vehicle Integration Office/Operations	Angela Hart
Systems Engineering Integration Team	Chris Johnson
CB	Lee Morin
Health and Medical Technical Authority	Mark Jernigan
Safety & Mission Assurance	John Trainor
Orion Chief Engineer	Julie Kramer White
Extravehicular Activity	Miriam Sargusingh
NESC	Nancy Currie

The steering committee chartered three tasks to coordinate these activities. The first team (Task 1) was chartered to address requirements and analysis techniques; this assessment encompasses the work of the Task 1 team. The Task 2 team examined alternate seat/attenuation solutions, and the Task 3 team performed the seat/attenuation system testing.

The Task 1 team was chartered with the following leadership, description, and requirements:

- Lead: JSC Human Adaptation and Countermeasure Office – Mr. Mike Gernhardt.
- Team: NESC, industry and academic experts, key stakeholders (Crew Office, JSC Engineering, and JSC Space Medicine and Human Engineering).
- Steering Committee Point of Contact: Dr. Nancy Currie.
- Task Description: Determine appropriate methods for modeling and prediction of potential crew injuries. Activities include conducting data mining of injury databases (e.g., NASCAR, Crash Injury Research Engineering Network, military, etc.) and

assessing impact simulation and injury prediction methodologies. Recommend techniques/changes to requirements appropriate for Orion, including stated limitations.

- Products:
  1. Periodic briefings to Steering Committee/CEV Project Office.
  2. Given driving load cases from the Orion Project Office, analyze Orion baseline design (606C) and alternate configurations developed by Task 2 team.
  3. Final report included recommendations for:
     a. Standard analysis techniques and models.
     b. Impact acceleration/occupant injury criteria appropriate for use by Orion.

This document fulfills the final product listed above as the final report for Task 1 and includes the recommendations and outcomes of this effort.

3.0 Data Analysis

3.1 Human Systems Requirements

3.1.1 BDR Model Acceleration Exposure Criteria Historical Background

3.1.1.1 Early Use of Simplified Exposure Limits

The BDR criteria were developed as a result of an evolutionary process to define the human dynamic response to, and exposure limits for, short duration accelerations (i.e., <500 msec) associated with spacecraft landing and emergency escape system performance. During the era of the Mercury, Gemini, and Apollo Programs, the encapsulated ejection seats for the B-58, XB-70 aircraft, and the cockpit crew escape system for the fighter/bomber (F/B)-111 aircraft for the USAF, occupant protection was a concern, and work was done to further develop and improve the impact exposure criteria. Acceleration limits were established [refs. 3 and 4] in terms of rate of onset, acceleration amplitude, and duration for areas known to be within voluntary tolerance and those known to cause moderate to severe injury. These acceleration limits were based upon the research of John P. Stapp and his contemporaries [ref. 4] using military volunteers, animal surrogates, and the results of accidental exposures of humans. However, the fitting of the trapezoidal acceleration-time histories was inadequate to assess the injury risk due to the complex, multi-directional landing impacts of these crew systems. The trapezoidal pulses were developed for ejection seats where the acceleration-time histories of the ejection catapult, rocket thrust, and deceleration due to aerodynamic forces could be controlled in terms of these acceleration-profiles.

Examples of other key research results include that of Beeding and Mosely [ref. 5], who conducted experiments using a horizontal deceleration facility to study the responses of volunteers to impact in forward-facing and rearward-facing seats with lap belt and shoulder harness restraints. They reported severe shock and repeated syncope with myalgia requiring one volunteer to be hospitalized for 5 days following his exposure to a 40-G sled acceleration with a rate of onset of 2,139 G/sec and a velocity change of 48.5 ft/sec in a rear-facing seat. Dr. Mosley reported that the subject may not have survived without immediate medical care. Prior exposures of volunteers in this position ranged from 25–40 G at onset rates from 1,034–2,139 G/sec for durations of 50 to 190 msec. Impact velocities were below 50 ft/sec. The acceleration-time histories could be defined in terms of the existing trapezoidal limits, although a half-sine pulse shape more approximated the applied acceleration.

3.1.1.2 Addressing Complex Multi-directional Accelerations

Based upon survived accidents, experimental data from tests with volunteers, tests with animals [ref. 6], and theoretical work based on the laws of mechanics, AFRL laid out an initial plan to investigate the acceleration profiles with high rates of onset using experimental and analytical approaches. NASA joined this effort to investigate human tolerance to landing impact conditions with rates of onset higher than had previously been considered safe.

To address this problem, Headley *et al*.[refs. 7 and 8] and Brinkley *et al*. [refs. 9 and 10] conducted experiments with volunteer subjects to explore the human responses to the complex waveforms associated with emergency escape capsule impact and the Project Mercury module launch abort landing impact. These experimental data demonstrated several relationships between the higher rates of acceleration onset, acceleration magnitude, and impact velocity change in the +Z- and +X-axes. During these experiments, Brinkley *et al*. [ref. 9] investigated the beneficial effects of an individually contoured body support constructed of fiberglass compared to a body support liner that could be formed to fit the occupant (Figure 3.1-1).

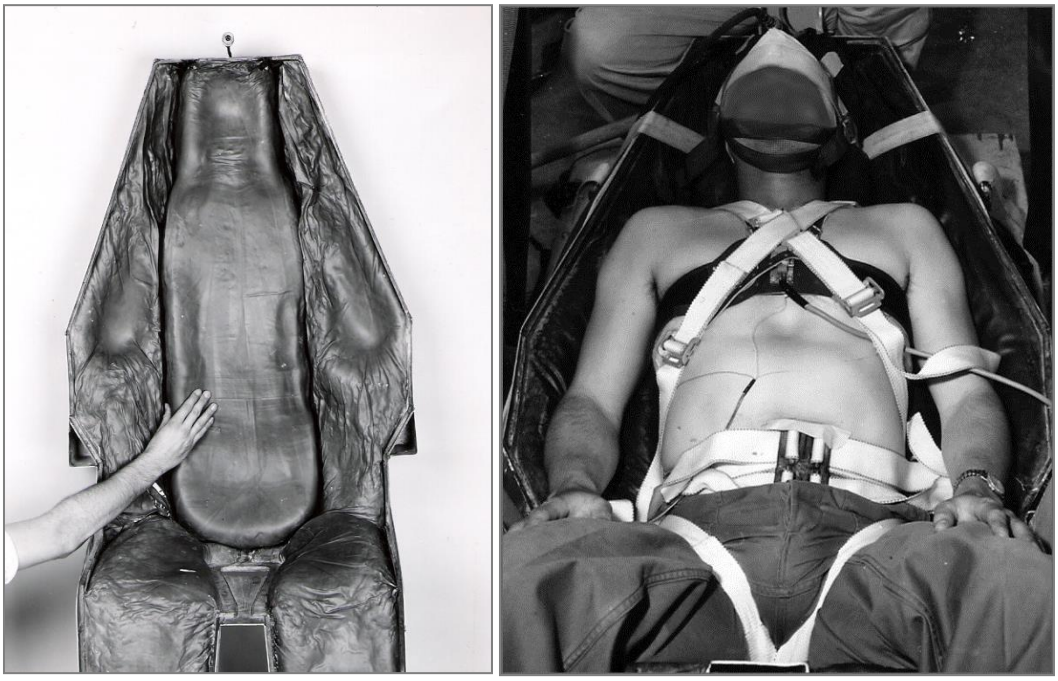

Figure 3.1-1. Photographs of a Volunteer Subject Prepared for an Impact Test Supported by Couch with a Form-fitting Liner and a Top View of the Liner Formed to Fit the Test Subject

During this same period, Payne [ref. 11] used the extensive human and animal impact exposure data assembled by Eiband [ref. 4], and Goldman and von Gierke [ref. 12] to study the feasibility of developing simple, lumped-parameter dynamic models that might describe the human response and likelihood of injury based on the experimental data. Payne developed numerical models of restraint and support systems to show the effects of their mechanical properties on the human responses to complex acceleration profiles.

In 1962, NASA began to organize efforts to design the Apollo crew systems. One of the efforts included the development of CM landing impact system human tolerance criteria. Initially, crew protection system designers were forced to accept a maximum acceleration of 10 G and a rate of onset of 250 G/sec as the limiting crew acceleration exposure criteria. A major analytical and

experimental program was organized by the NASA Manned Spacecraft Center (i.e., JSC) and was implemented by AFRL, the Naval Air Engineering Center, and the Armed Forces Institute of Pathology to identify potential critical modes of injury and likely adverse physiological responses, and to explore the effects of higher level multi-directional impacts "to assure astronaut functionality immediately after landing" [ref. 13].

The most immediate problem was to explore the human responses to sideward (Y-axis) impact. At that time, knowledge of human response to sideward acceleration was limited to the results of centrifuge experiments conducted by AFRL to sustained acceleration levels to 10 G [ref. 14]. In a study using a centrifuge, Hershgold examined the displacement of the volunteer subjects' internal organs during steady-state acceleration. His radiographs showed extensive displacement of thoracic and abdominal viscera to the dependent side of the body with acceleration as small as 6 G. Stapp [ref. 15] had not observed injuries to chimpanzees at calculated accelerations to 47 G with durations estimated to be 140 msec at the peak G level.

During this same time, impact tests of the B-58 encapsulated ejection seat were conducted with volunteer subjects [ref. 16]. The capsule was dropped with vertical velocities to 27 ft/sec (8.2 m/s) and landed on its back bulkhead with its occupant in a semi-supine position. The tests were conducted without detectable injury. During tests not reported in this article, the capsule was impacted with horizontal velocities to 34 ft/sec (10.4 m/s) in the sideward direction. An undetermined amount of energy was dissipated in tumbling and skidding of the capsule, making use and extrapolation of these data difficult. However, these tests demonstrated the tolerance to sideward impact was probably higher than the 10 G that had been investigated under steady-state acceleration of 10 G by Hershgold [ref. 14].

In preparation for a joint agreement with NASA to study the feasibility of higher impact exposure limits, Robinson *et al.* [ref. 17] conducted impact tests using Rhesus monkeys with sideward impacts to 75 G at terminal velocities to 32 ft/sec (9.8 m/s), with and without contoured body support systems. No post-mortem injuries were observed. Electrocardiographic evidence of transient abnormalities in conduction and rhythm were found following higher-level accelerations and impact velocities. Radiographs taken before and after the impacts showed an increase in the total heart shadow on the dependent side of the midline. Sequential radiographs revealed that the heart returned to normal within 3 hours after impact.

Based on the agreement between NASA and the Department of Defense (DoD), Schulman *et al*., [ref. 18] explored the effects of downward acceleration (–Z- axis) to 18.5 G with rates of onset to 1,540 G/sec. This research supplemented and extended USAF research that had been conducted with animals and volunteers to define criteria for downward ejection seats [ref. 19].

AFRL conducted impact tests to investigate the dynamic responses of military volunteers using a vertical deceleration tower. Acceleration, forces, physiological reactions, and subjective responses of volunteers were measured for sideward (Y-axis) impacts ranging to 21.5 G with rates of onset to 1,350 G/sec and impact velocities to 25.5 ft/sec (7.8 m/s) [ref. 20]. An individually fitted, semi-rigid body support was used with torso and extremity restraints. A Mercury pressure-suit helmet weighing 4.4 lbs (21 kg) was worn by the subjects in these tests. Plastic foam (0.5-inch-thick, 13-mm) pads were placed behind the helmet earphones and across the chin bar. The helmet was prevented from pitching motion, but not vertical motion by a 1.75-inch (44-mm) strap. The helmet microphone was removed and the impacts were tolerated by the male volunteer subjects.

A second series of impact tests jointly sponsored by the USAF and NASA were conducted to study the effects of seven impact vector directions and six acceleration profiles ranging in acceleration from 3–26 G, impact velocities ranging from 5–28 ft/sec (1.5–8.5 m/s), and onsets ranging from 200–2,000 G/sec. The seven seat orientations, including forward, upward, and sideward (right and left) acceleration components in 45-degree increments were used on a vertical deceleration tower. A drawing of the orientations, designated as vectors A through G, is shown in Figure 3.1-2 [ref. 21]. Force, acceleration, and physiological data were collected and analyzed. The volunteers were contained by an experimental restraint system and supported by a flat seat and seat back, and side panels to support the pressure-suit helmet, shoulders, and upper legs. The liner filled with small beads was not used in this second series of tests. The subjects needed assistance to ensure that the liner was adequately formed about their bodies and they were more confident in the support provided by a rigid seat. A test subject is shown restrained within the multi-directional impact test vehicle in Figure 3.1-2. The seat and its frame were attached to the AFRL vertical deceleration tower by rods that were instrumented with force measurement cells (see Figure 3.1-3). The restraint system is shown in Figure 3.1-4.

The subject panel included 20 male subjects. The acceleration and force data were subjected to extensive mathematical analysis based upon the Fourier Transformation [ref. 22]. The relationship between the measured forces and impact velocity, called mechanical impedance, was used to identify the human body dynamic response properties in terms of resonances similar to those of linear, second-order, spring-mass-damper systems. Broad, low-amplitude resonances were identified at 3.5, 5.5, 7.2, and 11.7 Hz. There was no gross distinction in the impedance magnitude or phase angle among the orientations studied. The subject impedance magnitude increased linearly with frequency to about 35 Hz. The analysis was not valid beyond this frequency because the velocity pulse did not contain significant frequency components beyond 35 Hz. Physiological and subjective response data that were collected indicated abrupt cardiac rhythm changes at the higher acceleration levels, wind knocked out, and various sites of transient pain, including the head. The investigators concluded the head would present a problem at higher impact levels. However, no voluntary tolerance limit was specified [ref. 21].

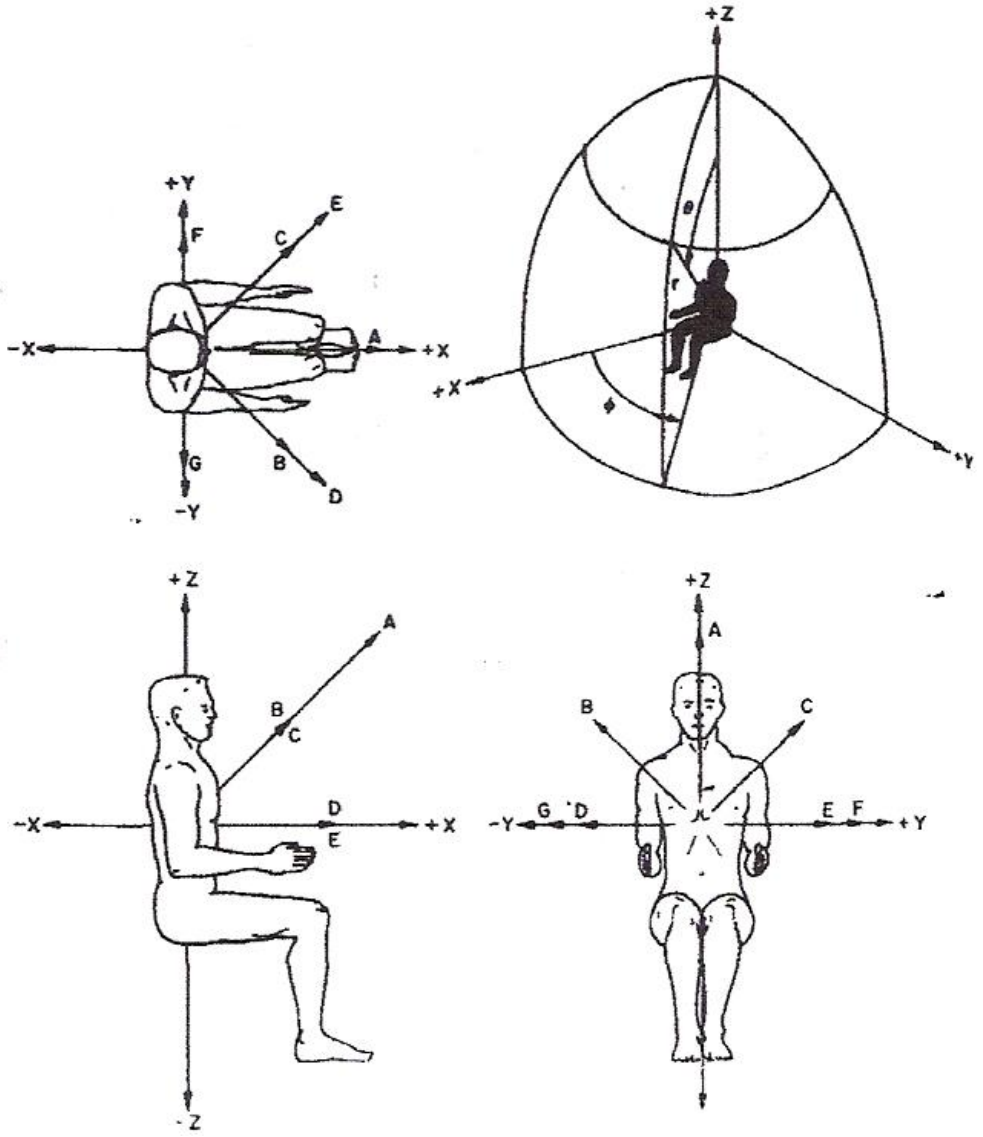

Figure 3.1-2. Acceleration Vectors

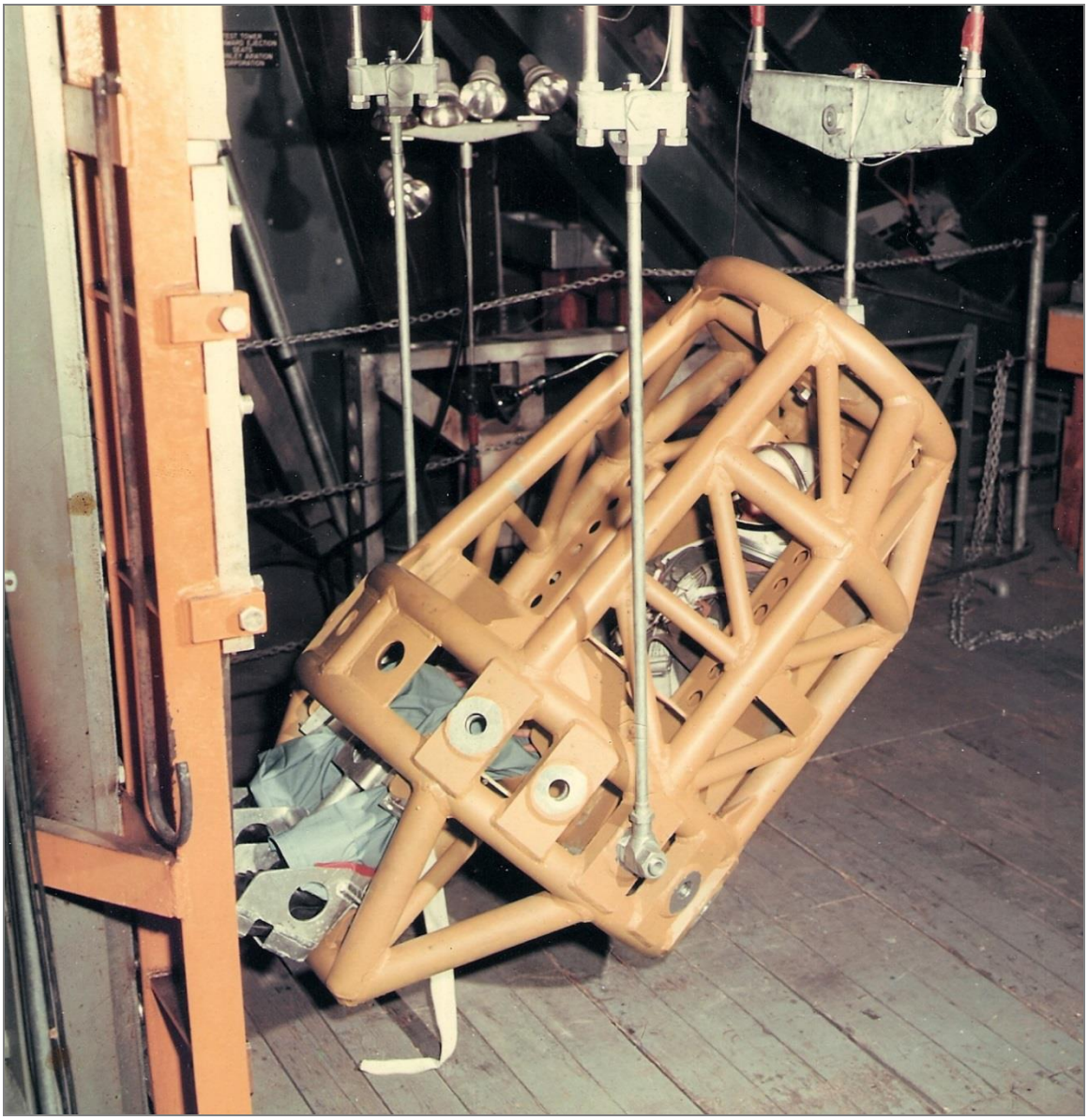

Figure 3.1-3. Multi-directional Impact Vehicle Showing Seat and Volunteer Subject (credit: USAF)

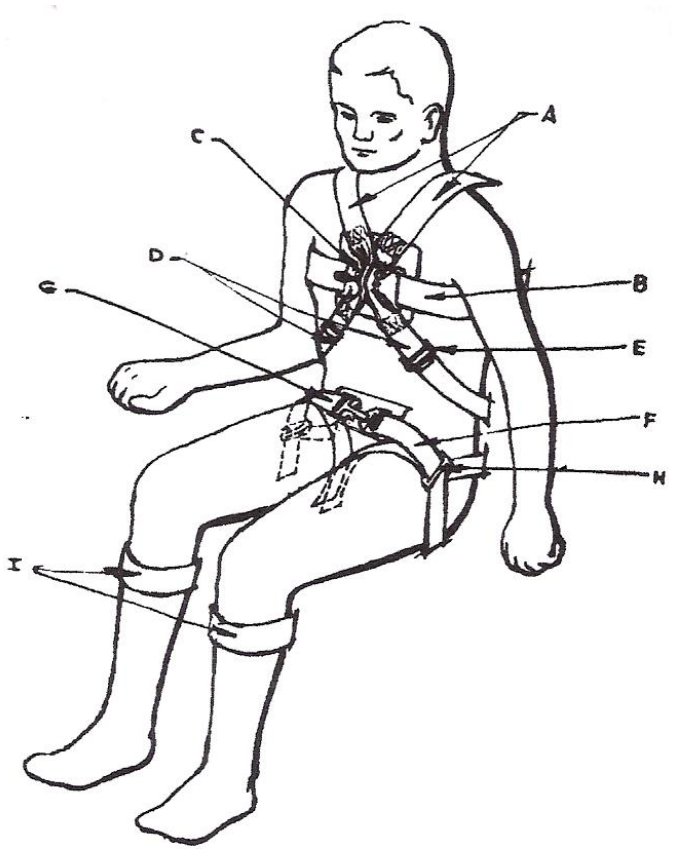

Figure 3.1-4. Restraint System Configuration

Further tests were accomplished by the USAF, as part of its joint effort with NASA, using a horizontal deceleration track at Holloman AFB, New Mexico. Stapp and Taylor [ref. 23] explored 16 different seat orientations with 58 volunteers. A total of 146 tests were conducted to explore the effects of accelerations ranging in magnitude from 10–25 G, rates of onset from 1,000–2,000 G/sec, and durations from 60 to 130 msec. A pneumatic piston accelerated a sled and subject, allowing it to coast and impact a water-filled decelerator at velocities ranging from 18–46 ft/sec (5.5–14 m/s). The subjects wore Mercury pressure-suit helmets and were restrained by the same developmental restraint system used by Weis *et al.* [ref. 21] at the WPAFB. The seat was constructed of flat panels to support and constrain the subject's movement in the rearward and sideward directions [ref. 23] (see Figure 3.1-5 and Figure 3.1-6). For smaller subjects, panels were used to ensure that there were no gaps between the subject and the seat.

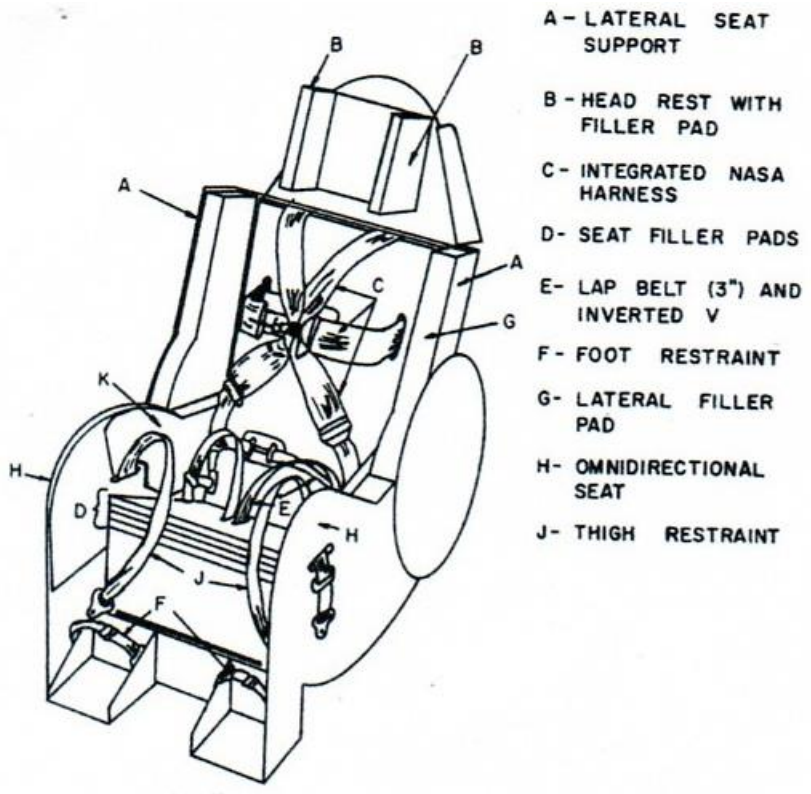

Figure 3.1-5. Seat and Restraint System

Figure 3.1-6. Photograph of Horizontal Deceleration Test Facility and Subject Restrained within the Multi-directional Test Apparatus

All body positions and impact conditions were within voluntary tolerance, except the forward-facing 45-degree reclining position at 25.4 G sled acceleration, with a rate of onset of 960 G/sec and a 97-msec duration. The subject experienced soft tissue pain and stiffness in the area of the 6th through 8th thoracic vertebrae for 60 days. Bradycardia was experienced in 55 electrocardiograms immediately after impact. The bradycardia was triggered by headward impact vectors due to stimulation of the carotid sinuses, dropping the heart rate as much as 90 beats per minute for 10–30 seconds. The restraint looseness was found to be a contributing factor. Persistent or severe pain was absent in 146 of 163 tests.

Brown *et al.* [ref. 24] extended the research of Weis *et al.* [ref. 21], and Stapp and Taylor [ref. 23] by conducting 288 impact tests with volunteers using the horizontal deceleration track to explore the responses of the nervous, cardiovascular, respiratory, and musculoskeletal systems. Twenty-four acceleration vector directions in 45-degree increments were studied using the same helmet, body support, and restraint in the two studies described above (see Figure 3.1-7). Seventy-nine subjects participated in this experimental study. At each seat orientation, the impact level was increased in increments of 2–5 G until the occurrence of an adverse reaction based upon the evaluation of the subjective, clinical, and physiological responses by the medical monitor, determined the maximum impact levels. Two tests were accomplished at each combination of position, acceleration level, and onset rate. The sled acceleration ranged from 5.5–30.7 G, the rate of onset was varied from 300–2,500 G/sec, and the impact velocity ranged from 9.3–45 ft/sec (2.8–13.7 m/s). The highest impact levels were achieved in positions 19 and 23, while lower levels were limited to 11.8 and 11.1 G in positions 9 and 13, respectively. The +Z- and –Z-axes orientations of positions 9 and 13 had been explored more thoroughly in the earlier tests by Schulman *et al.* [ref. 18], Weis *et al.*[ref. 21], and Stapp and Taylor [ref. 23].

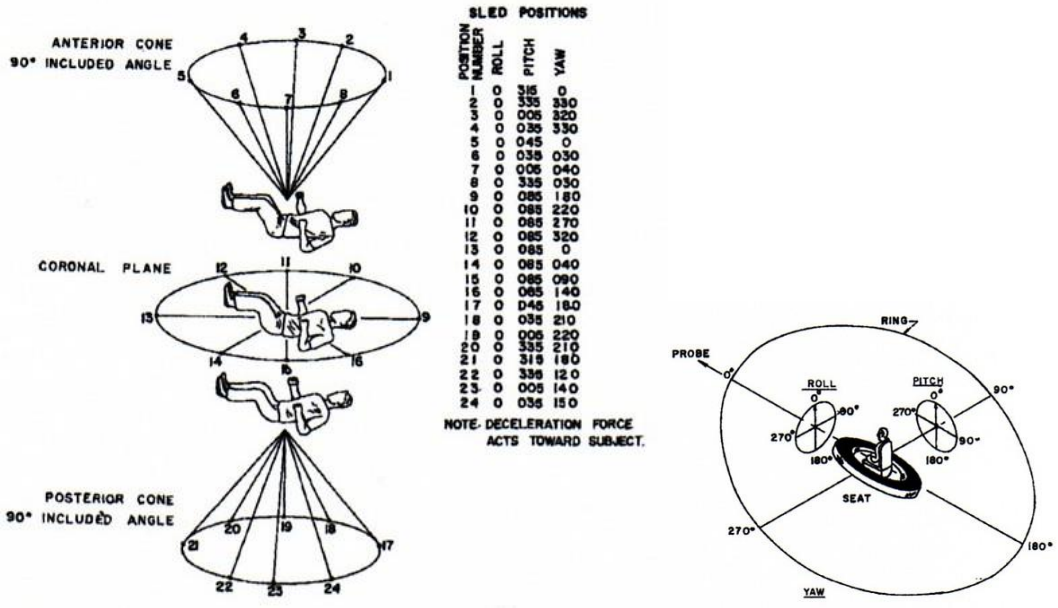

Figure 3.1-7. Force Vectors Orientation Applied to the Volunteers

The neurological effects observed were momentary stunning and disorientation, which lasted no more than 2 minutes. In one case, this response was noted at an impact level as low as 17.4 G, where the impact force vector was in orientation 17. Headaches lasting several hours were noted in nine tests. Shortness of breath and chest pain were experienced by the subjects in more than

one-half of the higher-level tests. Musculoskeletal complaints resulted primarily from muscle spasms and strains of the neck, back, and lower extremities.

Subsequently, additional tests were conducted with volunteers in developmental seats, restraints, and pressure suits, as shown in Figure 3.1-8 and Figure 3.1-9. Records of these tests have not been located. However, a fracture of the seventh thoracic vertebra occurred as a result of one of two tests conducted with the pressure suit partly inflated [ref. 25].

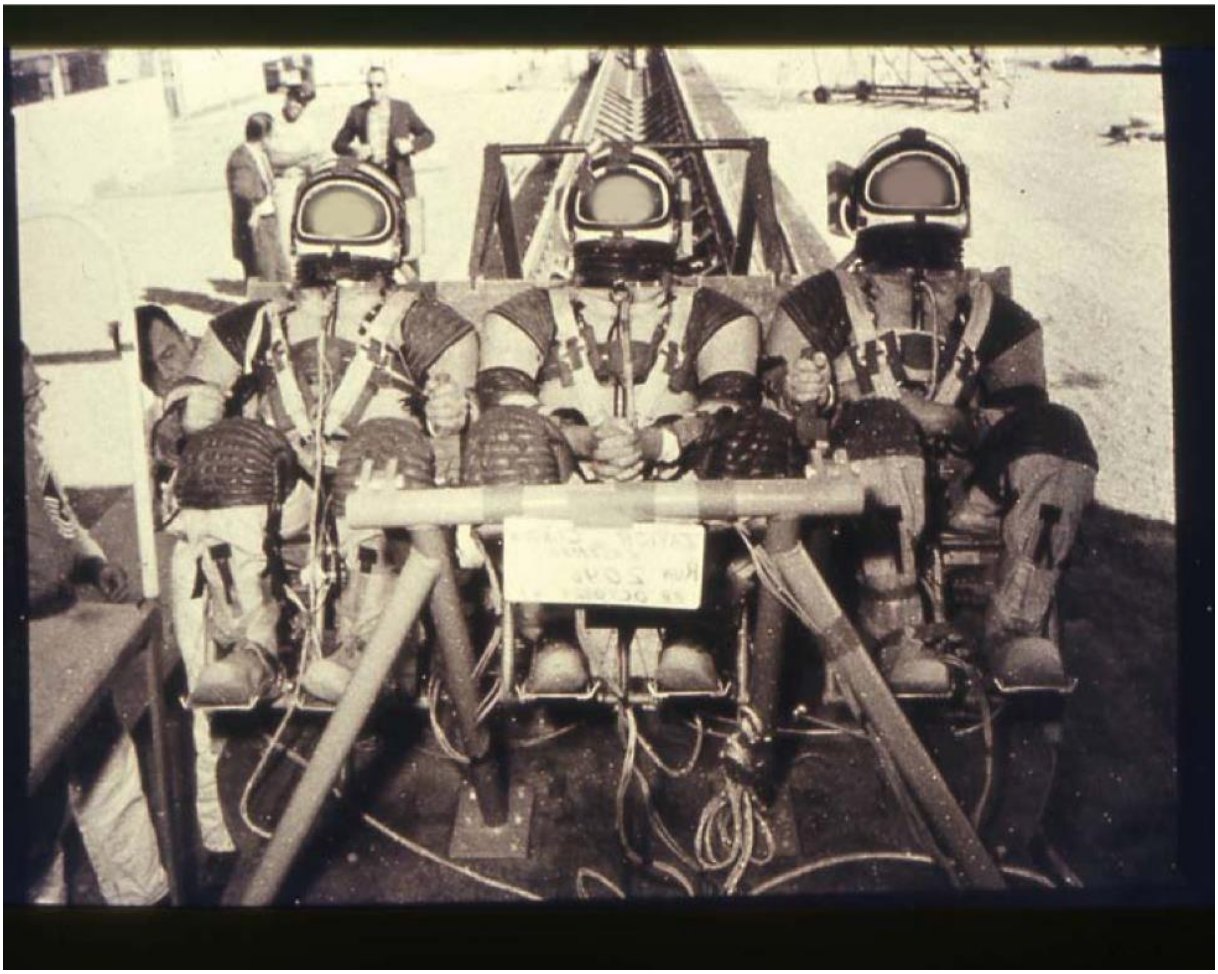

Figure 3.1-8. Volunteers Undergoing an Impact Test in a Developmental Seating System (credit: USAF)

Figure 3.1-9. A Volunteer Being Tested in a Developmental Pressure Suit (credit: USAF)

Payne [ref. 26] further developed numerical models of human body dynamics and studied the effects of body support and restraint systems in a research effort jointly funded by the USAF and NASA. Important analytical results influencing the design of restraint systems included studies of the restraint system slackness and preload using a lumped parameter model of human response.

3.1.1.3 Focus on the Development and Validation of a Spinal Injury Model

Payne suggested that two lumped parameter models could be used to describe the human responses to spinal (+Z-axis) and transverse (X-axis) impact conditions. NASA and AFRL sponsored a more detailed study of these models [ref. 27] using data from tests with human cadavers, and impact and vibration tests with volunteers.

Concurrently, AFRL conducted tests with human subjects to measure human responses to spinal acceleration since the USAF was planning to develop an ejection seat and would update its military specification for ejection seats. At the same time, the USAF and USN were developing a two-man, emergency escape crew cockpit for the F/B-111. The spinal injury model was used on an experimental basis to evaluate the crew escape system performance during developmental and qualification ejections from a rocket-propelled sled. Brinkley estimated the ground landing to have a probability of injury greater than 20 percent. After the system was operational, the spinal injury rate was found to be 29.5 percent (23/78) by Hearon *et al.* [ref. 28].

Brinkley [ref. 29] and Brinkley and Shaffer [ref. 30] conducted laboratory impact studies and evaluation of the spinal injury rates associated with operational USAF ejection seats using the dynamic response index (DRI) model developed by Steck and Payne [ref. 27]. Using the

operational ejection seat data, Brinkley and Shaffer validated the model using the injury probability from the work of Steck and Payne [ref. 27], but adjusted it to match the higher resistance to crew spinal injury shown in Figure 3.1-10 [ref. 30].

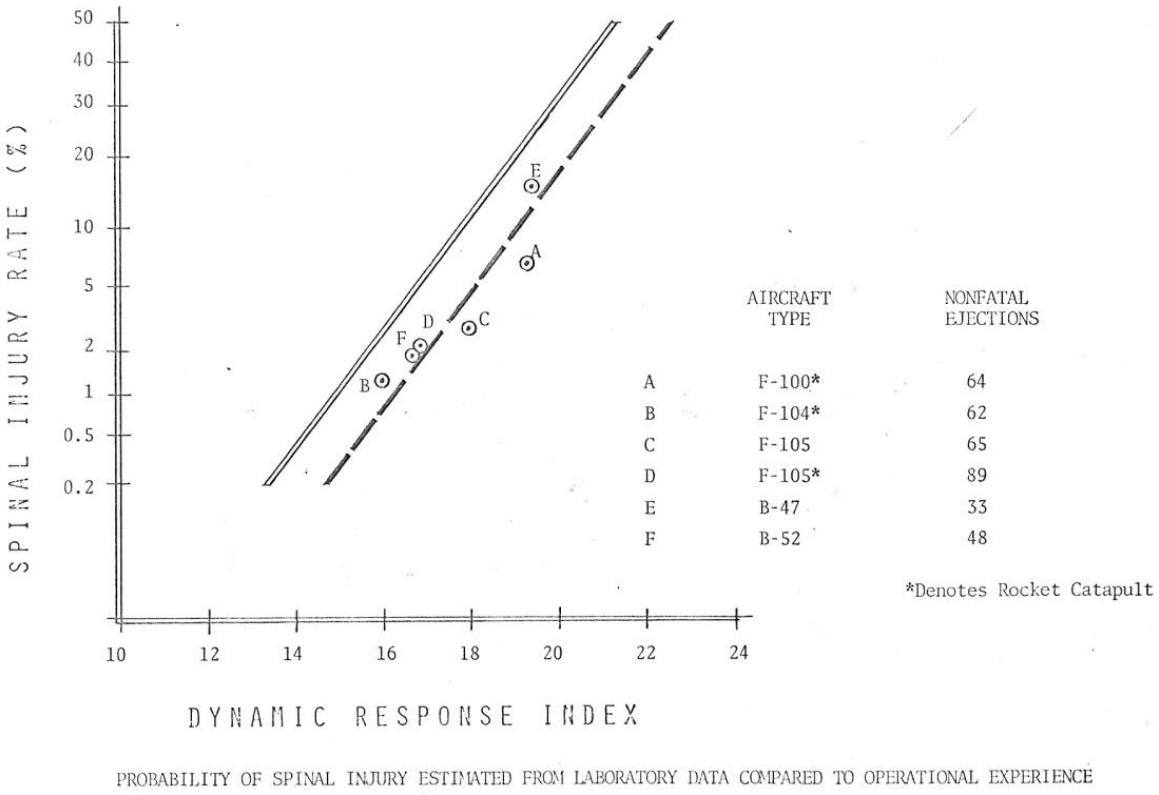

Figure 3.1-10. Probability of Spinal Injury Estimated from Operational Ejection Seat Experience

The DRI model estimates combined with ejection tests on volunteers were used to correct an extraordinarily high spinal injury rate associated with the ejection seat used in the F-4 aircraft. The complex curvature of the seat back and headrest caused the seat occupant to be forward of the ejection catapult thrust vector [refs. 30 and 31]. This caused the occupant's head and upper body to flex forward during ejection, lowering the threshold of compression injury to the thoracic spine. To correct the high injury rate, the ejection catapult thrust was reduced and a rocket was added to the seat bottom to sustain the acceleration after the seat separated from the aircraft. The seat-back geometry and thrust vector alignment could not be accomplished without a major seat redesign or replacement (see Figure 3.1-11). Because of the feasible changes, the spinal injury rate was reduced from 34 to 8 percent, as shown in Figure 3.1-12 [ref. 30].

The ability of the spinal column to withstand +Z-axis acceleration without injury may be significantly increased with proper spinal column alignment prior to impact.

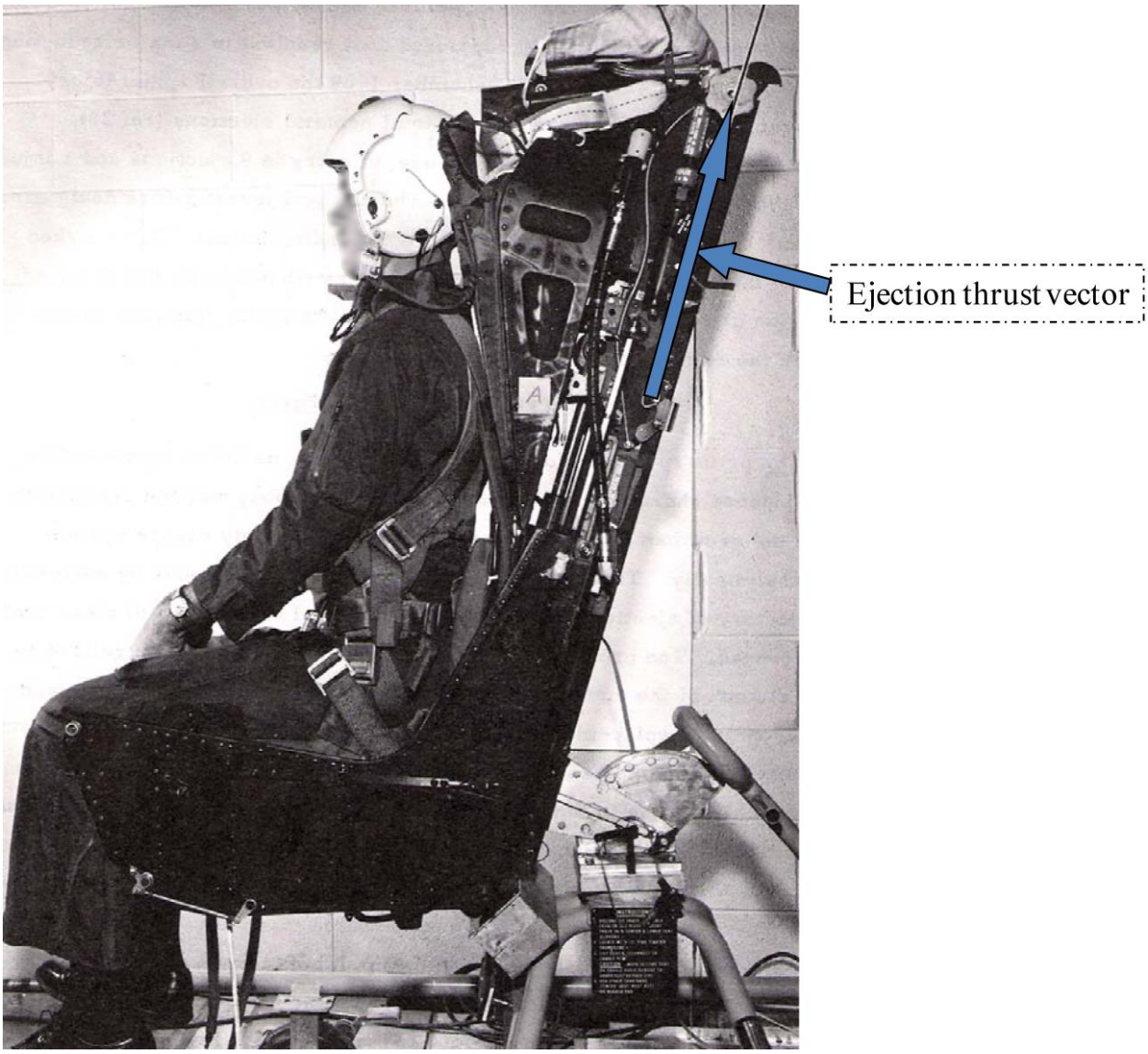

Figure 3.1-11. Seat-Back Geometry and Spine Alignment to the Ejection Thrust Vector

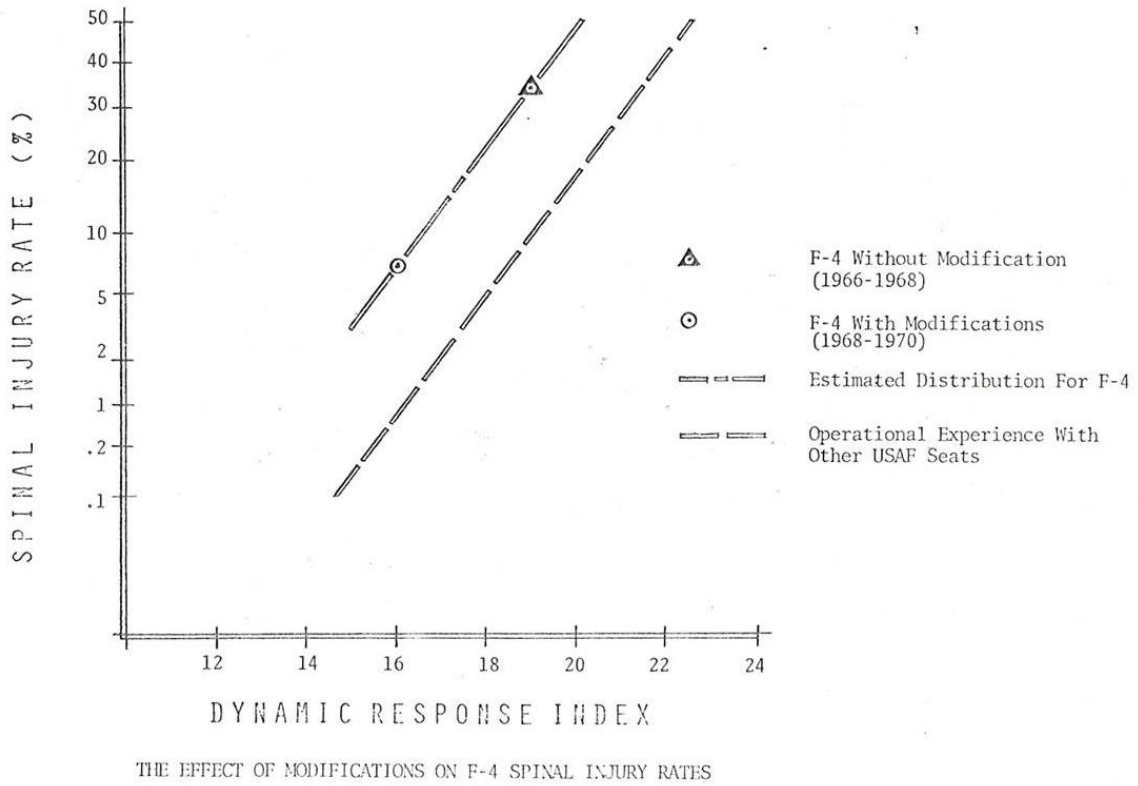

Figure 3.1-12. The F-4 Ejection Seat Injury Rates Associated with the DRI

3.1.1.4 Evaluating the Acceptability of Multi-directional Acceleration Conditions

During the 1970s, the USAF used a method to evaluate multi-directional acceleration environments that incorporated the DRI combined with a method to assess the magnitude of accelerations in the other principle axes that occurred within a moving 62-msec analysis window. A computer program was developed to accomplish this analysis incorporating look-up tables to assess the effects of the X-, Y-, and –Z-axes. While this method provided a consistent means to evaluate the performance of relatively conventional ejection seats, it did not provide a means to evaluate a new generation of ejection seats. These new ejection seat designs incorporated an array of attitude, altitude, and airspeed sensors; digital flight control; ejection catapult thrust control; and rocket thrust vector control. In situations where the conditions at ejection were benign, the escape system performance would be controlled to produce a low injury risk. Where the conditions presented a higher risk to the seat occupant, the ejection seat would produce accelerations with a higher injury risk, but a higher likelihood of a successful escape.

This concept led the USAF to generate a strategic plan for a development program to demonstrate the technologies required to demonstrate an advanced ejection seat that would have such flight control features, and be capable of safe escape at aircraft speeds to 700 knots (equivalent airspeed). The new technologies required to evaluate the performance of such an ejection seat included an ATD capable of measuring specific forces and moments at key internal locations and joints, a rocket sled capable of providing adverse attitudes and roll motion of an aircraft forebody at the time of an ejection test, and a means to sense and assess the injury risk associated with the escape system's performance [ref. 32].

3.1.1.5 Development of a Method to Assess the Injury Risk Resulting from Multi-axial Accelerations

Brinkley [ref. 33] proposed a means to evaluate the performance of an escape system using a whole body acceleration exposure limit method. Its primary objective was to compute a set of dynamic responses that could be used to estimate the injury risk levels. The computations would be based on measurements of linear acceleration and angular velocities at a known point. Brinkley proposed that if the linear acceleration at a point on the seat and the angular velocity were known, then the seat motion would be uniquely defined and the linear acceleration at any point in the seat coordinate system could be calculated. Brinkley proposed that a single-degree-of-freedom (DOF), lumped-parameter model could be used to assess the dynamic response of the human body in each orthogonal axis. The dynamic responses of the three orthogonal axes could be used to calculate a general whole body injury risk in terms of an ellipsoidal approximation.

Model parameters, natural frequency, and damping coefficients were selected on the basis of available laboratory data and existing lumped-parameter models. Injury risk levels were chosen on the basis of operational escape system experience and accidental injuries that had occurred in laboratory experiments. The DRI was adopted for the +Z-axis. A probability of spinal injury had been validated by ejection experience and non-injury and injuries experienced in the laboratory. The results of –Z-axis accelerations explored by investigators, such as Shaw [ref. 34] and Schulman *et al.* [ref. 18], and the USAF experience with downward ejection seats, were initially used to estimate low, moderate, and high risk levels. For simplicity, the DRI parameters were selected for the –Z-axis model.

Initial estimates of the X-axis models were derived from numerous reports of tests with volunteers by the USAF, USN, DoD contractors, and academic laboratories. The estimates supported the analytical work of Payne [ref. 26] and Steck and Payne [ref. 27].

Selection of model parameters for the Y-axis proved to be the most difficult due to the limited data. One set of sideward impact data was selected to be suitable for analysis [ref. 35]. Injury risk levels could not be developed with high confidence since few injuries had been observed beyond adverse cardiovascular responses [refs. 21, 23, 24 and 36] and syncope [ref. 36]. Unpublished experimental accidents with volunteer subjects conducted by aerospace contractors were added to estimate the high injury risk region. The influence of side support panels was also estimated.

In subsequent publications by Brinkley [ref. 37] and Brinkley, *et al.* [ref. 38], the results of laboratory experiments were used to improve the lumped-parameter models. For example, Brinkley, *et al.* [ref. 38] reported the results of impact experiments and analyses to better define the parameters for the –Z-axis model.

3.1.1.6 BDR Criteria Application

The BDR multi-axial dynamic response criteria have been used in numerous research and development applications. These include the:

- investigation of the Challenger accident,
- the development, test, and evaluation of the Crew Escape Technologies escape system demonstration ejection seat,
- evaluation of landing impacts of the Soyuz CM,
- the design and assessment of an escape system concept for the National Aerospace Plane,

- test and evaluation of the Russian K-36D ejection seat performance [ref. 39],
- development, test, and evaluation of the X-38 assured crew recovery system,
- development, test, and evaluation of the Soyuz TMA (Transport Modified Anthropometric) CM, and
- advanced development, test, and evaluation of the K-36D-3.5A ejection seat [ref. 40].

3.1.1.7 Impact Exposure Limits for NASA Standard 3001

In December 2004, Dr. Smith Johnston convened a panel of sustained and impact acceleration experts to review a draft NASA standard for CxP. The BDR model criteria were recommended to be incorporated in NASA Standard 3001 (NASA-STD-3001), *NASA Space Flight Human System Standard*. A draft was prepared, reviewed, and incorporated. Rotational limits were proposed and recommended.

3.1.1.8 Assumptions and Requirements for the BDR Model Criteria

- Accelerations of less than 500 msec (e.g., during liftoff, launch abort, landing impacts, and parachute deployments).
- Seated crew where seat padding or cushions preclude amplification of transient linear accelerations transmitted to the occupant.
- Crew contained by a restraint system that included pelvic, torso, and anti-submarining restraints that provide occupant confinement similar to a conventional five-point harness.
- During the experimental efforts, the restraint system was adequately pre-tensioned to eliminate slack. Pyrotechnically powered inertial reels were used to position escape system occupants and to eliminate slack in the restraint during the operation ejection cases that were used.
- The +Z-axis limits assume that the seat cushion materials do not amplify the acceleration transmitted to the seat occupant.
- The +X-axis limits assume that the seat occupant's head is protected by a flight helmet with a liner adequate to pass the test requirements of American National Standards Institute (ANSI) Z-90 (latest edition) or equivalent.
- The crew will be similarly restrained during all events that might require application of the BDR model criteria.
- The model cannot predict injury caused by rigid suit elements (i.e., localized blunt trauma, localized point loading, and interference with restraints).
- The testing used to develop the lateral dynamic response had minimal gap between the subject and the seating support surfaces. Additional space between the seat and subject will increase the injury risk, but this increased risk will not be reflected in the model predictions.

3.1.1.9 Recent Additions to the Supporting Database

Since the original BDR criteria publications, research has been continued by the AFRL Human Effectiveness Directorate to address specific issues associated with the criteria use. These issues included expansion of the empirical database to study the influence of variations in impact duration, impact magnitude, off-axis impacts, and the influence of a specific complex waveform on the dynamic response properties of volunteer subjects. Topics of interest have included linearity of human dynamic response properties, such as acceleration and externally measured forces.

Studies of the effects of helmet mass properties on the dynamic response of the head and neck have been of considerable interest to the USAF in view of the operational introduction of helmet-mounted displays and night-vision equipment. Now that women are flying fighter aircraft equipped with ejection seats, more emphasis has been given to the study of the dynamic response of both genders to the accelerations and forces generated during emergency escape.

Impact studies have been conducted with military volunteer subjects to evaluate impact profiles with acceleration levels of 3, 6.9, and 12 G and impact rise times varying from 30–130 msec and to study the amplification or attenuation of subject accelerations and forces reacted by the seat structure. The axes studied to date include the +Z, −Z, and X-Y and X-Z vectors, and vector combinations. More than 800 impact exposures have been accomplished with volunteers to explore their responses to these conditions. The +Z-axis study results have been analyzed and demonstrate that the measured seat pan force is linear over the range of acceleration levels explored. The impact force amplification or attenuation was found to be consistent with a simple, single-DOF, lumped-parameter model.

Strzelecki [ref. 41] experimentally studied the dynamic inertial response of volunteer subjects to determine if the simple lumped-parameter model used within the BDR model could adequately simulate the forces measured at the seat pan. The profile studied was unique in that it consists of a short-duration impact followed by longer duration acceleration. The study was accomplished using the AFRL vertical deceleration tower. The facility was modified to produce an impulsive deceleration prior to the impact carriage deceleration-metering pin striking the water-filled decelerator normally used to control the deceleration magnitude, rise time, and duration. The measured responses of the volunteer subjects for seat pan force and chest and head acceleration confirmed the DRI model predictions and that the dynamic preload impulse was effective in reducing the dynamic overshoot and thereby the injury potential associated with the following deceleration pulse.

The study of gender influence included reviews of the literature and experimental investigations. Allnutt [ref. 42] conducted a review of the medical and safety literature exploring differences between the responses of men and women to traumatic vehicular events. Allnutt provided ample evidence that the gender-specific biological and anatomical characteristics affect a body's likelihood of trauma. These characteristics include differences in stature, weight, tissue strength, and endocrine humoral factors. For example, bone from a female is different in density, structure, and strength, and changes with age from that of a male. Allnutt provided evidence showing that women's bones are smaller when comparing them to men of the same height and weight. The difference is not limited to the size of boney structures; the microscopic thickness of trabecular (spongy) and cortical (compact) bone is thinner in women and becomes thinner with age. These findings demonstrate the use of the simple scaling methods employed in the automotive industry to adjust for the sensitivity of women to impact is a simplification of the more complex relationship between male and females and bone strength. The findings highlight BDR criteria limitations since the majority of the data used to develop the exposure limits were based upon laboratory studies primarily using male volunteers.

With women now flying fighter aircraft, AFRL has undertaken literature reviews and experimental and analytical studies to investigate the influence of gender in sustained and impact acceleration conditions. Morris and Popper [ref. 43] studied the influence of gender and impact on neck motion. Buhrman and Wilson [ref. 44] conducted an initial study of gender and subject size on factors that might increase spinal injury risk during emergency escape from aircraft. The introduction of

helmet-mounted displays and night-vision systems has increased the USAF's concern for cervical spine injuries. Perry [ref. 45] conducted tests using a vertical deceleration facility along with male and female volunteers to study the influence of variations in the inertial helmet properties on the subjects' dynamic responses to +Z-axis impacts. In 2000, Perry conducted experiments to compare the responses of males and females to –Gx impacts [ref. 46]. More recently, Gallagher *et al.* [ref. 47] compared cervical stress and bone mineral density to subject size and gender during +Z-axis impacts conducted using the AFRL vertical deceleration tower. Gallagher *et al.* [ref. 48] conducted analyses of vertebral stress and bone mineral density during +Z-axis impacts.

In general, there was little difference between the physical responses of males and females. The natural frequencies that were determined revealed no statistically significant differences. The damping coefficient ratios were somewhat smaller. Computed stresses for +Gz studies showed that females experienced 15-percent greater cervical stress than males during 10-G impacts [ref. 47]. When normalized for weight, lumbar stress was 15 percent higher in the female subjects than in male subjects [ref. 49].

AFRL has conducted numerous experiments to evaluate the influence of factors, such as seat geometry, restraint system design features (including attachment position), and seat cushion properties on the likelihood of injury using vertical and horizontal impact facilities. Examples include: Perry *et al.* [ref. 50], a study of seat back angle effect on impact response; Hearon and Brinkley [ref. 51], a study of the influence of a negative-G strap; Hearon *et al.* [ref. 52], a study of factors influencing a high spinal injury rate during CM landings; and Hearon and Brinkley [ref. 53], a study of seat cushion effects on subject impact responses.

3.1.1.10 Recommended Topics for Continued Research

The influence of gender has been studied by tests of human tissues, analysis of automotive accidents, and impact tests with volunteers. Additional research is required to determine tolerance decrements for body segments and whole body impact exposure limits. Available data should be adjusted for the accident victim's age, or post-mortem human subject (PMHS).

Research on the effects of microgravity exposure on crew should be continued. Emphasis should be given to areas of the body that carry the highest impact loads during landing impact (e.g., hip, shoulder, and spinal column).

The influence of the distance between the load-carrying areas of the human body and the support structures should be evaluated analytically and experimentally.

The influence of pressure suits and their design features cannot be evaluated until specific developmental designs are defined. The topic of focused blunt trauma due to impact with mechanical design features of pressure suits remains relatively unexplored. The use of PMHSs remains a viable option for exploring this problem area.

3.1.2 Biodynamic Injury Criteria

For many years, the automotive industry has been interested in developing injury assessment methods to help design safer automobiles. Their goal is to relate the injury risk in a specific body region to measurements made in that corresponding region in an ATD or a computer-modeled ATD. Injury biomechanics research focuses on determining the appropriate injury mechanism parameters (e.g., acceleration, force, or structural deformation of body components) that can be measured in an ATD and determine limit values for those parameters for a certain level of injury risk in that body region. Accordingly, the design features of the ATDs and their limitations in

representing the human body and its organs play a role in how injury assessments are performed. These limit values for injury criteria are referred to as injury assessment reference values (IARV) in the automotive industry. The ATD most commonly used in current automotive safety evaluation is the Hybrid III midsize adult male ATD.

Mertz [ref. 54] provides a detailed injury risk assessments description based on ATD responses. Mertz describes the process as:

> "Injury assessment reference values (IARVs) were developed to assess the efficacy of General Motors (GM) restraint system designs under a variety of simulated frontal accident conditions using the Hybrid III midsize adult male dummy as the vehicle occupant. These design limit values were chosen such that if an IARV was not exceeded in the prescribed test, then the risk of the associated injury would be unlikely. "Unlikely" was defined as risk levels less than 5 percent. Since injury risk curves for the various dummy responses did not exist, the limit values that were chosen for the IARVs were simply conservative estimates of response values that would be consistent with the unlikely definition. These IARVs were published in 1984 as part of the GM petition of the NHTSA to allow the use of the Hybrid III midsize adult male dummy in Federal Motor Vehicle Standard (FMVSS) 208 testing. In 1993, IARVs were published for response measurements of the Hybrid III small female and large adult male dummies [refs. 55 and 56]. These values were obtained by applying constant failure stress scaling to the Hybrid III midsize adult male IARVs taking into account size differences.
>
> "In 1998, the American Automobile Manufacturers Association, which is now the Alliance of Automobile Manufacturers (Alliance) proposed to NHTSA that the FMVSS 208 certification limits should be set at the 5-percent injury risk level. This would put all FMVSS 208 limits on an equal injury risk level that is consistent with the "injury unlikely" intent of the IARVs while allowing for reasonable compliance margin. The injury risk curves used by the Alliance were based on those proposed by Mertz *et al.* [ref. 57] for responses of the Hybrid III family of dummies."

The tables for injury criteria limit values for crew protection (see Section 3.1.2.1) are based on the FMVSS 208 IARVs for the small female, large male, and midsize male Hybrid III ATDs. The tables list the corresponding values for the 2- and 0.5-percent risk levels taken from the IARV risk curves presented in Mertz [ref. 54]. Deconditioned values for these parameters, based on the procedures given in Section 3.1.2.6, are listed below.

3.1.2.1 Head Injury

3.1.2.1.1 Head Injury Criteria 15 msec

Assessing the potential for head injury (e.g., brain and skull) has been a primary focus in injury biomechanics research for over 40 years. The pioneering efforts by researchers to predict brain injury from head acceleration measurements led to the Wayne State Tolerance Curve (WSTC) [ref. 58]. Using the observation that most emergency room patients admitted with simple linear skull fractures were concussed (although not all concussed patients had skull fractures), they hypothesized that determining the translational head accelerations associated with the initiation of

linear skull fractures in drop tests of embalmed cadaver heads would give an estimate of concussion occurrence. The extreme association of the limit accelerations with the durations of impact found in those tests for contact durations below 4 msec led Gadd [ref. 59] to plot the data on a logarithmic scale, which exhibited a linear relationship with a slope of –2.5 between the peak acceleration and time duration on a log-log plot. Gadd proposed the Gadd Severity Index (GSI), a weighted impulse criteria in which the integral of the measured head acceleration over time, raised to the 2.5 power was a measure of head injury potential based on the WSTC. Because the time interval for calculating the GSI was not specified, this led to confusion over the interpretation of more complex head acceleration waveforms. Versace [ref. 60] proposed an optimization method to search for the acceleration time interval, (t_2-t_1), which would maximize the GSI. This is referred to as the Head Injury Criteria (HIC) and codified by the NHTSA. All passenger cars sold in the U.S. must meet a designated level of HIC in a 35-mph barrier crash test for the vehicle occupants.

Equation 3.1-1. HIC Formula

$$\boldsymbol{HIC(t) = \left[\frac{1}{t_2 - t_1}\int_{t_1}^{t_2} a_r dt\right]^{2.5}(t_2 - t_1)}$$

While there have been many efforts to improve the HIC predictive features, there have been no methods that appear to have advantages over the HIC in routine crash protective system testing. The only change in the automotive standards has been a lowering of the HIC limit from 1,000 to 700 for the midsize male. Since the HIC is felt to be most valid for head accelerations due to contact with a generally rigid surface, researchers [ref. 61] have selected a maximum HIC interval (t_2-t_1) of 15 msec or less based on biomechanical head impact research. Table 3.1-1 shows the original values included in the HSIR; and Table 3.1-2 lists the revised limit values for HIC for the small female, midsize male, and large male dummies at the 0.5- and 5-percent risk levels given in Mertz [ref. 54]. Crew deconditioning is not considered applicable to head injury assessment.

Table 3.1-1. Original HIC 15 msec (HIC15) HSIR Requirements

	0.5 percent			*2 percent*			*5 percent*		
	Small Female	*50th-percentile Male*	*Large Male*	*Small Female*	*50th-percentile Male*	*Large Male*	*Small Female*	*50th-percentile Male*	*Large Male*
HIC15	300			500			700		

Table 3.1-2. Proposed Revisions to HIC15 HSIR Requirements

	0.5 percent			*5 percent*		
	Small Female	*50th-percentile Male*	*Large Male*	*Small Female*	*50th-percentile Male*	*Large Male*
HIC15	278	250	239	779	700	670

3.1.2.1.2 Peak Head Acceleration

Mertz [ref. 54] presented risk curves for peak head acceleration without reference to pulse duration. The 5-percent risk limit was established as 180 G peak resultant head acceleration for the 50th-percentile (or midsize) male. Table 3.1-3 shows the original values included in the HSIR and Table 3.1-4 lists the revised limit values for the peak resultant head acceleration values for 0.5- and 5-percent risk level values for the three ATD sizes. Crew deconditioning is not considered applicable to head injury assessment.

Recent analyses of racing car accidents using onboard crash recording and a mathematical driver model have indicated that peak head and head rotational accelerations may be more predictive of head injury than the HIC [ref. 62]. A number of extensive head finite element models (FEMs) have been developed as research tools for studying head injury assessment methods. Most are still in the validation stage of development and are complex and time consuming to run. An exception is the Simulated Injury Monitor (SIMon) model developed by the NHTSA. It is a simplified brain model in which measurements of 3-dimensional (D) motion in the form of head translational accelerations, and rotational velocities and accelerations, measured in an ATD test, can be used to assess the risk of several forms of brain injury. This model is in the development phase of its implementation.

Table 3.1-3. Peak Head Acceleration HSIR Requirements

	0.5 percent			*2 percent*			*5 percent*		
	Small Female	*50th-percentile Male*	*Large Male*	*Small Female*	*50th-percentile Male*	*Large Male*	*Small Female*	*50th-percentile Male*	*Large Male*
Peak Head Acceleration (G) (deconditioned)	119	112	109	151	142	138	166	155	151
Peak Head Acceleration (G) (non-deconditioned)	138	130	127	176	165	160	193	180	175

Table 3.1-4. Proposed Revisions to Peak Head Acceleration HSIR Requirements

	0.5 percent			*5 percent*		
	Small Female	*50th-percentile Male*	*Large Male*	*Small Female*	*50th-percentile Male*	*Large Male*
Peak Head Acceleration (G)	138	130	127	193	180	175

3.1.2.2 Neck Injury Criteria

3.1.2.2.1 Peak Neck (Cervical) Bending Moments

The concept of predicting neck injuries due to bending has been studied for almost as long as head injury prediction. The present bending moment limit criteria for fore and aft bending (i.e., flexion and extension) are based on the work of Mertz and Patrick [ref. 63] in which the necks of volunteers and cadavers were inertially loaded by head motion in sled tests where the subjects were restrained by belt restraints or seatbacks without head support. The concept of neck injury due to bending is based on the concern for excessive bending motion (in flexion, extension, or lateral bending) causing ligamentous and boney damage as the vertebrae impinge in extreme motion. Since neck motion is difficult to measure with transducers in an ATD, the bending-moment levels associated with excessive motion in cadaver tests was used by Mertz and Patrick as an indicator of potential impingement. Mertz [ref. 54] does not give risk curves for neck compressive loading or neck shear loading. Lacking that information, a conservative estimate of low risk (~0.5 percent) can be made by taking the data on human volunteer static neck loading from Patrick and Chou [ref. 64] as a surrogate for low-risk dynamic loading in neck flexion and lateral bending. Mertz [ref. 54] presents a risk curve for extension moment values related to serious injury for the case of minimum muscle tone in various sized dummies.

Table 3.1-5 shows the original values included in the HSIR. Table 3.1-6 lists the revised limit values for the neck-bending moment limit values (i.e., 0.5- and 5-percent risk for the three ATD sizes for extension and 0.5- and 5-percent for flexion and lateral bending) for non-deconditioned and deconditioned crew. See Section 3.1.2.6 for information on the deconditioning factor.

Table 3.1-5. Peak Neck Bending Moment HSIR Requirements

	0.5 percent			*2 percent*			*5 percent*		
	Small Female	*50th-percentile Male*	*Large Male*	*Small Female*	*50th-percentile Male*	*Large Male*	*Small Female*	*50th-percentile Male*	*Large Male*
Peak neck (cervical) flexion bending moment (Newton meter (Nm)) (deconditioned)	42	83	83	57	108	125	89	163	222
Peak neck (cervical) flexion bending moment (Nm) (non-deconditioned)	49	96	96	66	126	145	104	190	258
Peak neck (cervical) lateral bending moment (Nm) (deconditioned)	33	65	65	41	82	82	62	123	123
Peak neck (cervical) lateral bending moment (Nm) (non-deconditioned)	38	75	75	48	95	95	72	143	143
Peak Neck (cervical) extension bending moment (Nm) (deconditioned)	15	34	42	27	49	67	28	56	75
Peak Neck (cervical) extension bending moment (Nm) (non-deconditioned	17	39	49	31	57	78	33	65	87

Table 3.1-6. Proposed Revisions to Peak Neck Bending Moment HSIR Requirements

	0.5 percent			*5 percent*		
	Small Female	*50th-percentile Male*	*Large Male*	*Small Female*	*50th-percentile Male*	*Large Male*
Peak neck (cervical) flexion bending moment (Nm) (deconditioned)	22	43	57	82	163	215
Peak neck (cervical) flexion bending moment (Nm) (non-deconditioned)	25	50	66	95	190	250
Peak neck (cervical) lateral bending moment (Nm) (deconditioned)	27	53	71	62	123	162
Peak neck (cervical) lateral bending moment (Nm) (non-deconditioned)	31	62	82	72	143	188
Peak Neck (cervical) extension bending moment (Nm) (deconditioned)	23	46	61	34	66	88
Peak Neck (cervical) extension bending moment (Nm) (non-deconditioned	27	54	71	39	77	102

3.1.2.2.2 Peak Neck (Cervical) Axial Tension

In analyzing the biomechanical database for neck tension, the Alliance noted there was one fatal neck lesion at the 5-percent risk level. As a result, the 3-percent risk level for neck tension was chosen for implementation in FMVSS 208 [ref. 54]. The worst case for neck tension loading is considered to be when the neck muscles are tensed only to the degree required to keep the head upright. Mertz [ref. 54] shows neck tension risk curves for serious neck injury limits with minimum muscle tone. Table 3.1-7 shows the original values included in the HSIR. Table 3.1-8 lists the revised limit values for the neck tension limit for the three ATD sizes with non-deconditioned and deconditioned values as described in Section 3.1.2.6.

Table 3.1-7. Peak Neck Axial Tension HSIR Requirements

	0.5 percent			*2 percent*			*5 percent*		
	Small Female	*50th-percentile Male*	*Large Male*	*Small Female*	*50th-percentile Male*	*Large Male*	*Small Female*	*50th-percentile Male*	*Large Male*
Peak neck (cervical spine) axial tension (Newton (N)) (deconditioned)	631	943	1,138	1,753	2,781	3,363	2,161	3,440	4,326
Peak neck (cervical spine) axial tension (N) (non-deconditioned)	734	1,097	1,323	2,038	3,234	3,910	2,513	4,000	5,030

Table 3.1-8. Proposed Revisions to Peak Neck Axial Tension HSIR Requirements

	0.5 percent			*5 percent*		
	Small Female	*50th-percentile Male*	*Large Male*	*Small Female*	*50th-percentile Male*	*Large Male*
Peak neck (cervical spine) axial tension (N) (deconditioned)	1,635	2,595	3,137	1,780	2,830	3,970
Peak neck (cervical spine) axial tension (N) (non-deconditioned)	1,901	3,017	3,647	2,070	3,290	3,970

3.1.2.2.3 Peak Neck (Cervical) Axial Compression

Neck compressive injury assessment focused on a number of possible injury modes. The most serious injuries occur when the spinal disruption compromises the spinal cord. These injuries are generally irreversible and can lead to weakness, paralysis, or death. Spinal structural element failure (i.e., vertebrae, discs, and ligaments) can lead to disruption of the cord from bone fragments impinging on the cord, or severe misalignment of the vertebrae causing cord disruption. There are many cervical spine compression failure modes. These modes depend on the spine configuration and the head attitude relative to the spine and torso when the load is applied to the head [ref. 65].

The normal cervical spine configuration in an upright, seated subject with the eyes looking forward is a concave to the rear curve (i.e., lordotic curve). As the head is rotated forward (flexion), the cervical spine lordotic curvature decreases and disappears as the spine becomes straight with forward bending. Continued forward bending of the head produces a concave to the front spinal curve (i.e., kyphotic curve). Research has shown that when the head is rotated (flexed) forward, the cervical spine becomes relatively straight with a slight kyphotic curvature, and a compressive load is applied to the top of the head, the spine is at risk of buckling with a subsequent dislocation

of adjacent vertebrae near the center of the cervical spine. Termed a fracture-dislocation, this injury can produce paralysis at a relatively low compressive force on the head. This injury is commonly seen in headfirst diving situations (e.g., water sports, automobile rollovers, and football spearing contacts). When the cervical spine is greatly curved in the forward or rearward direction, and the top of the head is loaded in compression, other failure modes, such as stretched ligaments, chipped vertebra, or crushed vertebra usually occur at sufficiently high forces. When the spine is straight and a force is applied rapidly to the top of the head, it is possible to produce a basal skull fracture instead of a cervical spine injury.

The compressive force limits chosen for the HSIR have been derived from the automotive injury biomechanics and injury assessment literature and as codified in the NHTSA FMVSS 208, *Occupant Crash Protection* (see Figure 3.1-13). FMVSS 208 specifies the maximum allowable compression force on the neck to be 4000 N for the 50th-percentile male Hybrid III ATD as it interacts with the interior of a vehicle in a 35-mph frontal barrier crash. The injury risk associated with the FMVSS 208 injury assessment numbers is considered to be at the 5-percent risk level. The HSIR lists the compressive force limits for the 5th-percentile female and the 95th-percentile Hybrid III ATDs. The HSIR document is concerned with injury assessment values for risk levels lower than 5 percent. However, Mertz [ref. 54] does not give risk curves for neck compressive loading or neck shear loading. Lacking that information, a conservative estimate of low risk (approximately 0.5 percent) can be made by taking the data on human volunteer static loading of the neck from Mertz [ref. 66] as a surrogate for low-risk dynamic loading in compression and shear. These values and deconditioned crew values (as described in Section 3.1.2.6) are given in Table 3.1-9.

Table 3.1-9. Peak Neck Axial Compression HSIR Requirements

	0.5 percent			*2 percent*			*5 percent*		
	Small Female	*50th-percentile Male*	*Large Male*	*Small Female*	*50th-percentile Male*	*Large Male*	*Small Female*	*50th-percentile Male*	*Large Male*
Peak neck (cervical spine) compression (N) (deconditioned)	596	946	1,142	1,067	1,694	2,046	2,167	3,440	4,154
Peak neck (cervical spine) compression (N) (non-deconditioned)	693	1,100	1,328	1,241	1,970	2,379	2,520	4,000	4,830

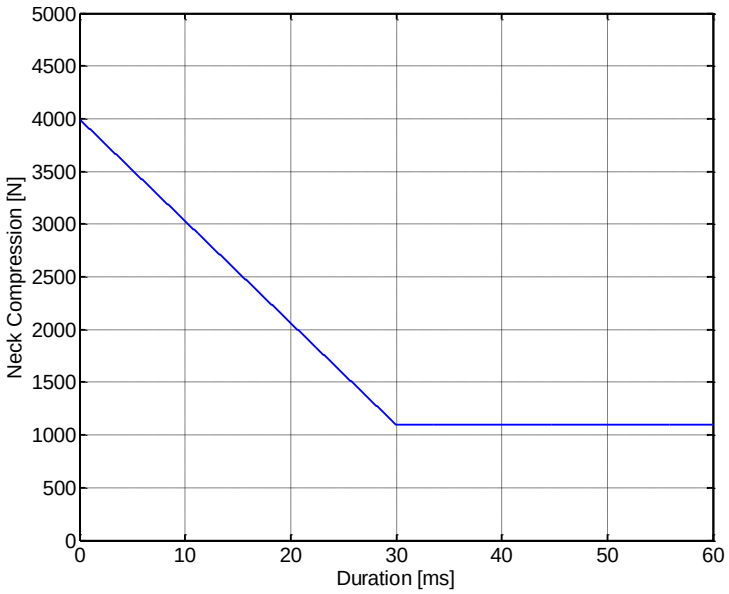

Figure 3.1-13. FMVSS 208 Neck Compression Limit for Severe Injury

Belt-restrained automobile occupants usually do not sustain loading to the top of the head in frontal crashes with the exception of some possible limited contact with the airbags. However, when a belt-restrained crew is in a spacesuit with an attached helmet, there is a possibility of compressive contact of the top of the head against the helmet interior during crash loading. A similar situation can occur in the development of head/neck restraints for racecar drivers. Some concepts use tethers that run vertically, rather than the horizontal tethers seen in the HANS® device. Vertical tethers can induce large compressive neck forces as the body moves forward into the restraint belts and the head interacts with the restrained helmet. To deal with this issue, the SFI 38.1 Standard [ref. 67] for head/neck restraints limits the maximum compressive load to 2500 N in a 70-G frontal crash test with a midsize male Hybrid III ATD. Design countermeasures to minimize contact of the top of the head with the interior of the space helmet are necessary to ensure that neck compressive forces are controlled to acceptable levels as defined by HSIR Table N4-2 Transient Force Application Limits (see Table 3.1-9). Revisions to the table (i.e., removal of the 2-percent limits) are shown in Table 3.1-10.

Table 3.1-10. Proposed Revisions to Peak Neck Axial Compression HSIR Requirements

	0.5 percent			*5 percent*		
	Small Female	*50th-percentile Male*	*Large Male*	*Small Female*	*50th-percentile Male*	*Large Male*
Peak neck (cervical spine) compression (N) (deconditioned)	596	946	1,142	2,167	3,440	4,154
Peak neck (cervical spine) compression (N) (non-deconditioned)	693	1,100	1,328	2,520	4,000	4,830

3.1.2.2.4 Peak Neck (Cervical) Shear Force

Mertz [ref. 54] does not give risk curves for neck compressive loading or neck shear loading. Lacking that information, a conservative estimate of low risk (~0.5 percent) can be made by taking the data on human volunteer static neck loading from Mertz [ref. 66] as a surrogate for low-risk dynamic loading in compression and shear. These values and deconditioned crew values are

described in Section N4.1 [ref. 1] and are given in Table N4-2 [ref. 1] (see Table 3.1-11). Revisions to the Table (i.e., removal of the 2-percent limits) are shown in Table 3.1-12.

Table 3.1-11. Peak Neck Shear Force HSIR Requirements

	0.5 percent			*2 percent*			*5 percent*		
	Small Female	*50th-percentile Male*	*Large Male*	*Small Female*	*50th-percentile Male*	*Large Male*	*Small Female*	*50th-percentile Male*	*Large Male*
Peak neck (cervical spine) shear force (N) (deconditioned)	593	946	1,142	919	1,462	1,766	1,680	2,666	3,219
Peak neck (cervical spine) shear force (N) (non-deconditioned)	690	1,100	1,328	1,069	1,700	2,053	1,953	3,100	3,743

Table 3.1-12. Proposed Revisions to Peak Neck Shear Force HSIR Requirements

	0.5 percent			*5 percent*		
	Small Female	*50th-percentile Male*	*Large Male*	*Small Female*	*50th-percentile Male*	*Large Male*
Peak neck (cervical spine) shear force (N) (deconditioned)	593	946	1,142	1,680	2,666	3,219
Peak neck (cervical spine) shear force (N) (non-deconditioned)	690	1,100	1,328	1,953	3,100	3,743

3.1.2.3 Lower Extremity Injury Criteria

Mertz [ref. 54] does not give risk curves for axial compressive loading for the lower extremities. Lacking that information, a conservative estimate of low risk (~0.5 percent) can be made by taking the data on knee long-duration or static-loading from Mertz [ref. 66] as a surrogate for low-risk compressive femur force limit and the peak knee force limit for short duration loading as the 5-percent risk femur compressive force limit.

Tibial plateau compressive force limits are given in Mertz [ref. 66] for the medial and lateral plateaus. A low-risk estimate of tibial axial compression can be estimated from assuming the single plateau limit force acting on the complete tibia and a 5-percent risk tibial axial compressive force limit as plateaus being simultaneously loaded, doubling the limiting force over the low-risk values. These values and deconditioned crew values are described in Section N4.1 [ref. 1] and are given in Table N4-2 [ref. 1] (see Table 3.1-13) Revisions to the table (i.e., removal of the 2-percent limits) are shown in Table 3.1-14.

Table 3.1-13. Peak Lower Extremity Axial Compression HSIR Requirements

	0.5 percent			*2 percent*			*5 percent*		
	Small Female	*50th-percentile Male*	*Large Male*	*Small Female*	*50th-percentile Male*	*Large Male*	*Small Female*	*50th-percentile Male*	*Large Male*
Peak femur axial compression (N) (deconditioned)	1,914	3,000	3,690	2,498	3,801	5,013	3,862	5,670	8,100
Peak femur axial compression (N) (non-deconditioned)	2,552	4,000	4,920	3,331	5,068	6,684	5,150	7,560	10,800
Peak tibia axial compression (N) (deconditioned)	1,914	3,000	3,690	2,490	3,900	4,800	3,825	6,000	7,380
Peak tibia axial compression (N) (non-deconditioned)	2,552	4,000	4,920	3,320	5,200	6,400	5,100	8,000	9,840

Table 3.1-14. Proposed Revisions to Peak Lower Extremity Axial Compression HSIR Requirements

	0.5 percent			*5 percent*		
	Small Female	*50th-percentile Male*	*Large Male*	*Small Female*	*50th-percentile Male*	*Large Male*
Peak femur axial compression (N) (deconditioned)	3,867	5,670	7,212	4,640	6,803	8,653
Peak femur axial compression (N) (non-deconditioned)	5,156	7,560	9,616	6,186	9,070	11,537
Peak tibia axial compression (N) (deconditioned)	1,914	3,000	3,690	3,825	6,000	7,380
Peak tibia axial compression (N) (non-deconditioned)	2,552	4,000	4,920	5,100	8,000	9,840

3.1.2.4 Restrained Body Movement and Deflection Injury Criteria

3.1.2.4.1 Chest Sternal-To-Spine Deflection

The Hybrid III ATD chest deflection has been shown to be a good indicator of chest injury potential in belt-restrained vehicle occupants [ref. 68]. When two parallel shoulder belts are used to restrain the upper torso, the loading from the belts should be considered distributed loading. Mertz [ref. 54] presents risk curves for normalized deflection. The HSIR 0.5-, 2-, and 5-percent risk limit values of sternal deflection for the three ATD sizes are given in Table 3.1-15 (not distributed load), with the proposed revisions shown in Table 3.1-16 (revised to reflect two shoulder belts instead of one).

Table 3.1-15. Chest Sternal-To-Spine Deflection HSIR Requirements

	0.5 percent			*2 percent*			*5 percent*		
	Small Female	*50th-percentile Male*	*Large Male*	*Small Female*	*50th-percentile Male*	*Large Male*	*Small Female*	*50th-percentile Male*	*Large Male*
Chest Sternal to Spine Deflection (millimeter (mm))	28	31	35	36	44	49	41	50	55

Table 3.1-16. Proposed Revisions to Chest Sternal-To-Spine Deflection HSIR Requirements

	0.5 percent			*5 percent*		
	Small Female	*50th-percentile Male*	*Large Male*	*Small Female*	*50th-percentile Male*	*Large Male*
Chest Sternal to Spine Deflection (mm)	33	41	45	39	48	53

3.1.2.5 Body Movement Limits

Dynamic overshoot occurs when the acceleration, forces, and moments measured on or within the human body or body segments exceed the input acceleration or forces that are imparted to the body. Dynamic overshoot is adverse only when the human body responses exceed the specified injury limits. The body movement limits are intended to control the amount of free space that will be permitted for body motion until the accelerating seat and restraint system contacts the occupant. Minimization of these movements reduces dynamic overshoot by coupling the occupant to the seat and restraint system. The indicators of acceptability are the Hybrid III ATD response parameters. Displacement measurements may be helpful in understanding the

relationship between free space and injury metrics, but the influence of free space on the potential for injury is a function of additional factors (e.g., impact acceleration, velocity change, and viscoelastic properties) and the injury tolerance of the impacted body segments. The restrained body movement limits are given in
Table 3.1-17 for the various directions of loading.

Table 3.1-17. Restrained Body Movement HSIR Limits

	Lateral *($\pm G_y$)*	*Anterior* *($+G_x$)*	*Posterior* *($-G_x$)*
Head Movement (mm)	75	125	25
Chest Movement (mm)	N/A	63	25
Pelvic Movement (mm)	37	50	25
Shoulder Movement (mm)	50	N/A	N/A

Caudal Pelvic Movement ($+G_z$) (mm)	50
Upward Head Movement ($-G_z$) (mm)	50

3.1.2.6 Derivation of Deconditioning Factor

Nominal landing limits are set for critical parameters (e.g., loads and deflections) to keep significant injury risk at the 0.5-percent risk level, with additional tolerance reductions resultant from the crew being deconditioned due to long-duration spaceflight and increased body movement presumed due to the launch/entry/landing suit. Therefore, a scaling factor has been applied to the non-launch abort landing scenarios in the form of a deconditioning coefficient that adjusts for the reduced crew capacity to endure flight/landing loads. It is assumed that the crew in all launch abort landing scenarios will not be deconditioned. The added body deflections due to wearing the flight suit cannot be estimated at this time. However, the body deflection constraints defined in CxP 70024 HS3130 will apply to the seat and the suit system. Therefore, a separate suit deflection coefficient is not required [ref. 1].

A deconditioning factor was estimated to adjust the maximum allowable loading at the femoral neck and the lumbar spine during a severe Orion reentry landing. The maximum allowable skeletal loading that can be experienced by an able-bodied person (i.e., no deconditioning) at the femoral neck, tibia, and lumbar spine during an Orion launch abort landing has been estimated from terrestrial crash impact data and other sources. This deconditioning factor is a function of measured human body physiological changes associated with dwell time away from the Earth's surface (i.e., reduced gravitational environment). The data for the deconditioned crew were derived from bone mineral density (BMD) measurements by dual-energy X-ray absorbance and quantitative computerized tomography, which can provide volumetric BMD changes in the trabecular bone compartment over a mission.

The deconditioning factor can be multiplied by the able-bodied loading estimates to account for the BMD loss. For purposes of this analysis, the deconditioning factor was assumed to be a proportionality factor relating the allowable pre- and post-flight skeletal loading after deconditioned BMD loss. It was further assumed that the same probability of injury should exist in pre- and post-flight cases. It should be noted that the highest likelihood contingency landing scenarios were drivers for establishing the following loading conditions: spine axial compressive loading in a seated crew; axial tibial compressive forces occurring during a seat stroke or crush in which the foot pan for a seated crew is pushed in the cephalic direction relative to the trunk; hip

loading due to a pure lateral blow to the greater trochanter of a seated crew; and hip loading due to a blow to the kneecap of a seated crew.

Therefore, the following deconditioning factors, mainly driven by spaceflight-induced musculoskeletal changes, have been applied to the values in Appendix N of CxP 70024 [ref. 1], Head Acceleration Limits, Neck Protection Criteria, and Transient Force Applications Limits as noted:

Φ - deconditioned crew coefficient for femur and tibia = 0.75

ξ - deconditioned crew coefficient for spinal elements and head = 0.86

3.1.2.7 Application of Occupant Protection Principles

The following are examples of industry application of restraint principles:

- The body may be restrained to maintain accelerations and loads to within the allowable limits.
- The torso may be restrained with a multiple attach point harness.
- The body may be supported with a conformal seat that is essentially rigid and fits the contours of the back and bottom of the torso, shoulders, pelvis, and legs.
- The sides of the head, shoulders, hips, and legs may be supported to reduce side-impact movement with close-fitting, conformal surfaces if required to maintain loads within the limits of human tolerance.
- The head and neck are supported such that loads and accelerations are within the limits of human tolerance.

Effective torso restraint in automobile racing (e.g., NASCAR and Indy Racing League (IRL)) and in space vehicle landing (e.g., Soyuz TM and TMA) has been accomplished with seats that conform to the crew's back and sides to provide continuous support for the pelvis, lumbar and thoracic spine, and helmeted head. Such a seat conforms to the shape of the back and is sufficiently stiff to support the back shape and spine during impact accelerations (i.e., the back of this seat is conformal to the body).

Effective car racing seats provide lateral support for sides of the pelvis, shoulders, and head. In the past, racing seats have commonly provided close-fitting pelvis lateral support, but such seats provided no motion control for the upper torso and head. The addition of panels that restrain the shoulders and head dramatically reduces injury potential in side impacts from automobile crashes.

3.2 Biodynamic Modeling

3.2.1 Coordinate System Definitions

This section describes the various coordinate systems employed. Appropriate data transforms were applied in all instances to ensure that the correct input and output orientations and polarities were obtained. All data were converted to Society of Automotive Engineering (SAE) J211/1 coordinate conventions to allow data comparisons [ref. 69]. The purpose of this section is to show the coordinate systems used and to provide the transformation matrices used to convert: input data from the environment specific coordinates to the SAE coordinate system; input data from SAE coordinates to the model specific coordinate system; and the model responses from the model specific coordinates back to the SAE coordinate system.

3.2.1.1 Environment Specific Coordinate Systems

3.2.1.1.1 WPAFB Horizontal Impact Accelerator (HIA) Coordinate System

The WPAFB HIA facility employs a Right-Hand Rule thumbs up, +X forward coordinate system for the sled. In addition, the impactor accelerates the sled from an initial velocity of zero, so no additional consideration is needed to correct for initial velocity. Because the coordinate system is fixed to the sled, the seat coordinate system varied depending on the seat orientation to the sled.

3.2.1.1.1.1 WPAFB –X (Frontal) Impact Runs

For this test condition, the ATD was facing the ram with its back toward the end of the track (Figure 3.2-1). Equation 3.2-1 to Equation 3.2-3 allow conversion from the seat coordinate system to the SAE coordinate system.

Equation 3.2-1. WPAFB –X to Sled Coordinate Transformation

$$\vec{a}_{sled} = \begin{bmatrix} -1 & 0 & 0 \\ 0 & -1 & 0 \\ 0 & 0 & 1 \end{bmatrix} \vec{a}_{-X}$$

Equation 3.2-2. WPAFB Sled to SAE Coordinate Transformation

$$\vec{a}_{SAE} = \begin{bmatrix} 1 & 0 & 0 \\ 0 & -1 & 0 \\ 0 & 0 & -1 \end{bmatrix} \vec{a}_{sled}$$

Equation 3.2-3. WPAFB –X to SAE Coordinate Transformation

$$\vec{a}_{SAE} = \begin{bmatrix} -1 & 0 & 0 \\ 0 & 1 & 0 \\ 0 & 0 & -1 \end{bmatrix} \vec{a}_{-X}$$

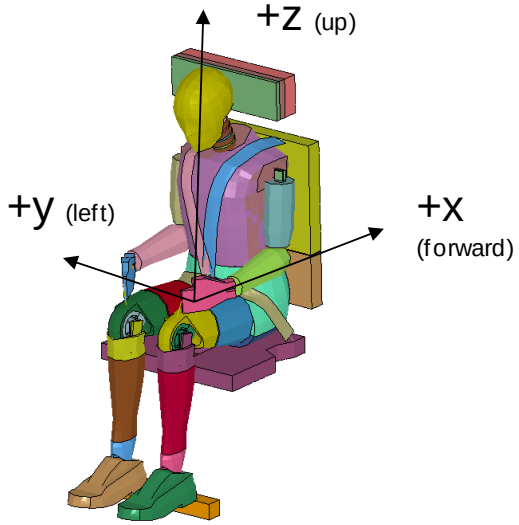

Figure 3.2-1. WPAFB Horizontal Sled –X (Frontal) Test Condition Coordinate System

3.2.1.1.1.2 WPAFB +X (Rear) Impact Runs

For this test condition, the ATD was facing the end of the track (Figure 3.2-2), so the seat and sled coordinate systems are aligned. Equation 3.2-4 to Equation 3.2-6 allow conversion from the seat coordinate system to the SAE coordinate system.

Equation 3.2-4. WPAFB +X to Sled Coordinate Transformation

$$\vec{a}_{sled} = \begin{bmatrix} 1 & 0 & 0 \\ 0 & 1 & 0 \\ 0 & 0 & 1 \end{bmatrix} \vec{a}_{+X}$$

Equation 3.2-5. WPAFB Sled to SAE Coordinate Transformation

$$\vec{a}_{SAE} = \begin{bmatrix} 1 & 0 & 0 \\ 0 & -1 & 0 \\ 0 & 0 & -1 \end{bmatrix} \vec{a}_{sled}$$

Equation 3.2-6. WPAFB +X to SAE Coordinate Transformation

$$\vec{a}_{SAE} = \begin{bmatrix} 1 & 0 & 0 \\ 0 & -1 & 0 \\ 0 & 0 & -1 \end{bmatrix} \vec{a}_{+X}$$

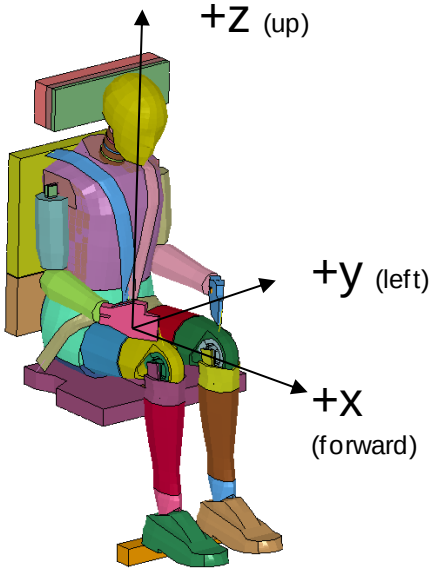

Figure 3.2-2. WPAFB Horizontal Sled +X (Rear) Test Condition Coordinate System

3.2.1.1.1.3 WPAFB –Y (Lateral) Impact Runs

For this test condition, the ATD was facing to the right with the left shoulder toward the end of the track (Figure 3.2-3). Equation 3.2-7 to Equation 3.2-9 allow conversion from convert the seat coordinate system to the SAE coordinate system.

Equation 3.2-7. WPAFB –Y to Sled Coordinate Transformation

$$\vec{a}_{sled} = \begin{bmatrix} 0 & -1 & 0 \\ 1 & 0 & 0 \\ 0 & 0 & 1 \end{bmatrix} \vec{a}_{-Y}$$

Equation 3.2-8. WPAFB Sled to SAE Coordinate Transformation

$$\vec{a}_{SAE} = \begin{bmatrix} 1 & 0 & 0 \\ 0 & -1 & 0 \\ 0 & 0 & -1 \end{bmatrix} \vec{a}_{sled}$$

Equation 3.2-9. WPAFB –Y to SAE Coordinate Transformation

$$\vec{a}_{SAE} = \begin{bmatrix} 0 & -1 & 0 \\ -1 & 0 & 0 \\ 0 & 0 & -1 \end{bmatrix} \vec{a}_{-Y}$$

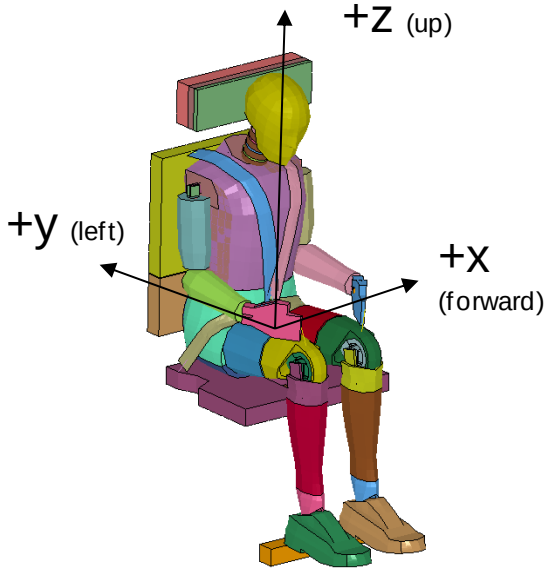

Figure 3.2-3. WPAFB Horizontal Sled –Y (Lateral) Test Condition Coordinate System

3.2.1.1.1.4 WPAFB +Z (Spinal) Impact Runs

For this test condition, the ATD was facing up with the head toward the end of the track (Figure 3.2-4). Equation 3.2-10 to Equation 3.2-12 allow conversion from the seat coordinate system to the SAE coordinate system.

Equation 3.2-10. WPAFB +Z to Sled Coordinate Transformation

$$\vec{a}_{sled} = \begin{bmatrix} 0 & 0 & 1 \\ 0 & -1 & 0 \\ 1 & 0 & 0 \end{bmatrix} \vec{a}_{+Z}$$

Equation 3.2-11. WPAFB Sled to SAE Coordinate Transformation

$$\vec{a}_{SAE} = \begin{bmatrix} 1 & 0 & 0 \\ 0 & -1 & 0 \\ 0 & 0 & -1 \end{bmatrix} \vec{a}_{sled}$$

Equation 3.2-12. WPAFB +Z to SAE Coordinate Transformation

$$\vec{a}_{SAE} = \begin{bmatrix} 0 & 0 & 1 \\ 0 & 1 & 0 \\ -1 & 0 & 0 \end{bmatrix} \vec{a}_{+Z}$$

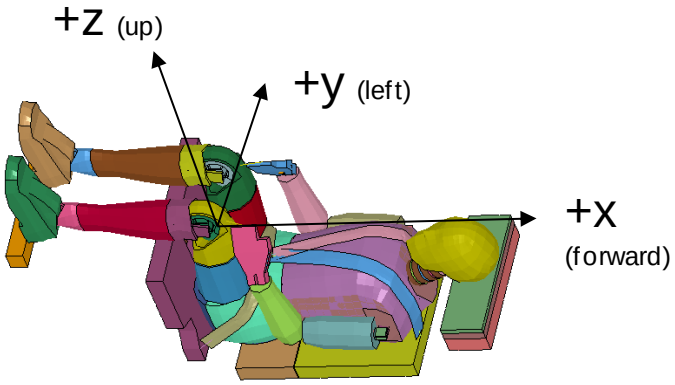

Figure 3.2-4. WPAFB Horizontal Sled +Z (Spinal) Test Condition Coordinate System

3.2.1.2 LS-DYNA® Specific Coordinate Systems

Because LS-DYNA® allows for a custom coordinate system definition, additional consideration is needed for the numerical models run with each LS-DYNA® seat model.

3.2.1.2.1 WPAFB LS-DYNA® Seat Model Coordinate System

Because the WPAFB testing has an initial velocity of zero, accelerations were from zero, so no additional consideration was needed to correct for initial velocity. Equation 3.2-13 shows the transformation employed to convert from SAE coordinates to the WPAFB LS-DYNA® model coordinates (Figure 3.2-5). Equation 3.2-14 shows the transformation to convert the Constellation Crew Injury Prediction (CCIP) ATD output to SAE coordinates. Equation 3.2-15 shows the transformation to convert the FTSS ATD output to SAE coordinates. Equation 3.2-16 shows the transformation used to convert the THUMS output to SAE coordinates.

Equation 3.2-13. WPAFB Seat SAE to Model Coordinate Transformation

$$\vec{a}_{model} = \begin{bmatrix} 1 & 0 & 0 \\ 0 & -1 & 0 \\ 0 & 0 & -1 \end{bmatrix} \vec{a}_{SAE}$$

Equation 3.2-14. WPAFB Seat CCIP to SAE Coordinate Transformation

$$\vec{a}_{SAE} = \begin{bmatrix} 1 & 0 & 0 \\ 0 & 1 & 0 \\ 0 & 0 & 1 \end{bmatrix} \vec{a}_{CCIP}$$

Equation 3.2-15. WPAFB Seat FTSS to SAE Coordinate Transformation

$$\vec{a}_{SAE} = \begin{bmatrix} 1 & 0 & 0 \\ 0 & -1 & 0 \\ 0 & 0 & -1 \end{bmatrix} \vec{a}_{FTSS}$$

Equation 3.2-16. WPAFB Seat THUMS to SAE Coordinate Transformation

$$\vec{a}_{SAE} = \begin{bmatrix} -1 & 0 & 0 \\ 0 & 1 & 0 \\ 0 & 0 & -1 \end{bmatrix} \vec{a}_{THUMS}$$

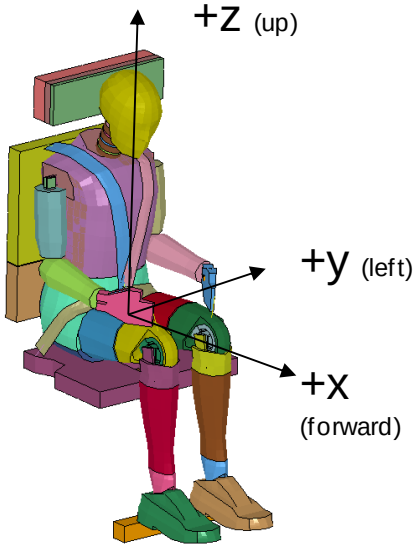

Figure 3.2-5. WPAFB LS-DYNA® Seat Model Coordinate System

3.2.1.3 MADYMO Specific Coordinate Systems

MADYMO employs a Right-Hand Rule thumbs up, +X forward coordinate system (Figure 3.2-6). For WPAFB, no initial velocity condition must be accounted for, so Equation 3.2-17 was used. To convert the MADYMO output to SAE coordinates, Equation 3.2-18 was used.

Equation 3.2-17. SAE to WPAFB MADYMO Model Coordinate Transformation

$$\vec{a}_{WPAFB} = \begin{bmatrix} 1 & 0 & 0 \\ 0 & -1 & 0 \\ 0 & 0 & -1 \end{bmatrix} \vec{a}_{SAE}$$

Equation 3.2-18. MADYMO Output to SAE Coordinate Transformation

$$\vec{a}_{SAE} = \begin{bmatrix} 1 & 0 & 0 \\ 0 & -1 & 0 \\ 0 & 0 & -1 \end{bmatrix} \vec{a}_{MADYMO}$$

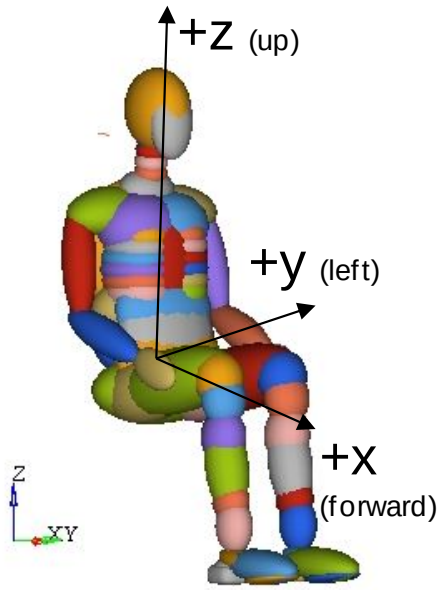

Figure 3.2-6. MADYMO Model Coordinate System

3.2.1.4 BDR Model Specific Coordinate System

The BDR model employs a Right-Hand Rule thumbs up, +X forward coordinate system (Figure 3.2-7). For WPAFB sled testing, Equation 3.2-19 was used. To convert the BDR output to SAE coordinates, Equation 3.2-20 was used.

Equation 3.2-19. SAE to WPAFB BDR Model Coordinate Transformation

$$\vec{a}_{WPAFB} = \begin{bmatrix} 1 & 0 & 0 \\ 0 & -1 & 0 \\ 0 & 0 & -1 \end{bmatrix} \vec{a}_{SAE}$$

Equation 3.2-20. BDR Model Output to SAE BDR Model Coordinate Transformation

$$\vec{a}_{SAE} = \begin{bmatrix} 1 & 0 & 0 \\ 0 & -1 & 0 \\ 0 & 0 & -1 \end{bmatrix} \vec{a}_{Brinkley}$$

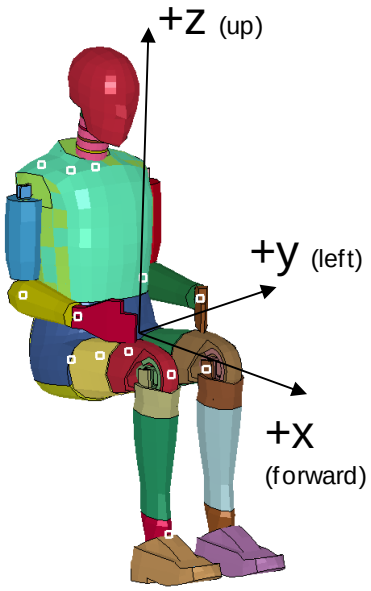

Figure 3.2-7. BDR Model Coordinate System

3.2.2 Model Development

3.2.2.1 WPAFB Configuration

3.2.2.1.1 Introduction and Description of Test Facility

The purpose of the WPAFB sled tests was to provide ATD sled test data under a variety of loading conditions so a comparison could be made between measured ATD impact responses and predictions made with numerical models. The Hybrid III and side-impact dummy (SID) ATDs were used for this study. As currently envisioned by NASA, the Hybrid III ATD will be used to evaluate the effectiveness of Orion CM crew protection systems. The Hybrid III ATD was originally designed to evaluate frontal impacts (–X-axis impacts ±45 degrees) for the automotive industry. The primary impact vectors that are expected during an Orion CM landing are combinations of +X- and +Z-axes acceleration vector components and lateral Y-axis components. Therefore, concerns have been raised regarding the Hybrid III ATD response adequacy and corresponding numerical simulations to these loading directions. Furthermore, since the numerical

models are validated to represent the Hybrid III ATD rather than the specialized dummies used by the automobile industry to evaluate sideward and rearward impacts, concerns have been raised regarding its usefulness when the impact vectors are in these other directions. No dummies have been validated for all the combinations of loads, which are expected for Orion landings. While the sled testing did not determine the overall usefulness of using the Hybrid III for CxP, it did determine the numerical model accuracy for predicting the ATD response in loading directions other than frontal impact.

The test impacts varied in acceleration vector direction and magnitude, impulse duration, and body support and restraint configuration. The basic study approach was to collect the ATD's dynamic accelerations and loads in an impact environment and compare these responses to the predicted ATD responses in the identical environment using the numerical models. Sled testing was performed using the AFRL HIA facility. The HIA is a multi-axial, high-G test facility that has been used for numerous human- and ATD-impact studies. For this study, a flat seat-pan/seat-back fixture with added leg support fixture and optional side support fixture was used. Two-seat configurations were used and are referred to as the Baseline 2 seat and the Baseline 2 plus side-supports seat (Baseline 2 + S). The Baseline 2 seat has a rigid backrest, a rigid seat pan, a rigid footrest, and a leg support panel. The Baseline 2 + S seat is identical to the Baseline 2 seat with the addition of side supports that restrict the motion of the head, shoulders, hips, and legs during lateral impact.

A five-point restraint system was used to confine the ATD in the seat. The restraint system consisted of two shoulder straps, a lap belt, and a negative-G strap. Provisions were made to tether/restrain the ATD's hands and feet to designated attachment points on the seat structure and footrest. Instrumented ATDs and associated fixtures were provided. Drawings for the seat configurations for FEM purposes and the mechanical properties of the restraint system materials for numerical modeling were provided (Figure 3.2-8). Padding used for the ATD's head protection was tested to determine the material's mechanical properties.

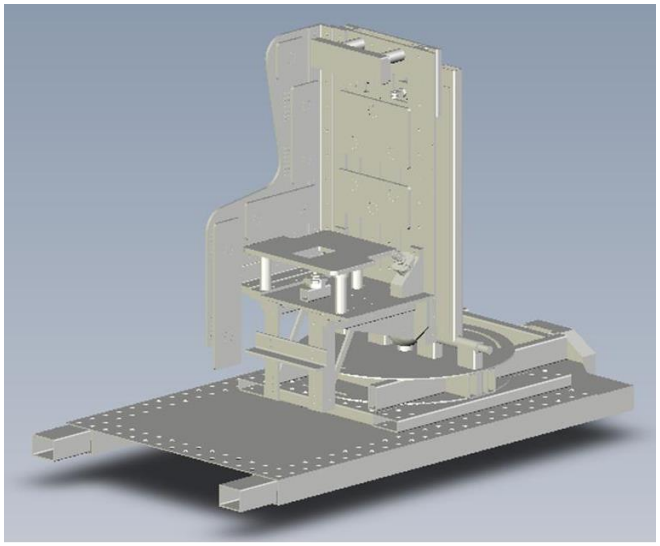

Figure 3.2-8. Computer-Aided Design (CAD) Model of Seat Used for WPAFB Sled Testing

The test setup included two instrumented ATDs: a 50th-percentile male Hybrid III automotive ATD and a 50th-percentile male Hybrid III aerospace ATD. The majority of testing was performed using the Hybrid III automotive ATD. The automotive ATD was used for testing in all four directions

(i.e., frontal, rearward, spinal, and lateral) and the aerospace ATD was used for comparison to the automotive ATD for spinal direction impacts. The aerospace ATD is identical to the automotive ATD except for the mechanical components used to represent the spine.

Follow-on tests were later performed using a European side-impact dummy (EuroSID) and a 50th-percentile male Hybrid III automotive ATD exposed to lateral loadings so that a comparison could be made between the Hybrid III response in the lateral direction and the EuroSID. The current plan for assessing crew injuries during Orion landings is to use the Hybrid III FE ATD. The crew response will be obtained by loading the ATD with landing-load acceleration obtained from vehicle-landing simulations, which are currently being performed using LS-DYNA®. The landing-load accelerations, which are combinations of X-, Y-, and Z-axes accelerations, will be applied to LS-DYNA® models consisting of the Hybrid III FEMs placed in the Orion seat designs. Injury criteria will be extracted from the simulations (e.g., neck forces, head accelerations, pelvic motion) and compared against the recommended injury criteria established in the HSIR requirements. An issue related to this approach is that the Hybrid III is not validated for lateral impact. While Orion landings generally produce primarily rear and spinal direction loading, there are landing conditions, particularly when vehicle roll is prevalent, where lateral loading occurs. Furthermore, the HSIR requirements include lateral direction-related criteria (e.g., neck loadings and body movements) which must be satisfied.

The principle objective of the SID tests is to compare the Hybrid III lateral response to the EuroSID response with particular emphasis on comparing the HSIR lateral-loading criteria between the Hybrid III and EuroSID for identical seats and loading conditions. If it is determined that the Hybrid III produces similar results to the EuroSID for similar lateral loading, the Hybrid III can then be used for the above approach involving multi-axial landing simulations and data extraction. If the Hybrid III does not produce similar results to the EuroSID, then the above planned approach may not be workable and an alternate approach will need to be developed. It is expected that the results will be different and some adjustments will need to be made to the injury criteria.

The ATD, seat system, and restraints were instrumented sufficiently to provide reliable data collection over the duration of the load application and subsequent ATD dynamic response. In addition to standard Hybrid III measurement response, forces were measured at the restraint attachment points and along the interface between the lateral seat supports and the instrumented ATD. Acceleration measurements were taken on the sled and seat. High-speed video and photographic documentation of the test series was collected for all test runs. The pre-impact positions of specific points located on the head, shoulders, hips, and knees were measured prior to each test with respect to the seat to ensure uniformity of the location of these anatomical points from test to test.

Two test acceleration profiles were selected based on predicted nominal and contingency landing conditions of the Orion capsule, and best acceleration properties to elicit a range of ATD response properties for validating the numerical models. Preliminary predictions of peak acceleration conditions are 10 G nominal and 20 G contingency. The acceleration profile used for most test conditions will have a time-to-peak of approximately 70 msec. The time-to-peak will be varied in several cells to evaluate the frequency sensitivity of the ATDs and the numerical models. Example pulses and configurations are shown in Figure 3.2-9 to Figure 3.2-11.

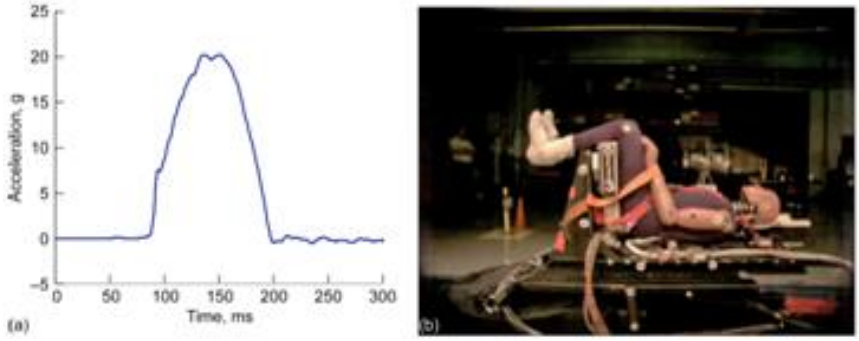

Figure 3.2-9. Sled with a 20-G Impulse in the Z-Direction. Sled Motion is to the Right. (a) Acceleration Pulse, (b) ATD Position

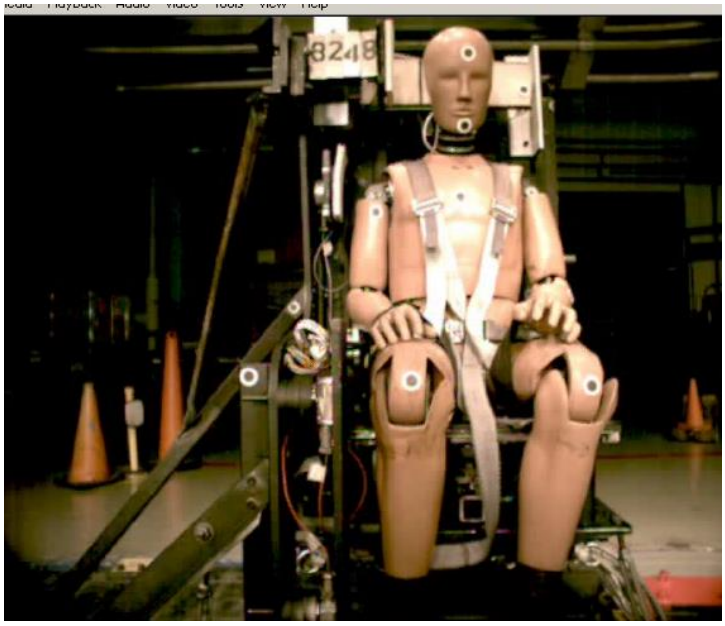

Figure 3.2-10. Seat with Side Impact Constraints Added and Oriented for Lateral Impact Loads

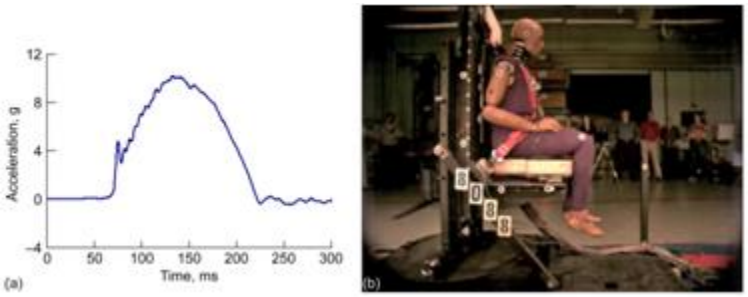

Figure 3.2-11. Sled Test with a 10-G Impulse in the X-Direction. Sled Motion Is to the Right. (a) Acceleration Pulse, (b) ATD Position

Table 3.2-1 shows the four directions of impact loading that were applied to the automotive ATD and the spinal and front impact loadings that were applied to the aerospace ATD. The identical seat configuration was used for all impact directions except for the lateral direction, where some of the tests were performed without side supports, some with side supports at a full gap distance, and some with 50-percent gaps. Peak G impact and the rise time-to-peak G levels were varied.

Table 3.2-1. WPAFB HIA Test Matrix

Test Cell	Impact Vector	Impact Direction	Impact Level (G)	Pulse Length (ms)	Manikin Type	Seat Configuration	Test No.	Test No.	Test No.	ΔV [m/s]	DR
A	+Z	Spinal	10	70	Hybrid III Auto	Baseline 2	8207	8208	8209	10.0	12.3
A1	+Z	Spinal	10	70	Hybrid III Auto	Baseline 2	8258[a]			10.0	13.7
B	+Z	Spinal	10	30	Hybrid III Auto	Baseline 2	8193			7.4	14.7
C	+Z	Spinal	10	110	Hybrid III Auto	Baseline 2	8198[b]	8199		13.2	10.1
D	+Z	Spinal	20	70	Hybrid III Auto	Baseline 2	8206			15.2	29.0
E	*+Z*	*Spinal*	*10*	*70*	*Hybrid III Aero*	*Baseline 2*	*8253*	*8254*	*8255*	*9.8*	*13.4*
F	*+Z*	*Spinal*	*15*	*70*	*Hybrid III Aero*	*Baseline 2*	*8256*			*12.7*	*21.1*
F1	+Z	Spinal	15	70	Hybrid III Auto	Baseline 2	8257			12.6	21.0
G	-X	Frontal	10	70	Hybrid III Auto	Baseline 2	8201	8202	8204	10.2	15.3
H	-X	Frontal	10	30	Hybrid III Auto	Baseline 2	8192			7.3	18.2
I	-X	Frontal	10	110	Hybrid III Auto	Baseline 2	8200			13.1	10.3
J	-X	Frontal	20	70	Hybrid III Auto	Baseline 2	8205			15.1	35.3
K	*-X*	*Frontal*	*10*	*70*	*Hybrid III Aero*	*Baseline 2*	*8250*	*8251*		*9.8*	*15.2*
L	*-X*	*Frontal*	*20*	*70*	*Hybrid III Aero*	*Baseline 2*	*8252*			*14.7*	*34.3*
M	+X	Rear	10	70	Hybrid III Auto	Baseline 2	8210			10.1	13.4
N	+X	Rear	20	70	Hybrid III Auto	Baseline 2	8211[c]	8212[d]		15.1	28.4
O	+X	Rear	10	30	Hybrid III Auto	Baseline 2	8194[e]	8195		7.4	14.4
P	+X	Rear	10	110	Hybrid III Auto	Baseline 2	8196	8197[f]		13.2	10.6
Q	-Y	Lateral	10	70	HybridIII Auto	Baseline 2+SG	8239			9.9	15.2
Q1[g]	-Y	Lateral	10	70	HybridIII Auto	Baseline 2+SG	8240[h]	8241[i]		10.0	14.9
S	-Y	Lateral	10	70	HybridIII Auto	Baseline 2+SG	8242			10.0	14.8
T	-Y	Lateral	20	70	HybridIII Auto	Baseline 2+SG	8243			14.7	32.6
U[j]	-Y	Lateral	10	70	HybridIII Auto	Baseline 2+SG	8244	8245		10.1	14.9
U[j]	-Y	Lateral	20	70	HybridIII Auto	Baseline 2+SG	8246			14.7	32.6
V[k]	-Y	Lateral	20	70	HybridIII Auto	Baseline 2+SG	8247	8249		14.7	32.6
V[k]	-Y	Lateral	10	70	HybridIII Auto	Baseline 2+SG	8248[l]			10.1	32.6
A4	*-Y*	*Lateral*	*10*	*70*	*EuroSID*	*Baseline 2+SG*	*8285*	*8286*		*9.9*	*14.4*
B4	*-Y*	*Lateral*	*10*	*70*	*EuroSID*	*Baseline 2+SG*	*8287*	*8288*		*9.9*	*14.2*
B5	*-Y*	*Lateral*	*10*	*70*	*EuroSID*	*Baseline 2+SG*	*8289*	*8290*		*9.9*	*14.2*
C4	*-Y*	*Lateral*	*20*	*70*	*EuroSID*	*Baseline 2+SG*	*8291[m]*	*8292*		*14.8*	*31.8*
C5	*-Y*	*Lateral*	*20*	*70*	*EuroSID*	*Baseline 2+SG*	*8293*			*14.8*	*31.5*
D4	-Y	Lateral	10	70	HybridIII Auto	Baseline 2+SG	8294			9.9	14.2
E4	-Y	Lateral	10	70	HybridIII Auto	Baseline 2+SG	8295			10.0	14.3
F4	-Y	Lateral	20	70	HybridIII Auto	Baseline 2+SG	8296			14.8	31.9

Baseline2+S is baseline 2 seat with added side supports

Baseline2+SG is baseline 2 seat with gap as specified in revised HSIR document

Dummies removed from the seat and instrumentation re-zeroed after each test

a Headrest Modified to provide 1" offset from plane of headrest to plane of backrest

b Test Redone because acceleration input exceeded requirement

c Lost dummy data cable

d lost lumbar z accelerometer

e test without brace at footrest

f headrest 1" aft of dummy head

g Cell Q1 added to test lateral impact with no lateral head support

h Upper limbs restrained to seat fixture with velcro straps

i Upper limbs restrained with velcro strap run beneath thigh. Felt pad (13mm thk) added to shoulder plate

j Cell U tests conducted with 50% recommended Gaps between manikin and lateral reaction load plates

k Cell V tests conducted with 100% recommended Gaps between manikin and lateral reaction load plates

l Crossbar added to lateral reaction plate for head. Tie down straps added to lower seat for additional motion control during impact

m neck x,y force not working

Four numerical models were used in the present study for comparison to the data obtained in the sled tests at WPAFB. Results from each model were compared to the test data and to each of the other models to determine the strengths and weaknesses and their applicability to CxP and the types of landings expected during Orion landings. Three of the models are numerical models of the Hybrid III automotive ATD: the Livermore Software Technology Corporation (LSTC) Hybrid III FEM, the FTSS Hybrid III FEM, and the TNO Automotive Safety Solutions (TASS) MADYMO multi-rigid body model. The fourth model was the THUMS human body FEM.

3.2.2.1.2 CxP Crew Injury Protection ATD Model

The Hybrid III automotive FE ATD used in this assessment was developed and validated by LSTC (see Figure 3.2-12). A full set of LSTC Hybrid III FE dummies has been modeled in LS-DYNA® format and set up according to the SAE calibration procedures for Hybrid III ATDs. The FE ATD used in this study was modeled using a combination of rigid and deformable parts. This ATD was validated by LSTC using standard impact tests in four different locations and positions, including head impact, neck flexion and extension, chest impact, and knee impact. These particular tests were selected because the intended use for this model is for frontal impact automobile crashes. However, this ATD was not validated for impacts in all possible orientations. The intent of the present testing was to identify how this model emulates the Hybrid III ATD for loadings other than the frontal impact direction. The LSTC Hybrid III FE ATD model can be used without charge, which provides an advantage over other numerical models.

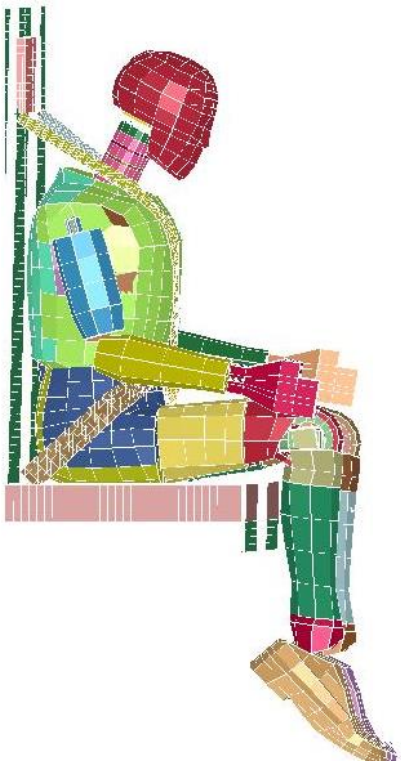

Figure 3.2-12. LSTC Hybrid III FEM in WPAFB Seat Model

The FE ATD was imported into the preprocessor LS-PrePost® to orient it in the desired positions so that the numerical model matched the position of the test ATD. In addition, limb operations were available to position the arms and legs properly. The neck was in a standard position that could not be altered. In the new ATD models currently in development by LSTC, the neck can be

rotated to better match the test setup. However, this model has not been validated and was not used for this study. Since the validated FE neck model cannot be positioned arbitrarily, for the model to be entirely consistent with the test, it was necessary to position the test ATD's neck to match the FEM.

Seatbelts were modeled with the preprocessor LS-PrePost®. The FE ATD was imported into the preprocessor; then "segment sets" were defined on the FE ATD where the seatbelts were to be positioned. Once these sets were defined, the seatbelts were positioned on the set and tensioned to make the belts fit to the contour of the ATD. The belts can be modeled with seatbelt elements (1-D beamlike elements) or 2-D shell elements. The shell model is the most appropriate model for capturing the seatbelt/ATD interaction. The pre-tension in the seatbelt is modeled by defining a local coordinate system on the belt ends. A load is defined in this coordinate system with a magnitude equal to the preload applied in the test setup. The load must be ramped to the full magnitude. Applying full-magnitude tension at time zero can lead to unrealistic oscillations in the system response and to inaccurate simulation results.

3.2.2.1.3 FTSS Hybrid III 50th-percentile LS-DYNA® Model

Following a peer review conducted by the NESC [ref. 70], the Orion Project coordinated a pilot study using the FTSS[1] LS-DYNA® Hybrid III 50th-percentile v7.0 ATD model for numerical comparisons with the WPAFB sled test data (see Figure 3.2-13). FTSS is a primary provider of physical test ATDs and their numerical models to the automotive industry ATDs. FTSS has extensive history and experience with test and numerical ATDs, including the Hybrid III. The FTSS Hybrid III was selected for the pilot study to identify this model's performance for replicating the test data and to perform a comparison between the FTSS model and the other models investigated in this study.

Figure 3.2-13. FTSS Model in WPAFB Sled Test Seat

[1] Note that since the original writing, First Technology Safety Systems has merged with Denton to become Humanetics.

The FTSS pilot study was conducted in two phases. In the first phase, predictive simulations were performed without having access to the test time history data as only test videos were provided. After that, the test data was supplied and the models were further refined to match the test as closely as possible. The purpose of the first phase was to identify how well the numerical models can predict test results (pre-test) without the use of the test data to guide model development. The second phase was to determine how well the models could match test results when modeling refinement is performed post-test. Both phases were valuable as they show how the models performed when test data are not available, or when test data are available and allow for modeling refinement. In some cases, no test data may be available and in other cases test data are used to improve modeling fidelity and the model is subsequently used for similar configurations or for alternate loading conditions.

From the test videos and provided data it was evident that the simulation was less constrained and allowed more ATD motion in the pelvis and chest. The tests showed similar trends, but key behaviors were delayed and the associated data signals contained large spikes. Visual indicators like the belt exit angle at the shoulder and deformation of the shoulder suggested that the FE ATD needed to be moved down and belt tension introduced to reduce allowable ATD motion. Situations such as these are common modeling complications and further exemplify the challenge of using these complex models without the benefits of having test data specific to the application to anchor the model.

To improve the correlation between the observed test response and the simulation, several improvements were made to the model. First, the ATD position was updated to achieve more contact with the back of the fixture.

The pelvis was rotated allowing additional torso rotation. The torso rotation allowed additional neck rotation, which allowed the pelvis to be moved rearward allowing a shorter lap belt. The shoes were removed from the baseline ATD model allowing the legs to be rotated down. The legs were spread apart as evident in the test video (see Figure 3.2-14). The arms and hands were repositioned accordingly and pre-loading was added prior to the start of the input acceleration.

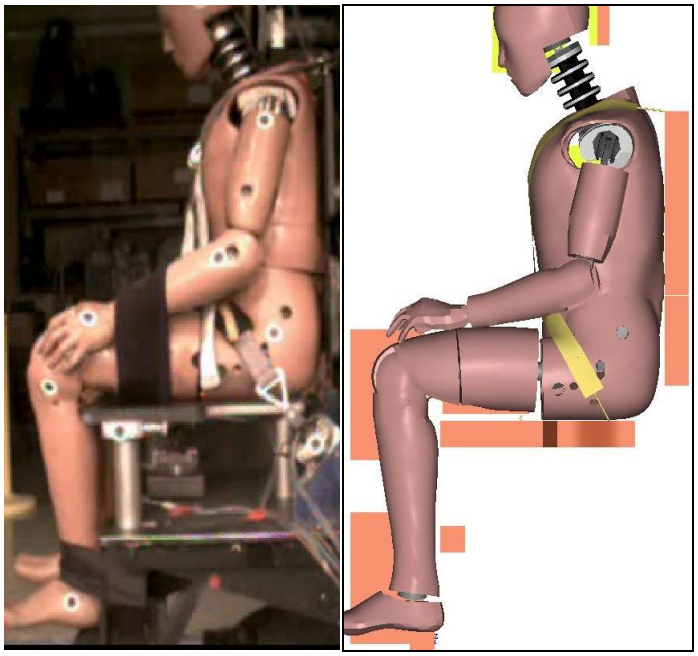

Figure 3.2-14. FTSS Hybrid III Re-positioned to Better Match Test Video

The test videos showed a black band restraining the hands to the leg (see Figure 3.2-15). Also visible were similar bands restraining the lower legs to the test fixture. Six-DOF directional springs were defined to constrain the wrists to the legs. The spring was set to have an axial direction that moved with the tibia axis. For the lower leg, a simple unidirectional spring was used to constrain the lower leg to the seat structure.

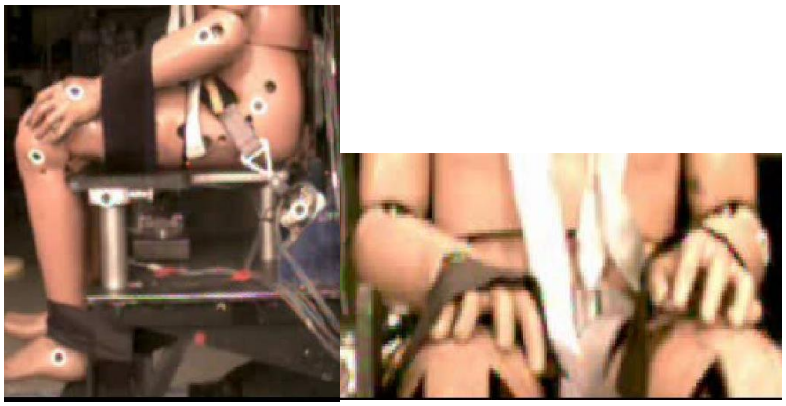

Figure 3.2-15. Physical ATD Hand and Feet Constraints

Three methodologies were utilized to develop three models to match the initial conditions viewed in the videos (see Figure 3.2-16).

FEM 1—Belt pre-tensioners were used to pull in the belts with loads approximated from the provided test data. This required that the applied input accelerations be delayed or offset in time while the ATD was pulled into the seat. A locking retractor was used to lock the belt length just prior to the start of the applied accelerations.

FEM 2—As in method FEM 1, pre-tensioners and retractors were used. Additionally, the pelvis was displaced downward (as a result of gravity) into the fixture over a period of 62 msec. The retractor was modified to lock at 62 msec.

FEM 3—The ATD mesh was pre-deformed to a position that was similar to those achieved in FEMs 1 and 2 methods. The pre-tensioners and retractors were still utilized to keep the belts as tight as possible and achieve the preloads reflected in the test data.

Note that FEMs 1 and 2 are identical at the initial position, but FEM 3 is the pre-deformed ATD mesh and was visually lower and more rearward in the fixture.

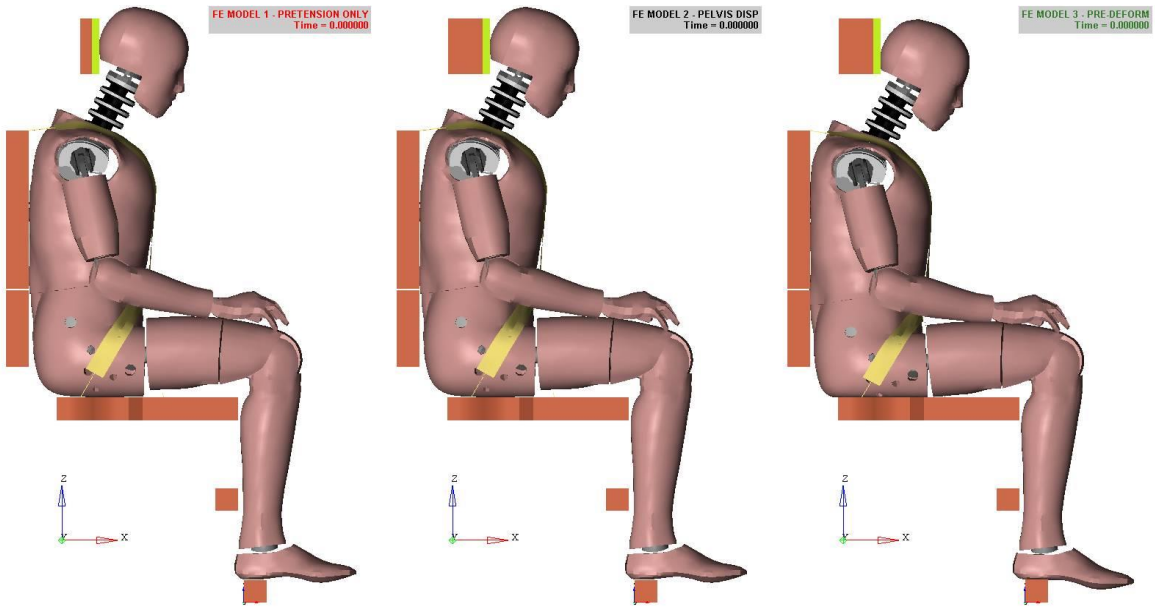

Figure 3.2-16. Comparison between Three Preload Methods

All three FEM methods added additional run time to the beginning of the simulation to allow for settling the ATD due to gravity and/or the introduction of belt tension. In addition, all three methods improved the correlation by reducing belt slack, reducing the free belt length, and settling the ATD into a configuration similar to the test condition. For FEM 1, the approach did pull tension in the belts. However, it is not a robust method for tuning a defined preload. In addition, despite the belts being visibly tightened, little load was measured in the belt ends. The pre-tension and retractor allowed tight control over the belt preload and slack reduction. The rate of application of the pre-tension can introduce undesired dynamic effects at the start of the simulation. Slowly ramping the pre-tension requires more simulation time at the start to allow the ATD to fully settle. The ATD did not settle as much in FEM 1 as it did in FEMs 2 and 3.

It is possible that the sequence of timing of the tension between the lap and shoulders could affect the final position, but that scenario was not investigated.

For FEM 2, the desired deformed configuration can only be obtained after test or after knowledge of similar test conditions has been obtained. The introduction of the pelvis motion in the 62-msec period introduced a bouncing effect of the upper body and subsequent noise at the start of the simulation. As the shoulders bounced, some of the desired belt tightening was lost. This motion could be removed with approaches, such as additional run time and simultaneous enforced displacement of part of the upper body skeleton. Since the gravity load was introduced through fixture motion, the desired pelvis relative motion needs to take into consideration the fixture motion.

An initial simulation was required to understand the unmodified ATD behavior to judge how much motion to introduce.

For FEM 3, the desired deformed configuration can only be obtained after test or after knowledge of similar test conditions has been obtained. This method requires a pre-simulation to get the ATD into the desired deformed configuration. This deformed model must be updated every time there are system changes that affect the boundary conditions enough to affect the initial deformed shape (e.g., belt anchor locations, supporting structure modifications, occupant seating position, etc.). The configuration was obtained through trial and error by comparison to the available video. If setup information is available (e.g., test data of the pelvis location and other key points and angles), then the ATD could be moved into the position more reliably. As the mesh was pre-deformed, stresses that would normally be present were not, causing excessive further mesh deformation. This would have to be monitored to determine if the affected areas introduce negative effects to the overall simulation.

As the mesh is deformed, some elements become distorted, decreasing the solution time step, thus increasing the run time. The time step can be artificially increased through added mass techniques. This mass-scaling technique would have to be monitored to understand the potential effects to the solution. Run time is needed to tension the belts to remove excess slack. The 80-msec was kept in this case for comparison to the other FEM methods. Less time could be needed as less slack needs to be taken up because less ATD settling occurs.

The belt tension/slack condition was influencing the ATD motions. Understanding the belt lengths, end conditions, and pre-loading will help set up the simulation and improve correlation. Utilization of pre-tensioners and retractors is recommended to achieve the proper pretest conditions.

The pre-deformed (FEM 3) approach allowed for good correlation with the available data. It can reduce some run time added at the beginning for settling. However, the extent to which the mesh had to be deformed to represent the test video added significant run time to the overall solution. In a development environment, the ATD may not be as tightly constrained thus requiring less initial deformation and consequently less mesh distortion. Mass scaling could be introduced to offset some of the added run time with minimal detrimental effects to the overall solution.

The use of lower-leg and arm restraints should be considered for future development. Constraining the leg motion can influence the pelvis motion, loading, and load timing. Similarly, the motion and loading due to the arm behavior can affect the chest, neck, and head responses.

The belt condition at the location of the five-point restraint buckle was undefined. In the simulation, the belts were constrained at that location resulting in no relative motion. The constraint condition could affect the belt slip/loading and subsequent ATD motions.

The physical presence of the five-point hardware may be introducing ATD contact or restraint at the pelvis and torso joint. In the simulation, the torso skin was allowed to flow freely over the top of the pelvis. It is unclear if the physical hardware might affect the behavior.

The 1-D seatbelt material that was supplied to FTSS appeared to have an improperly defined mass. It should be cross-referenced to ensure that no unintended inertia effects are introduced.

Capturing more information of the physical test setup would allow for more accurately configuring the simulation and eliminate some analyses, which were performed to study possible setup conditions. A better understanding of the physical setup procedure may increase understanding on an approach that could facilitate a better simulation method.

The following might be considered in future testing to help with post-test correlation;

- Collect test setup measurements and photographic documentation.
- Additional camera with an orthogonal viewpoint would be beneficial in helping to understand the physical behavior especially if the development inputs become more complex.
- A grid board as background in the camera view to provide a reference for distances,
- Strobe lighting timed with the fixture trigger to provide a definitive indicator of time zero.
- Belt marking graduated to a known distance to help understand belt motion and relative motions between the belt and the ATD.
- Rolling, clipping, or treatment of excess belt material to improve clarity of the image.
- Painting fixtures in a bright color so that it provides a background and helps discern different parts of the image.
- Utilizing secondary measuring devices could validate if there were fixture motion.

Following the pilot study, it was decided to continue use of the FTSS ATD model for all WPAFB sled test comparisons using the FEM 3. All references to FTSS in succeeding sections relate to this ATD configuration.

3.2.2.1.4 MADYMO Modeling Using the Hybrid III 50th-percentile ATD

The 50th-percentile Hybrid III Ellipsoid model (Figure 3.2-17) version 6.4 as supplied by TASS was used without modification. It consists of 37 rigid bodies and 69 contact ellipsoids. Various kinds of joints were used to join the bodies. Properties of the joints are generally not known, as they are internal to the model and unavailable to the user. For example, the neck is represented by five kinematic joints located in the centers of the four rubber disks and on the rotation axis of the nodding joint. The rubber disks are represented by spherical joints and the nodding joint by a revolute joint [ref. 71].

Extensive component tests have been done by TASS to characterize the joint functions and segment contact characteristics. These include: neck, clavicles, shoulders, elbows, wrists, thorax, abdomen, lumbar spine, hip, knees, ankles, and feet. Details of the testing procedures and results can be obtained from the MADYMO Theory Manual [ref. 72]. The standard ATD calibration tests (shown for the LSTC model) were among the validation tests in addition to full ATD tests with belts on a rigid seat, vertical drop tests, and airbag tests. As with the LSTC model, the ATD was not validated for all impact orientations since the Hybrid III ATD was designed primarily for frontal impact use.

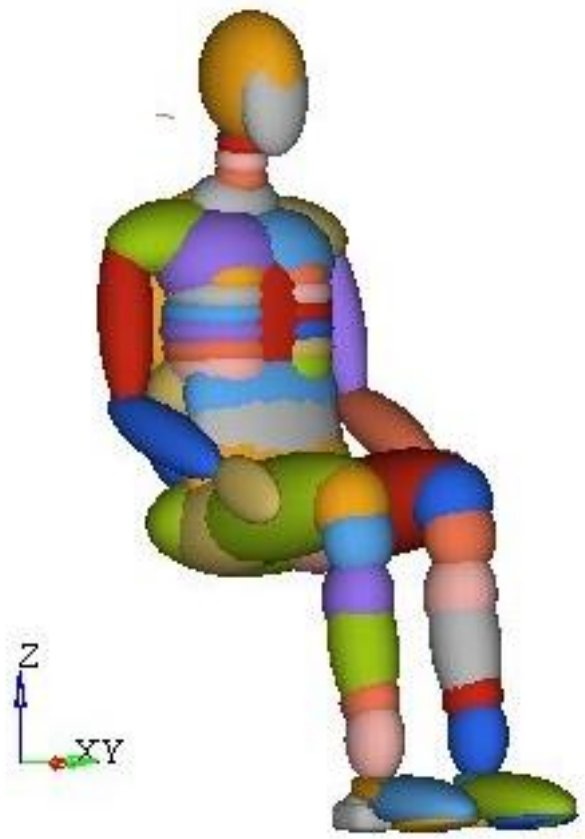

Figure 3.2-17. MADYMO Hybrid III 50th-percentile ATD – Version 6.4

The FE seat model used for the LS-DYNA® simulations was imported into MADYMO. Thus, the seat geometry was identical to that of the LS-DYNA® model. Flat surfaces (e.g., seat back, headrest, and lateral supports) were converted to plane surfaces. Three-inch-wide FE belts were generated using MADYMO-provided software and fitted as a five-point restraint system. Belt attachment points were in line with those used in the test, but more distant to accommodate retractors that were used to pre-tension the belts. At approximately 150 msec prior to the onset of the sled acceleration, the pre-tensioners were activated to apply approximately 100 N of pre-tension on each belt anchor point after the occupant "settled." Gravitational acceleration was applied. It was found that it took approximately 150 msec for the occupant to stabilize to the reaction of gravity and belt pre-tension. Since the seat was assumed to be rigid (except where padding was used), the contact characteristics supplied with the MADYMO ATD were used. The specified sled test accelerations were applied to the seat as shown in Figure 3.2-18.

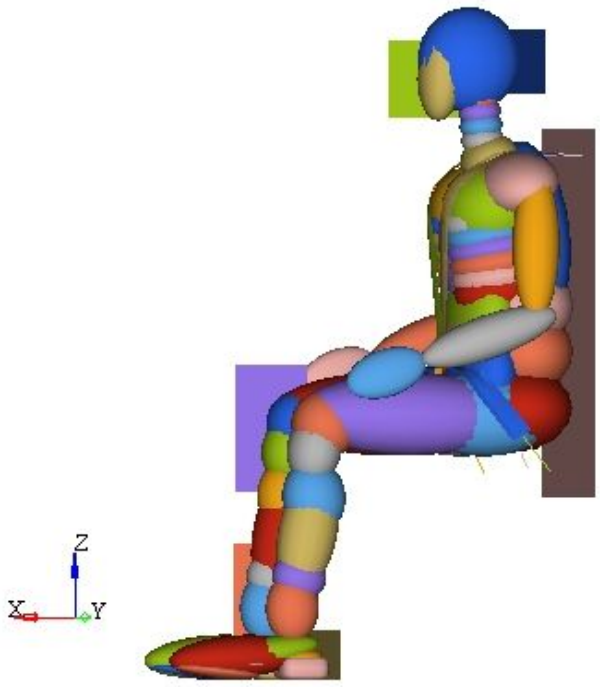

Figure 3.2-18. WPAFB Configuration

3.2.2.1.5 THUMS Model

The THUMS model was developed for use in automotive testing and has been extensively validated against PMHS data [ref. 73] primarily for automotive applications. The THUMS model results were compared to sled test results for the Hybrid III ATD to evaluate predictions from THUMS, the Hybrid III, and test data. Injury responses were extracted from the THUMS model, were examined, and are discussed in detail in Appendix E.

The FEM used in this analysis was a modified version of the THUMS version 1.61c. This model had been previously modified for NASA simulations to stabilize the model response in Z-loading configurations. The original THUMS model could not successfully be run to completion without incurring numerical problems because of elements exceeding their failure limits. To circumvent this problem, modifications were implemented, including different response curves for the pelvis flesh and lung tissue. Additionally, all element failure criteria were removed to assess loading values in all the elements for the entire simulation.

The seat configuration and material properties used were the same as the WPAFB sled test seat. This seat consisted of a rigid back with a cushioned headrest and seat bottom. A floorboard was included and the feet of the THUMS model were restrained to this component. The floorboard used with the THUMS model was translated in the X-direction to accommodate the original model knee bend. It was simpler to relocate the floorboard since the THUMS model cannot be easily articulated to arbitrary positions. It is expected that relocating the floorboard from its position would not considerably affect the results of the simulations. The WPAFB restraint system is a five-point harness configuration. Figure 3.2-19 illustrates the initial THUMS model before placement in the seat. Figure 3.2-20 and Figure 3.2-21 illustrate the WPAFB seat configurations.

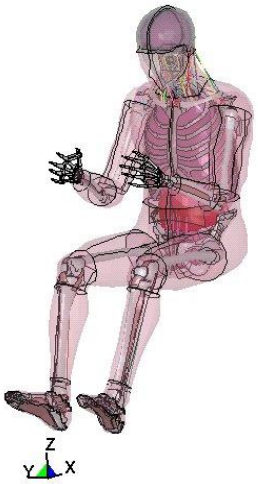

Figure 3.2-19. Isolated THUMS Model Prior to Integration with the Seat

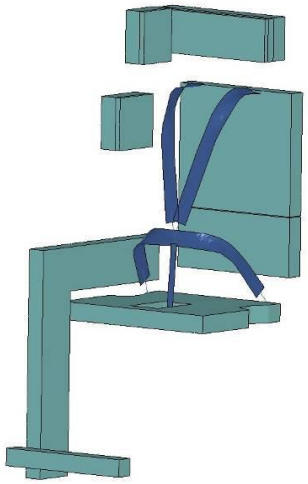

Figure 3.2-20. Seat Configuration for Lateral Loading Simulations

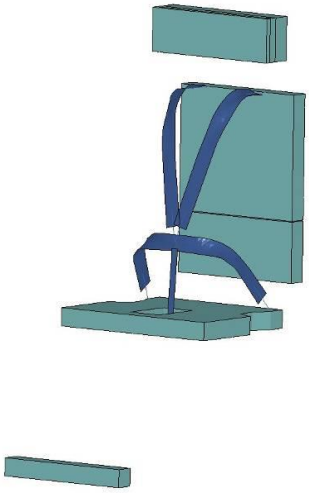

Figure 3.2-21. Seat Configuration for Anterior/posterior and Inferior/superior Loading Pulses

There were four landing scenarios modeled in the simulations with corresponding tests conducted at WPAFB. The four tests selected were 8202, 8208, 8212, and 8245 (Table 3.2-1). These tests were selected to represent loading in the frontal (8202), spinal (8208), rear (8212), and lateral (8245) directions (see Figure 3.2-22). The input for the THUMS simulations, similar to that for the FTSS, LSTC Hybrid III FEM, and MADYMO simulations was the measured acceleration of the seat. This acceleration was applied directly to the modeled seat.

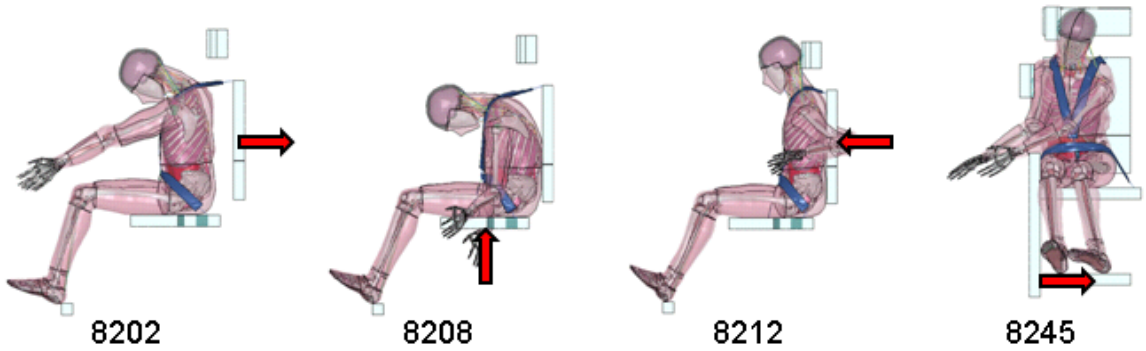

Figure 3.2-22. Illustration of Seat Directions for Each Pulse

The metrics selected to compare to the test data were the head and chest acceleration and seatbelt forces. Peak head acceleration was measured by the nodal acceleration of a single node located at the center of the head (node 8890001) as shown in Figure 3.2-23. Accelerations at this node were compared to the accelerations obtained during the WPAFB sled tests with the Hybrid III. Additionally, the belt tension and the seat acceleration were evaluated for each simulation and compared to the test data. Visual inspection of the sled test videos was used to compare the overall kinematics of the THUMS and sled results.

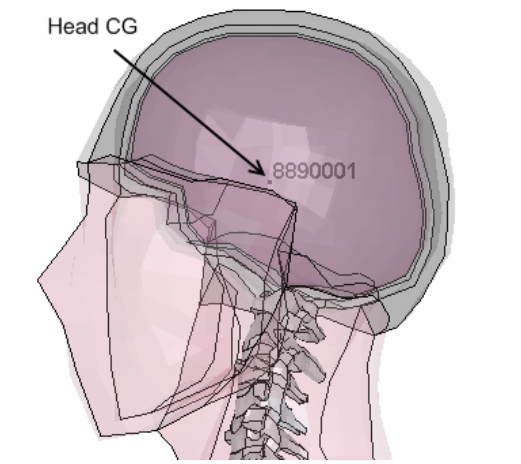

Figure 3.2-23. Location of the Node Used to Record Head Acceleration in the THUMS Model

3.2.3 Filtering Specifications

With the exception of the LSTC Hybrid III FEM ATD, all data were filtered in accordance with SAE J211/1 filtering specifications [ref. 69]. The one exception was the chest accelerations, which were filtered at channel frequency class (CFC) 1000 instead of CFC180 (see

Table 3.2-2 through

Parameter	*Filter Specification*
Head Accelerations	SAE J211/1 CFC1000
Head Velocity	SAE J211/1 CFC1000
Head Displacement	SAE J211/1 CFC1000
Chest Acceleration	SAE J211/1 CFC1000
Sternal Deflection	SAE J211/1 CFC600
Chest Displacement	SAE J211/1 CFC1000
Neck Forces	SAE J211/1 CFC1000
Neck Moments	SAE J211/1 CFC600
Lumbar Forces	SAE J211/1 CFC600
Lumbar Moments	SAE J211/1 CFC600
Pelvis Acceleration	SAE J211/1 CFC1000
Pelvis Displacement	SAE J211/1 CFC1000
Femur Forces	SAE J211/1 CFC600
Tibia Forces	SAE J211/1 CFC600
Restraint Forces	SAE J211/1 CFC60

Table 3.2-5). For the LSTC Hybrid III FEM ATD, CFC180 filters were applied to all but the leg axial and restraint forces, which were filtered using CFC60 filters per the developer's recommendations [refs. 77 and 78] (see Table 3.2-6).

Table 3.2-2. Physical ATD Filter Specifications

Parameter	***Filter Specification – SAE J211/1***		
	CFC60	***CFC600***	***CFC1000***
Head Accelerations			X
Head Velocity			X
Head Displacement			X
Chest Acceleration			X
Sternal Deflection		X	
Chest Displacement			X
Neck Forces			X
Neck Moments		X	
Lumbar Forces		X	
Lumbar Moments		X	
Pelvis Acceleration			X
Pelvis Displacement			X
Femur Forces		X	
Tibia Forces		X	
Restraint Forces	X		

Table 3.2-3. FTSS ATD Filter Specifications

Parameter	*Filter Specification*
Head Accelerations	SAE J211/1 CFC1000
Head Velocity	SAE J211/1 CFC1000
Head Displacement	SAE J211/1 CFC1000
Chest Acceleration	SAE J211/1 CFC1000
Sternal Deflection	SAE J211/1 CFC600
Chest Displacement	SAE J211/1 CFC1000
Neck Forces	SAE J211/1 CFC1000
Neck Moments	SAE J211/1 CFC600
Lumbar Forces	SAE J211/1 CFC600
Lumbar Moments	SAE J211/1 CFC600
Pelvis Acceleration	SAE J211/1 CFC1000
Pelvis Displacement	SAE J211/1 CFC1000
Femur Forces	SAE J211/1 CFC600
Tibia Forces	SAE J211/1 CFC600
Restraint Forces	SAE J211/1 CFC60

Table 3.2-4. MADYMO ATD Filter Specifications

Parameter	*Filter Specification*
Head Accelerations	SAE J211/1 CFC1000
Head Velocity	SAE J211/1 CFC1000
Head Displacement	SAE J211/1 CFC1000
Chest Acceleration	SAE J211/1 CFC1000
Sternal Deflection	SAE J211/1 CFC600
Chest Displacement	SAE J211/1 CFC1000
Neck Forces	SAE J211/1 CFC1000
Neck Moments	SAE J211/1 CFC600
Lumbar Forces	SAE J211/1 CFC600
Lumbar Moments	SAE J211/1 CFC600
Pelvis Acceleration	SAE J211/1 CFC1000
Pelvis Displacement	SAE J211/1 CFC1000
Femur Forces	SAE J211/1 CFC600
Tibia Forces	SAE J211/1 CFC600
Restraint Forces	SAE J211/1 CFC60

Table 3.2-5. THUMS Model Filter Specifications

Parameter	*Filter Specification*
Head Accelerations	SAE J211/1 CFC1000
Head Velocity	SAE J211/1 CFC1000
Head Displacement	SAE J211/1 CFC1000
Chest Acceleration	SAE J211/1 CFC1000
Sternal Deflection	SAE J211/1 CFC600
Chest Displacement	SAE J211/1 CFC1000
Neck Forces	SAE J211/1 CFC1000
Neck Moments	SAE J211/1 CFC600
Lumbar Forces	SAE J211/1 CFC600
Lumbar Moments	SAE J211/1 CFC600
Pelvis Acceleration	SAE J211/1 CFC1000
Pelvis Displacement	SAE J211/1 CFC1000
Femur Forces	SAE J211/1 CFC600
Tibia Forces	SAE J211/1 CFC600
Restraint Forces	SAE J211/1 CFC60

Table 3.2-6. LSTC Hybrid III ATD Filter Specifications

Parameter	*Filter Specification*
Head Accelerations	SAE J211/1 CFC180
Head Velocity	SAE J211/1 CFC180
Head Displacement	SAE J211/1 CFC180
Chest Acceleration	SAE J211/1 CFC180
Sternal Deflection	SAE J211/1 CFC180
Chest Displacement	SAE J211/1 CFC180
Neck Forces	SAE J211/1 CFC180
Neck Moments	SAE J211/1 CFC180
Lumbar Forces	SAE J211/1 CFC180
Lumbar Moments	SAE J211/1 CFC180
Pelvis Acceleration	SAE J211/1 CFC180
Pelvis Displacement	SAE J211/1 CFC180
Femur Forces	SAE J211/1 CFC60
Tibia Forces	SAE J211/1 CFC60
Restraint Forces	SAE J211/1 CFC60

3.2.4 Model Correlation

3.2.4.1 Error Measure for Comparing Transient Response Histories

To assess model acceptability, the Sprague-Geers (S&G) method was employed. The method assesses magnitude and phase errors and consists of three metrics. *Magnitude Error* compares the areas under the curves and peak measurements. This measure is insensitive to phase differences. *Phase Errors* are measured without being affected by magnitude effects. *Total Error* is the root sum of squares of the magnitude and phase errors. The method is biased toward the reference data. Equation 3.2-21 through Equation 3.2-26 show the application of the method.

Equation 3.2-21. S&G Total Error

$$T = \sqrt{M^2 + P^2}$$

Equation 3.2-22. S&G Magnitude Error

$$M = \sqrt{\frac{I_{gg}}{I_{ff}}} - 1$$

Equation 3.2-23. S&G Phase Error

$$P = \frac{1}{\pi} \cdot cos^{-1} \frac{I_{fg}}{\sqrt{I_{ff} \cdot I_{gg}}}$$

Equation 3.2-24. S&G I_{ff} Definition

$$I_{ff} = \frac{1}{t_2 - t_1} \int_{t_1}^{t_2} f^2(t) dt$$

Equation 3.2-25. S&G I_{gg} Definition

$$I_{gg} = \frac{1}{t_2 - t_1} \int_{t_1}^{t_2} g^2(t) dt$$

Equation 3.2-26. S&G I_{fg} Definition

$$I_{fg} = \frac{1}{t_2 - t_1}\int_{t_1}^{t_2} f(t) \cdot g(t)dt$$

Where:

f(t) is the reference data (sled test results)
g(t) is the signal being evaluated (numerical prediction of the response)
M is the magnitude error ($-1 \leq M \leq 1$)
P is the phase error ($-1 \leq P \leq 1$)
T is the total shape error ($0 \leq T \leq 1$)

This method was studied by the FAA with other model validation methods and was found to be the best at describing variations [ref. 79]. In addition, the FAA conducted a study comparing 39 test/simulation time histories. A panel of 16 subject matter experts (SMEs) evaluated the model performance and the results were compared to the S&G results. This panel found good correlation between the S&G and their results, with the recommended classifications shown in Table 3.2-7.

Table 3.2-7. S&G Classifications

SME Rating	*S&G Percent Error*
Excellent	0–4
Good	4–10
Fair	10–20
Poor	20–30
Very Poor	>30

Table 3.2-8 shows the classifications that were adopted for this study to quantify the model correlation to the sled test data. All S&G results are shown in Appendices B and C. Some responses are not valid in each impact orientation because the responses were small and any discrepancy between the model and test data shows a large S&G error, which may be erroneous.

For the discussions in subsequent sections of this report, the column titled Qualitative Description of Correlation in Table 3.2-8 were used to judge the results. The column in the table titled SME Qualitative Description lists the correlation ratings used by the FAA to measure the quality of numerical ATD predictions for commercial aircraft qualification. These ratings differ from the rating used in the present study. However, the qualitative descriptions of the correlation between test and numerical predictions were arbitrary and were selected for the present study based on reasonable expectations for the modeling predictions.

Table 3.2-8. Relation between S&G Numerical Value and Qualitative Description of Test-predication Correlation

S&G Percent Error	*Qualitative Description of Correlation*	*SMEs Qualitative Description*
0–4	Good	Excellent
4–10	Good	Good
10–20	Good	Fair
20–30	Fair	Poor
30–40	Poor	Poor

3.2.4.2 WPAFB Sled Tests

The objective of comparing the numerical models to test data was to assess the numerical model's ability to model and simulate the Hybrid III ATD. This objective was not completely straightforward since the numerical response was affected by the ATD model accuracy, and by the ATD seat, harness, and the interaction with these components. To eliminate modeling discrepancies resulting from limitations in the seat model, responses that occur as a result of the ATD impacting the seat or the padding on the seat wereignored. Although the data traces show complete transient responses, not all of the responses were used for the S&G comparison calculations, which are used to quantify the correlation between test and numerical predictions. When the data in the traces were not used for the quantitative comparisons, they were indicated by the data trace line changing from a solid to a dashed line (shown in Appendix C).

3.2.4.2.1 Front Impact

Front impact sled data were compared to the numerical models for a variety of front loading conditions. Front impact is unlike the condition expected for Orion landings since the crew is oriented to land primarily with a rearward impact. However, front impact is one of the primary conditions for automobile qualification and is the condition that the Hybrid III ATD was designed to replicate. Therefore, it was expected that the numerical models would perform best for front impact since both the models and ATD have undergone validation for this condition.

3.2.4.2.1.1 Test Cases

Six sled tests were run for front impact using the Hybrid III automotive ATD with a curved spine and an additional three tests using the Hybrid III aerospace ATD with the straight spine. All tests were run near the 10-G level except for test 8205, which was run near 20 G. The pulse duration was 70 msec unless otherwise noted in the test matrix. Test numbers 8201, 8202, and 8204 were duplicate tests to assess the repeatability of the physical sled tests and obtain data to compare the numerical models to the test data. Maximum G level and delta velocity and the seat acceleration transient profiles (Appendix C-1.1) were found to be repeatable indicating the reliability of the sled and loading generation system. For the 10-G and 20-G sled tests, the loadings were relatively mild, indicated by the low BDR (Appendix C-1.2) even for the 20-G load case where the BDR injury risk criterion was 0.64 and the allowable limit was 1.0. Since all the loadings are in a relatively low range, it is expected the ATD will not experience extreme loading conditions and the ATD and the numerical models should produce good results.

3.2.4.2.1.2 Harness Loads

The first step toward producing good numerical results is for the numerical model to constrain the ATD in the seat by having an accurate representation of the harness and how it constrains the ATD during loading. If the harness belt forces do not match what is measured in the physical sled test, then there will be a mismatch in how the ATD is constrained, making it doubtful that the internal ATD measurements will match the numerical model.

For the left shoulder belt forces (Appendix C-1.38), all of the models predict the belt force within an approximate 10-percent range, with the exceptions of the MADYMO model and the FTSS model for the 20-G case. For the 20-G case the FTSS model under-predicts the belt force by nearly 30 percent. The MADYMO model consistently predicted a left belt force that differed by nearly 30 percent. This probably indicates that the harness was not sufficiently modeled and as such, the prediction was not a deficiency in the MADYMO ATD representation. For the right shoulder belt force, all of the models reasonably predict the belt force. Considering the numerical models should

be symmetric, it is surprising the predicted right belt forces correlate while the left shoulder belt forces do not. Small out-of-place sled seat accelerations combined with the exact manner in which the left and right shoulder belts are placed in the model may be leading to larger discrepancies in the left and right belt forces than are seen in the test data where the measured left and right belt forces are closer to each other in magnitude. The measured left and right shoulder belt forces are similar for each of the three repeat tests.

None of the numerical models predicted the right or left lap belt forces reliably (Appendix C-1.36), except for the THUMS model, which was within 5 percent of the test data for the single frontal impact case where THUMS was used to generated numerical predictions. The test data were repeatable for each of the three repeat tests, and the left and right lap belt forces were similar in magnitude. With additional study of the harness and ATD positioning, the numerical models may be made to better match the test data. However, these results are indicative of the challenge of using the models for pre-test predictions when many of the specific conditions are not well known. The correlation between test and models is worse for the crotch belt force (Appendix C-1.40) where there is essentially no correlation between test and model predictions. The FTSS model does the best job of predicting the measured crotch belt force while some of the other models are off by an order of magnitude. These large discrepancies between test and predictions may be a result of the models transferring the shoulder belt loads directly into the crotch belt and transferring less of the load into the lap belts. Whereas in the tests, the crotch belt was carrying less load compared to the lap belts. The lap and shoulder belts, and the crotch belt feed into a common attachment point above the ATD crotch, creating a complex condition that was difficult to model. Major issues for Orion occupant protection are the type, configuration, and preload of the harness. Based on the present results it is questionable whether the ATD numerical models can be used to assess the differences and effectiveness of different harness configurations reliably.

3.2.4.2.1.3 Head and Neck Results

Head and neck results are important since the BDR model does not consider this region of the body, and injury criteria, such as those discussed in Section 3.1.2 are important as a supplement to the BDR to quantify the potential of injury to this region. During the initial transient response, the head X acceleration (Appendix C-1.3) follows the magnitude and shape of the driving seat acceleration. The acceleration magnitude was 10–30 G and within the allowable 100-G peak HSIR limit. Near 200 msec, the head impacts the chest leading to a sharp peak in the head acceleration. For the three repeat tests, the measured peak acceleration was around 80 G, while all of the models predicted considerably higher peak accelerations. For the 20-G sled test (8205), the peak measured acceleration appeared to be clipped and missing the peak while the predicted peak accelerations far exceeded the allowable 100-G HSIR limit. Note that the S&G calculations are performed for the response before rebound only, so they do not include the discrepancies in the large peaks. Considering the large difference between test and prediction, it might not be reliable to use the numerical models for predictors of the peak-acceleration-injury criteria. Using acceleration as injury criteria may make sense from an occupant protection perspective, but it is impossible for the models to accurately predict peak accelerations. If the desire is to use numerical models for predicting injury metrics, then it is unwise to use peak accelerations as injury predictors. For Z-axis direction acceleration (Appendix C-1.5) none of the models predict the peak acceleration or the acceleration profile leading to the peak accurately.

It is useful to compare the head translation X velocity and the acceleration. Since velocity is an integral part of acceleration, it is expected, and verified by a comparison of the results, that the

models would better correlate with velocity than acceleration (Appendix C-1.7). Before and during the head to chest impact, there was good correlation between the measured and predicted head velocity for all of the models. It is interesting to note the discrepancy between the results for the peak head acceleration and velocity injury criteria. More thought should be given to consider which of these criteria would be more useful for Orion-type applications.

The head rotational acceleration (Appendix C-1.11) and velocity (Appendix C-1.12), and the head translation X acceleration and velocity follow similar trends in terms of matching test and predictions. While it is difficult to match test and predictions for the rotational acceleration, the rotational velocity match is more consistent. It appears there is a sign difference between test and predictions, but the head is moving forward and rotating downward toward the chest during the frontal impact tests. The test data show a positive head rotation, except for test 8202, where there was an unexplained sign change in the test data.

HIC was calculated from test and predictions for HIC15 (15 msec, Appendix C-1.15) and HIC36 (36 msec, Appendix C-1.16). Although both HIC are compared, only HIC15 is used in the HSIR requirements. For HIC36, the LSTC Hybrid III and the THUMS models did a good job of predicting HIC before the head impact with the chest (only 8202 was run with THUMS). Beyond impact, all of the models predicated different HIC values from the test data. None of the models (expect for THUMS) accurately predicted HIC15, and THUMS did not predict HIC15 accurately during the impact region. While the peak X acceleration exceeded the HSIR injury criteria for most of the cases, HIC36 was within the allowable range for every case, including the 20-G sled test (8205).

For front impact, upper neck X shear force (Appendix C-1.18) and axial force (Appendix C-1.20) were compared to the test data. All of the numerical models (except the LSTC Hybrid III FEM) do a good job of predicting the neck X shear force to the point of head impact with the chest. The LSTC Hybrid III FEM follows the general trend of the neck X shear force. However, it predicts an oscillation in the neck force that is not seen in the test data or the other models. Around the time of impact, none of the models accurately predicts the shear force. All of the neck shear forces were within the HSIR allowable, including the 20-G test case. All of the models produced wide variations in the neck axial force when compared to the test data, although none produced axial forces that exceeded the HSIR limit except for the 20-G case (where all the models predicted a force exceeding the limit). Similar to the neck shear force, the LSTC Hybrid III FEM predicted a large oscillation in the neck axial force. This oscillation may be due to how the ATD model was constrained in the seat rather than to a problem with the ATD model. With additional refinement to the pre-loading and placement of the ATD in the seat, it is expected that much of this oscillation could be eliminated.

It is important to note that the models over-predicted the measured test axial neck force. This is important because neck axial forces obtained from the ATD in Orion landing conditions have exceeded the HSIR occupant injury limits for several landing conditions. The limits are more prone to be exceeded when a helmet is placed on the occupant's head due to the added weight of the helmet. Since the limits are sometimes exceeded and the models appear to be overestimating the axial neck force, it is important to examine this value and verify the predicted results with test measurements.

For upper neck flexion/extension moment (Appendix C-1.22), the MADYMO model correlates with the test data while the other models do a poor job of matching the test data. There is less of a

problem with test and model correlation during the time of impact of the head and chest since moments are dependent on rotation, which is limited once the head impacts the chest. None of the flexion/extension moments exceeds the HSIR requirement. It may be that this requirement is never or rarely exceeded since the head rotation is always limited by the chest in flexion and the seat back in extension. The neck N_{ij} is a combination of neck axial force and flexion/extension moment. Correlation between test and predictions for this injury metric is useful since this metric has potential as a valid measure of neck injuries for Orion. For all test cases, the MADYMO was within 20 percent of the test N_{ij} before head impact with the chest while the other models generated larger differences. In the region of head impact, none of the models produced reliable results.

3.2.4.2.1.4 Chest Response

Chest acceleration and displacement, and sternal displacements were predicted using the models, although only chest acceleration (and for a limited number of cases, body movement) was measured during testing. It was expected that the models would do a good job of predicting chest acceleration since the ATD is constrained to the seat with the harness and the ATD should typically follow the prescribed seat acceleration. As expected, all of the models track the chest X acceleration to the time of maximum forward excursion (Appendix C-1.26). The MADYMO model predicted the largest deviation from the test results, but was within 20 percent of the test data. The deviation can likely be attributed to modeling of the harness and not to the ATD numerical model. As mentioned previously, utilizing peak accelerations for the numerical models is unreliable since the models are unable to match peak accelerations with the measured test accelerations.

None of the models were able to predict the peak Z acceleration (Appendix C-1.28) that occurs during the time of maximum forward excursion, or the acceleration profile leading to the peak. As seen in previous results, the LSTC Hybrid III FEM predicts large oscillations about the test data, which are attributed to how the ATD is held with the harness rather than to the ATD numerical model. It could be expected that the numerical ATDs would produce a worse match for Z-axis direction response than for X-axis direction since the Hybrid III ATD is designed primarily for X-axis direction loadings.

3.2.4.2.1.5 Lumbar Response

The models did not accurately predict the lower lumbar shear X (Appendix C-1.33). The MADYMO model consistently under-predicted the shear force while the rest of the models over-predicted the force. For all of the test cases, including the 20-G case, the X shear force was below the HSIR limit. For the lower lumbar axial force, the results were somewhat scattered; sometimes the models correlated with the test data and other times they did not. In general, the lumbar axial force was below the HSIR limit as would be expected for frontal impact loadings. The lower lumbar flexion/extension moments (Appendix C-1.35) were under-predicted by the MADYMO model and over-predicted by the other models. Pelvis X-direction acceleration was not measured with the physical Hybrid III. However, all of the models predicted similar acceleration profiles for this parameter and none of the predictions exceeded the HSIR limit.

3.2.4.2.1.6 Body Movement

During the sled tests, video data were obtained for each test and targets were placed on the ATD making it possible to perform video analysis to obtain body movements, including head movement. Head movement was computed for some of the test cases and when available was compared to the predicted data. It was not practical to post-process all of the test data to the obtained body

movements. While there was large disagreement in the various models' predicted forward head movement (Appendix C-1.13), the MADYMO model consistently predicted the correct forward head movement. Chest movement in the X-direction (Appendix C-1.30) predicted by the models varied from approximately 30 to 90 mm for the FTSS model for the 10-G sled tests. For the 20-G sled test, the variation in predicted chest movement was of a similar magnitude. The physical Hybrid III ATD is capable of measuring sternal deflection. However, the ATD used for the WPAFB tests was not instrumented to record this value.

3.2.4.2.2 Rear Impact

Rear-impact sled data were compared to the numerical models for a variety of rear loading conditions. Rear impact is one of the primary impact directions expected for Orion landings. However, the Hybrid III is not normally used for rear impact testing. Since Orion loadings are combinations of loading directions and it is desirable to use a single ATD for numerical predictions and physical testing, it was desirable to assess the test versus model correlation for this direction of loading. While it is important that the numerical model replicate the physical ATD for rear impact, additional work will be necessary to determine the applicability of the injury criteria and their limits for this direction of loading. Since the ATD is pushed into the seat during rear impact, it was expected that accurate modeling of the harness would be less important and many of the device internal loads would be small since it is constrained by the seat.

3.2.4.2.2.1 Test Cases

Seven sled tests were run for rear impact using the Hybrid III automotive ATD (Appendix C-3.1). All tests were run near the 10-G level except for tests 8211 and 8212, which were run near 20 G. The pulse duration was 70 msec unless noted otherwise in the test matrix. No repeat tests were planned for rear impact. However, some of the tests had faulty data channels so the tests were repeated to obtain complete data sets. All tests were performed with the identical seat except for test 8197 where the seat headrest was moved from the Hybrid III head, leaving a 1-inch gap between the headrest and the back of the ATD head. For all other rear impact tests, the ATD head was placed against the headrest. For the 10-G sled tests, the loadings were relatively mild, indicated by the low BDR. For the 20-G test cases, the sled loading was amplified in the BDR and the peak dynamic response was close to 35 G, which is just at the limit for a low BDR score. It is interesting to note that while the sled peak acceleration was 20 G, the BDR to this 20-G input was close to 35 G.

3.2.4.2.2.2 Harness Loads

For the left and right shoulder belt forces, none of the models reliably predicts the belt forces (Appendix C-3.38 and C-3.39). During the initial segment of the ATD response, the device is pushed into the seat, the belts are relaxed, and the forces are relatively small. During this segment, a large percentage difference in belt force is less significant since the magnitudes of the belt forces are small. Once rebound of the ATD with the seat occurs and the device bounces back, the belt forces increase and the mismatch between tests and prediction is more pronounced. During this segment, the numerical models did not reliably predict the belt forces, and the test data were not symmetric. For rear impact, where the seat loadings are symmetric, it was expected that the belt forces would be symmetric. Furthermore, the numerical models were symmetric and their predicted belt forces were not as symmetric as expected. Comparing the left and shoulder belt forces for test case 8194, the measured peak left and right belt forces are 120 and 225 lbs, respectively, which is impossible for the numerical model to predict since the

models themselves are symmetric. Correlations for the lap and crotch belts are just as poor as they are for the shoulder belts. As mentioned in the results for the frontal impact cases, assessment of the harness is an important factor of occupant protection for Orion and the inability of the numerical models to predict harness lading accurately is an important deficiency of the numerical models.

3.2.4.2.2.3 Head and Neck Results

All of the models perform well for predicting the head X acceleration peaks and shape (Appendix C-3.3). It is not surprising that the models reliably predict head X acceleration for rear impact, since the ATD head is pushed into the seat headrest and the device mostly follows the seat motion, which is relatively smooth and defined by the driving sled acceleration. For the Z-direction acceleration (Appendix C-3.5), all of the models reasonably predict the acceleration. The FTSS model predicts the largest discrepancy between test data and analysis results. However, it appears that the FTSS predictions are higher frequencies and there may be justification for filtering the results at a lower frequency to provide a better match with the test data. The Z-direction acceleration, resulting from rear impact, is small for this direction so a lack of correlation is far less important than for some of the other parameters.

It is useful to examine the head translation X velocity (Appendix C-3.7) and acceleration. Since velocity is an integral part of acceleration, it is expected the models would be able to predict velocity better than acceleration. Similarly to frontal impact, all of the models were able to predict head X velocity accurately for rear impact loading. Head movement (Appendix C-3.13) was not recorded for all of the models, but in general, the models correctly predicted the head was pushed into the headrest and rebounded. As expected, there was more of a difference among the models' predictions during the rebound segment.

In general, none of the numerical models did a good job of predicting the HIC15 (Appendix C-3.16). The models did a better job of predicting the HIC36 (Appendix C-3.17), which was expected since the HIC36 was integrated over a longer period of time. The FTSS model did a good job of predicting the HIC36 for all but one case. For HIC15 and HIC36, the peak values were below the HSIR limit, which was expected since the ATD head is prevented from moving and protected by the seat headrest. As mentioned in Section 3.2.4.2.1, frontal impact, from a modeling perspective, the HIC36 may be a more useful occupant injury criterion since the models are more capable of reliably predicting the HIC36 than peak acceleration.

For rear impact, upper neck X shear force and axial force are compared to the test data (Appendix C-3.18 and C-3.20). None of the models did a good job of predicting the neck shear or the axial forces. These predictions may be a result of the Hybrid III physical ATD and the numerical model not being designed for rear impact loading. The measured maximum axial neck tension load was near 200 N for every case except 8197, where the measured peak neck tension was near 1000 N. Test case 8197 was a repeat of 8196 so it was surprising that the neck force was so large in 8197. The tensions were expected to be almost identical since they were repeat tests. The predicted neck axial forces were more in the range of 600–1000 N. It should be noted that, similarly to frontal impact, the neck axial force was always over-predicted by the numerical models. Caution must be used since the neck axial force limit in the HSIR is a criterion that is sometimes exceeded during analysis of Orion landing conditions. Since the models appear to over-predict axial neck tension, occupant injuries may be predicted when they are not occurring. Upper neck flexion/extension

moment and neck N_{ij} were not reliably predicted by the models and in general, the numerical models over-predicted the parameters.

3.2.4.2.2.4 Chest Response

Chest acceleration and displacement, and sternal displacements were predicted using the models, although only chest acceleration was measured during testing. It was expected that the models would do a good job of predicting chest acceleration, since during rear impact the ATD is pushed back into the seat and the ATD should follow the prescribed seat acceleration. As expected, all of the models track the chest X acceleration (Appendix C-3.26). None of the models, except for the THUMS model, is able to predict the Z acceleration (Appendix C-3.28) accurately. However, the magnitude of the Z acceleration is small and less significant for rear impact when compared to the X-direction of loading.

3.2.4.2.2.5 Lumbar Response

Similar to frontal impact, all of the models (except MADYMO) accurately predicted the lower lumbar shear X force (Appendix C-3.33). For all the test cases, including the 20-G case, the X shear force was below the HSIR limit. None of the models consistently predicted the lower lumbar axial force (Appendix C-3.34). The sign of the lumbar axial force is opposite between test and predicted. The test predicted tension while the models predicted compression. It is expected that during rear impact the lumbar load would be compressive. The models did not reliably predict the lower lumbar flexion/extension moments. Pelvis X-direction acceleration was not measured with the physical Hybrid III. However, all of the models predicted similar acceleration profiles for this parameter and none of the predictions exceeded the HSIR limit.

3.2.4.2.3 Spinal Impact

Spinal impact sled data were compared to the numerical models for a variety of rear loading conditions. Spinal and rear impacts (discussed in Section 3.2.4.2.2) are two of the primary impact directions expected for Orion landings. Similar to rear impact, the Hybrid III is not normally used for spinal impact testing. Since Orion landings are combinations of loading directions and it is desirable to use a single ATD for numerical predictions and physical testing, it was advantageous to assess the test versus model correlation for this direction of loading. While it is important that the numerical model replicate the physical ATD for spinal impact, additional work will be required to determine the applicability of the injury criteria and their limits for this direction of loading. The BDR has been validated for spinal impact direction loadings so any spinal direction occupant injury criteria based on the ATD behavior should be compared to BDR results.

3.2.4.2.3.1 Test Cases

Nine sled tests were run for spinal impact using the Hybrid III automotive ATD (Appendix C-4.1). Tests were run at the 10- and 20-G levels and an additional test was run at 15 G. Various pulse durations were used and are shown in Table 3.2-1. Tests 8207, 8208, and 8209 were 10-G repeat tests. For frontal and rear impact, the 10-G sled test loadings were relatively mild indicated by the low BDR. For spinal impact, the same level of loading (10 G) produced a BDR that exceeded the low level of injury (Appendix C-4.2). The reason that the BDR criterion was exceeded for spinal impact is that the model allowable for spinal direction loading was lower than the allowable for rear or front impact. This is due to the human tolerance being considerably lower in the spinal direction. For the 10-G spinal loadings, the BDR was lower for the 110-msec rise time pulse than for the 70-msec pulse since the latter pulse was closer to the BDR model resonance frequency. The 110- and 70-msec rise times correspond to 2.3- and 3.6-Hz driving frequencies,

respectively. The BDR model responds most strongly near 10 Hz so it is expected the 70-msec rise time pulses would lead to a higher BDR. The 15- and 20-G pulses produced a BDR that exceeded the low BDR limit regardless of the rise time.

3.2.4.2.3.2 Harness Loads

For the repeat tests, the left and right shoulder belt forces were repeatable and symmetric (Appendix C-4.38, C-4.39). The minimum shoulder belt tension was 250 N and the maximum is 500 N, so while the belt forces were symmetric and repeatable, there was a spread of 250 N. None of the models predicted the belt forces reliably and there was less correlation between test and models for the lap and crotch belt than for the shoulder belts.

3.2.4.2.3.3 Head and Neck Results

Unlike frontal and rear direction loadings, peak head X accelerations are less important for spinal loading. Overall, the models do an adequate job of predicting the head X accelerations and as expected the X acceleration was relatively small, since the primary loading was in the Z-direction (Appendix C-4.3). For Z-direction acceleration (Appendix C-4.5), all of the models reasonably predict the acceleration. The LSTC Hybrid III FEM did not meet the 'good' correlation for three of the nine cases and the THUMS model was 'fair' for case 8208. For all of the test cases, the measured and predicted HIC15 was small (Appendix C-4.16) and below the occupant injury criterion of 300. Since the HIC was so small, discrepancies between test and predictions are not important. For front impact, upper neck X shear force and axial force are compared to the test data (Appendix C-4.18, C-4.20). None of the models did a good job of predicting the neck X shear or axial forces. The one exception was the FTSS model, which did a good job of predicting the neck axial force for all but one of the test cases. All the models over-predicted the forces.

3.2.4.2.3.4 Chest Response

Chest Z acceleration is of primary importance for spinal direction loading (Appendix C-4.28). All of the models did a good job of predicting the chest Z acceleration. The one exception was the LSTC Hybrid III FEM, which exhibited large oscillations about the measured Z acceleration. It was expected that the models would do a good job of predicting chest Z acceleration since during spinal impact the ATD is pushed back into the seat pan and the ATD should follow the prescribed seat acceleration. As noted previously, although the models received a 'good' grade from the S&G correlation metric, there are peaks in the predicted response that do not correlate with the test data. When only the peaks were selected for the occupant injury criterion, there were larger disagreements between test results and the numerical model predictions.

3.2.4.2.3.5 Lumbar Response

None of the models consistently predicted the lumbar shear X force (Appendix C-4.33). The FTSS was good for 4 of the 9 cases, but not good for the remainder of the test cases. For all of the test cases, including the 20-G case, the test and predicted X shear forces were below the HSIR limit. While lumbar axial force is not currently an HSIR occupant protection criterion, numerous discussions have been made concerning this criterion and its use for occupant protection. The BDR criteria is thought to be a superior criteria for spinal direction loading and though the criterion does not address head and neck injuries, it does capture the effect of lumbar loadings. An important consideration for including lumbar axial forces as injury criteria is the models' ability to predict reliably and to measure this force physically during testing. It was unexplained during this assessment why the test results showed the ATD lumbar force to be positive (tension lumbar force)

in 2 of the 9 test cases when the ATD lumbar load was expected to be compressive for all nine cases. The models always predicted a compressive lumbar force. If the sign difference between test and predictions was ignored, then the MADYMO model generated a 'good' correlation for all test cases and the LSTC Hybrid III and FTSS models predictions ranged from poor to good, depending on the test case.

The models consistently over-predicted the magnitude of the lumbar force, which has been the case for most, if not all, of the model predictions for all of the parameters examined in this study. The argument could be made that since the models tend to over-predict the injury criteria the reductions are conservative and the occupant will be protected. This argument may be valid for occupant protection. However, if the over-predicting leads to the injury criterion not being met, then the occupant protection will need to be re-designed or the landing loads reduced. This situation could lead to unnecessary design changes, added vehicle weight, and compromises to other vehicle functions (e.g., egress or occupant mobility). The models did not reliably predict the lower lumbar flexion/extension moments (Appendix C-4.35). Pelvis X-direction acceleration was not measured with the physical Hybrid III. However, all of the models predicted similar acceleration profiles for this parameter and none of the predictions exceeded the HSIR limit.

3.2.4.2.3.6 Comparison of ATD Lumbar Loads to Brinkley Z-Axis Response

As part of this study, there was discussion to add the ATD lumbar axial load as injury criteria. Considerable discussion has taken place concerning the applicability of the lumbar axial load limit used for other applications outside of Orion and how this limit might be applied or modified for Orion and the loadings expected for spacecraft landings. One issue with using these criteria is that it appears that the limits used in such applications as automotive or military have different loading conditions and limits may not be easily transferrable to Orion crew loading conditions. The FAA currently uses a 1500-lb limit for commercial aircraft seat qualification. However, this limit is associated with a higher tolerance for injury than is acceptable for Orion. Data for lower injury risks are not currently available.

Another issue associated with using the ATD lumbar axial load as injury criteria is the relationship between the lumbar criteria and the results generated by the BDR in the spinal (Z-axis) loading direction. The two criteria should be consistent since they address spinal injuries. There is concern that the two criteria are not consistent. The BDR model considers the effect of the loading pulse amplitude and shape, and the dynamic response of the human in the spinal loading direction. The ATD lumbar load limits currently available were derived for specific loading conditions, and may not be applicable for other loading conditions. Resolving this issue is beyond the scope of this assessment. However, a comparison between the ATD lumbar axial force and the axial BDR is provided in the following section.

Figure 3.2-24 shows the BDR limits for the high, moderate, and low levels of injury risk for the spinal direction. These limits were derived from human testing [ref. 37] and include the effect of the human body frequency response to pulse shape. For short pulses, the human body does not have time to respond and the allowable level of acceleration is therefore high. For long-duration pulses, the tolerable acceleration level is less than for short pulses; for pulses just below 10 Hz, the tolerance level is lowest since the human body peak response is near this frequency.

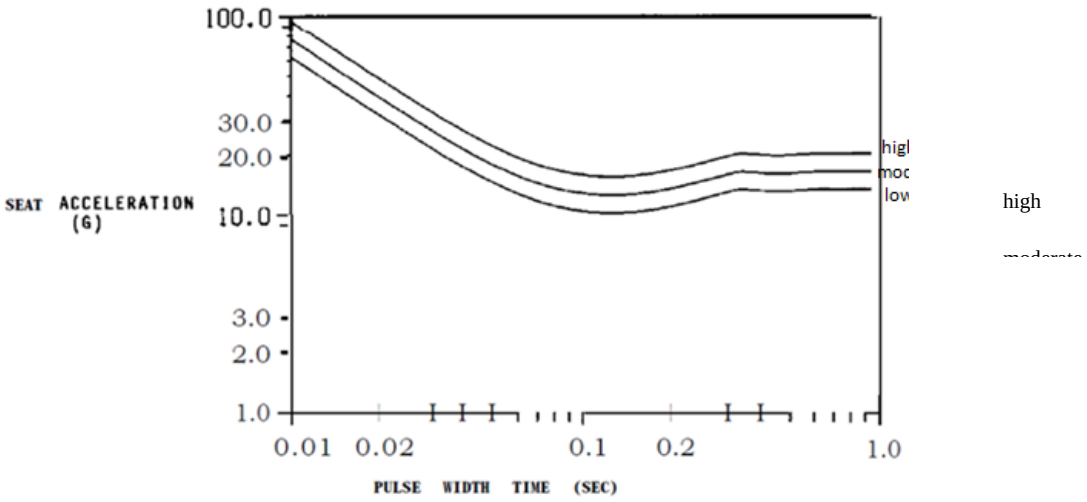

Figure 3.2-24. Limits for +Z-axis Acceleration as a Function of the Time-to-Peak Acceleration for Half-sine Acceleration Profile

Figure 3.2-25 shows a comparison between various spinal direction input pulses and resulting ATD lumbar forces. A combination of pulses that produced low (DR_z = 13.0 G) and moderate (DR_z = 15.4 G) BDR injury levels was obtained from Figure 7.2-33, and those pulses were used as input to load the Hybrid III numerical model. The lumbar force was extracted from the Hybrid III and the results were used to generate the comparison shown in Figure 7.2-34. As mentioned, the BDR model was sensitive to how the human body responds to pulse magnitude and duration while the Hybrid III ATD is thought to be less human-like in this direction and probably not a good predictor of spinal loading for a range of pulse durations. As shown in Figure 3.2-25, the peak ATD lumbar force varies depending on pulse magnitudes that generate identical BDRs. There were inconsistencies between the ATD lumbar load predictions and the BDR predicted injury levels.

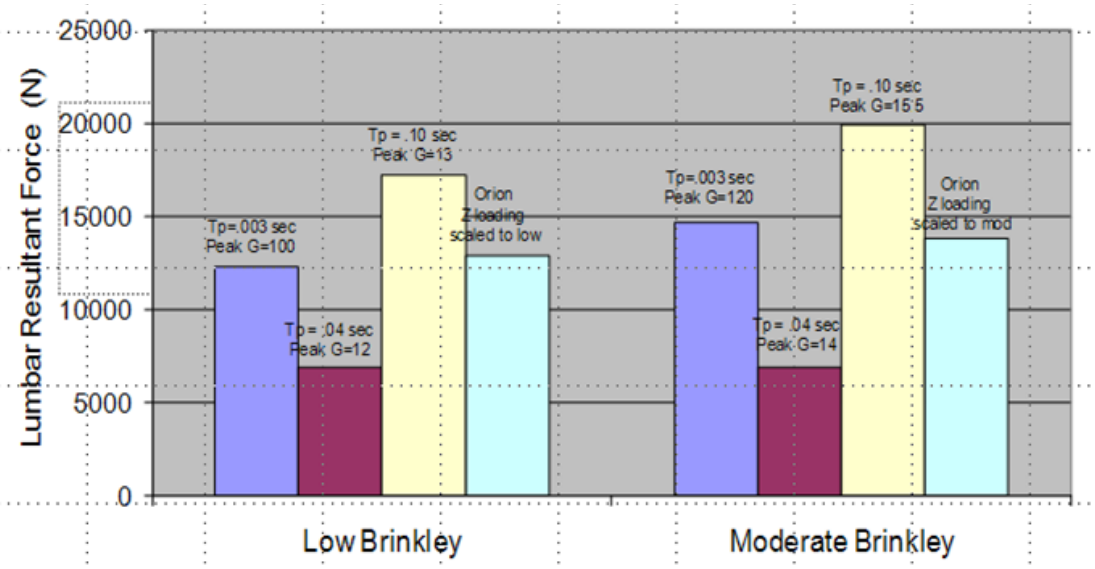

Figure 3.2-25. Comparison of +Z BDR Low and Moderate to ATD Lumbar Forces

3.2.4.2.4 Lateral Impact

Lateral impact sled data were compared to the numerical models for a variety of loading conditions. The Hybrid III is not normally used for lateral impact direction loadings so it is important to assess the numerical models' abilities to predict the ATD response in this direction. Furthermore, if the models are able to predict Hybrid III lateral response, then the applicability of the injury criterion developed for this direction loading to the Hybrid III ATD will need to be assessed. This issue is discussed in detail in Section 3.2.4.2.5 where the response of the Hybrid III is compared to the EuroSID ATD.

3.2.4.2.4.1 Test Cases

Fourteen sled tests were run for lateral impact using the Hybrid III ATD (Appendix C-2.1). For lateral testing, seat side supports were added to limit ATD lateral motion. Test 8239 was run without side supports, but there were concerns that the ATD would be damaged since it could not be constrained by the harness. A combination of 10- and 20-G load cases was run with a pulse length of 70 msec. A constant pulse length was used for the lateral testing to eliminate the time required to convert the sled-driving mechanism to the 110-msec pulse setup. Three-sided support configurations were used. A no gap configuration was used where the side supports the head, shoulder, and pelvis/leg region were placed directly against the ATD to provide full lateral support with no motion permitted between the ATD and the side supports. The second configuration was a 50-percent gap where the distance was 50 percent of the HSIR body movement requirements. The head, shoulder, and pelvis/leg side supports have difference gaps based on these body movement requirements. The final configuration tested had a gap equal to 100 percent of the HSIR body movement requirements. The ATD injury parameters derived from these tests did not provide direct insight into the effectiveness of the body movement requirements since the test loadings are different from spacecraft landing loads, but the results did provide a sense of the relationship between restricted body movement and resulting injury criterion.

Human tolerance to impact loading is far lower in the lateral direction than for the rear, frontal, and spinal directions. This lower tolerance level is seen in the BDR where the 20-G sled tests exceed the BDR low level of injury (Appendix C-2.2). A number of the 10-G impact tests exceed the low BDR limit, although the results were at the low limit. The remainders of the 10-G test cases do not exceed the BDR low level. The BDR model was obtained for a specific seat design with side supports so the results obtained were not accurate since this seat differs from the seat used to develop the BDR model. The only way to remedy this complication is to redevelop the BDR model using the same seat that was used for the test, or in the case of a space vehicle, redevelop the BDR model using the spacecraft seat.

3.2.4.2.4.2 Harness Loads

Predicting harness loads is more challenging for lateral direction impacts than for the other directions. For the other directions, the loading is essentially symmetric and the loading in the belts is primarily tensile, providing less of a challenge for the models' predictive capabilities. For side impact, the ATD belts are loaded in a complex manner and it is more difficult to predict the loads with accuracy. Additionally, for side impact, the seat side supports provide most of the lateral constraint and the harness is less important than for the other loading directions (i.e., where the harness provides the only constraint).

3.2.4.2.4.3 Head and Neck Results

For lateral impact, the head and neck do not only move in the lateral direction. Instead, the head and neck motion is complex and the total loading is a combination of loadings in all three translational and rotational directions. As a result, it is important to consider other directions in addition to the lateral direction-oriented injury criteria. It is important to note that the injury criteria used in the HSIR were derived primarily for single-direction impacts. For combined loading, it is not clear how to combine injury criteria. At this time, the HSIR requirements for head and neck load limits treat each loading direction as though they act independent from each other.

None of the models were able to predict the peak head resultant acceleration reliably (Appendix C-2.6). This result was not surprising since the ATD head impacts the side support, and for many of the test cases, it repeatedly impacts the side support causing multiple peaks in the acceleration profile. It is difficult to predict these peak-impact loads numerically, leading to the question of whether it is practical to utilize peak head resultant acceleration as an occupant injury criterion. Even though the HIC is computed from an integral of the acceleration and tends to smooth out discrepancies in peak accelerations, the HIC15 was not well predicted by the models since the discrepancies in the acceleration predictions were too large for the smoothing to have much effect on the correlations (Appendix C-2.16).

The correlation between test and predictions for the neck force in the X, Y, and Z directions ranged from "good" to "poor" for all of the models. The lateral Y force (Appendix C-2.19) was less reliable than the X-direction (Appendix C-2.18) predictions, which were expected since the ATD is not designed for loading in this direction, and the models were not expected to perform well in this direction as for frontal impact. The neck N_{ij} and the neck lateral moment (Appendix C-2.22) were not well predicted by the models.

3.2.4.2.4.4 Chest Response

All the models did a "good" to "fair" job predicting chest Y acceleration (Appendix C-2.27). There was no trend between the level of load or the distance between the ATD and side supports. It was expected that the impact resulting from the gap between the seat side supports and ATD would challenge the models' ability to predict the response accurately. However, the models generated reasonably correlated acceleration predictions.

3.2.4.2.5 EuroSID Lateral Test Results

An issue related to the above approach is that the Hybrid III is not normally used or validated for lateral impact. While Orion landings generally produce primarily rear- and spinal-direction loading, there are landing conditions (particularly when vehicle roll is prevalent) where lateral loading occurs. Furthermore, the HSIR requirements include lateral direction-related criteria that must be satisfied. The EuroSID may be used for pure lateral loading. However, Orion loading is multi-axial and the EuroSID would not be amenable for use in the above approach. To date, NASA has no procedure for separating the multi-axial landing loads into individual directions so that direction-specific dummies (the EuroSID) may be used for assessing crew injuries during landings.

The objective of the test plan was to compare the Hybrid III lateral response to the EuroSID response with particular emphasis on comparing the HSIR lateral loading criteria between the Hybrid III and EuroSID for identical seats, constraints, and loading conditions. If it is determined that the Hybrid III produces similar results to the EuroSID for lateral loading, then the Hybrid III can be used for the approach involving multi-axial landing simulations and data extraction. If the

Hybrid III does not produce similar results to the EuroSID, then the above planned approach may not work and an alternate approach will need to be developed.

During sled testing at WPAFB, additional testing was completed with the EuroSID2 for comparison to the Hybrid III lateral response (see Table 3.2-9). The EuroSID2re was tested in the same conditions as the Hybrid III with 10- and 20-G pulses, and with no gap and a 50-percent gap between the ATD and the side supports (seeTable 3.2-10). The EuroSID2 was designed specifically for side impacts and was useful to compare how the Hybrid III compares to this ATD for side impacts. Comparisons were made for head, shoulder, pelvis, thigh, and knee lateral forces. Comparisons could not be made between internal ATD forces since the EuroSID was not instrumented in the same manner as the Hybrid III. Overall, the Hybrid III and EuroSID produced similar lateral forces. Since internal forces were not compared, and it is the internal forces that are used as injury criteria, it was not possible to draw a conclusion as to whether the Hybrid III can be used in place of the EuroSID for side impacts.

Table 3.2-9. Lateral Impact Test Matrix

lateral test	Sister Test	Dummy	Impact Level,	head side plate	head plate gap	shoulder side plate	shoulder plate gap	hip/leg side plate	hip/leg plate gap
8239		HybridIII Auto	10	none	na	none	na	none	na
8240		HybridIII Auto	10	none	na	long plate-no padding	no gap	no padding	no gap
8241		HybridIII Auto	10	none	na	long plate-6x6 padding	no gap	no padding	no gap
8242		HybridIII Auto	10	with padding	no gap	long plate-tiny padding	no gap	no padding	no gap
8243		HybridIII Auto	20	with padding	no gap	long plate-tiny padding	no gap	no padding	no gap
8244		HybridIII Auto	10	with padding	50% gap (1.5 inch)	6x6 inch plate - tiny padding	50% gap (1 inch)	no padding	50% gap (.75 inch)
8245		HybridIII Auto	10	with padding	50% gap (1.5 inch)	6x6 inch plate - 6x6 padding	50% gap (1 inch)	no padding	50% gap (.75 inch)
8246		HybridIII Auto	20	with padding	50% gap (1.5 inch)	6x6 inch plate - 6x6 padding	50% gap (1 inch)	no padding	50% gap (.75 inch)
8247		HybridIII Auto	20	with padding	50% gap (1.5 inch)	6x6 inch plate - 6x6 padding	50% gap (1 inch)	no padding	50% gap (.75 inch)
8248		HybridIII Auto	10	with padding	100% gap (3 inch)	6x6 inch plate - 6x6 padding	100% gap (2 inch)	no padding	100% gap (1.5 inch)
8249		HybridIII Auto	20	with padding	100% gap (3 inch)	6x6 inch plate - 6x6 padding	100% gap (2 inch)	no padding	100% gap (1.5 inch)
8285	8242	EuroSID	10	with padding	no gap	6x6 inch plate - 6x6 padding	no gap	no padding	no gap
8286	8242	EuroSID	10	with padding	no gap	6x6 inch plate - 6x6 padding	no gap	no padding	no gap
8287	none	EuroSID	10	with padding	0.5 inch	6x6 inch plate - 6x6 padding	0.5 inch	no padding	0.5 inch
8288	none	EuroSID	10	with padding	0.5 inch	6x6 inch plate - 6x6 padding	0.5 inch	no padding	0.5 inch
8289	8244, 8245	EuroSID	10	with padding	50% gap (1.5 inch)	6x6 inch plate - tiny padding	50% gap (1 inch)	no padding	50% gap (.75 inch)
8290	8244, 8245	EuroSID	10	with padding	50% gap (1.5 inch)	6x6 inch plate - tiny padding	50% gap (1 inch)	no padding	50% gap (.75 inch)
8291*	8243	EuroSID	20	with padding	no gap	6x6 inch plate - 6x6 padding	no gap	no padding	no gap
8292	8243	EuroSID	20	with padding	no gap	6x6 inch plate - 6x6 padding	no gap	no padding	no gap
8293	8246, 8247	EuroSID	20	with padding	50% gap (1.5 inch)	6x6 inch plate - tiny padding	50% gap (1 inch)	no padding	50% gap (.75 inch)
8294	8242 repeat	HybridIII Auto	10	with padding	no gap	6x6 inch plate - 6x6 padding	no gap	no padding	no gap
8295	8244, 8245 repeat	HybridIII Auto	10	with padding	50% gap (1.5 inch)	6x6 inch plate - tiny padding	50% gap (1 inch)	no padding	50% gap (.75 inch)
8296	8243	HybridIII Auto	20	with padding	no gap	6x6 inch plate - 6x6 padding	no gap	no padding	no gap

Table 3.2-10. EuroSID Testing Matrix

G Level	Sled Y	Gap (percent)	DR_y	Case	ATD
10	10.7	0	14.4	8285	EuroSID2re
10	10.3	0	14.3	8286	EuroSID2re
10	10.8	17	14.2	8287	EuroSID2re
10	10.5	17	14.2	8288	EuroSID2re
10	11.6	50	14.3	8289	EuroSID2re
10	12.1	50	14.3	8290	EuroSID2re
20	20.6	0	31.2	8291	EuroSID2re
20	21.3	0	31.8	8292	EuroSID2re
20	23.1	50	31.5	8293	EuroSID2re
10	10.8	0	14.8	8242	Hybrid III
10	10.5	0	14.2	8294	Hybrid III
10	11.5	50	14.9	8244	Hybrid III
10	11.7	50	14.8	8245	Hybrid III
10	11.2	50	14.3	8295	Hybrid III
10	13.5	100	15.0	8248	Hybrid III
20	22.0	0	32.6	8243	Hybrid III
20	21.9	0	31.9	8296	Hybrid III
20	22.9	50	32.6	8246	Hybrid III
20	23.7	50	32.3	8247	Hybrid III
20	27.0	100	32.2	8249	Hybrid III

3.2.4.2.5.1 Headrest Lateral Force

During testing, the ATD head impacts the headrest with different magnitudes. Figure 3.2-26 shows the relationship of head lateral forces between the EuroSID and Hybrid III dummies.

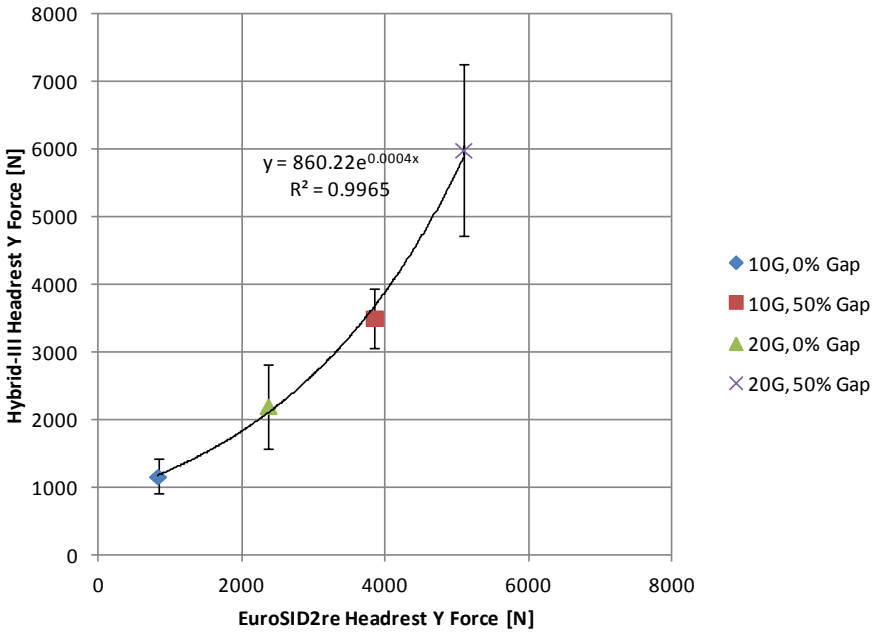

Figure 3.2-26. EuroSID/Hybrid III Headrest Lateral Force Comparison

3.2.4.2.5.2 Shoulder Lateral Force

Figure 3.2-27 shows the relationship of shoulder lateral forces between the EuroSID and Hybrid III dummies.

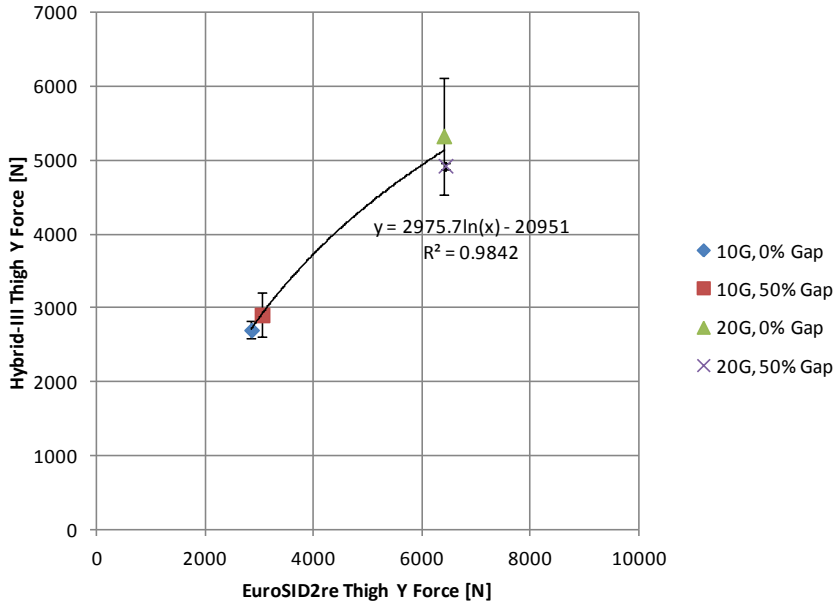

Figure 3.2-27. EuroSID/Hybrid III Shoulder Support Lateral Force Comparison

3.2.4.2.5.3 Pelvis Lateral Force

Figure 3.2-28 shows the relationship of pelvis lateral forces between the EuroSID and Hybrid III dummies.

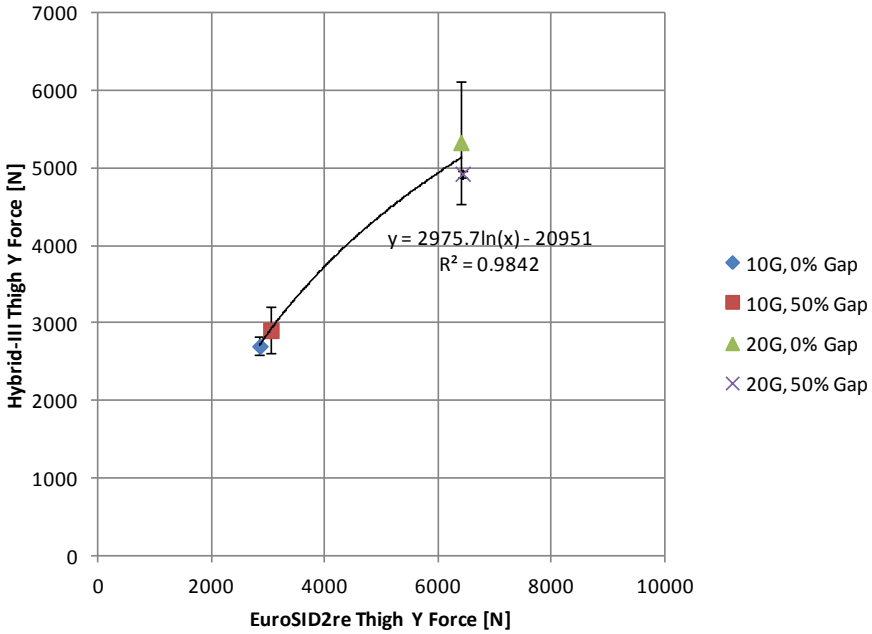

Figure 3.2-28. EuroSID/Hybrid III Pelvis Support Lateral Force Comparison

3.2.4.2.5.4 Thigh Lateral Force

Figure 3.2-29 shows the relationship of thigh lateral forces between the EuroSID and Hybrid III dummies.

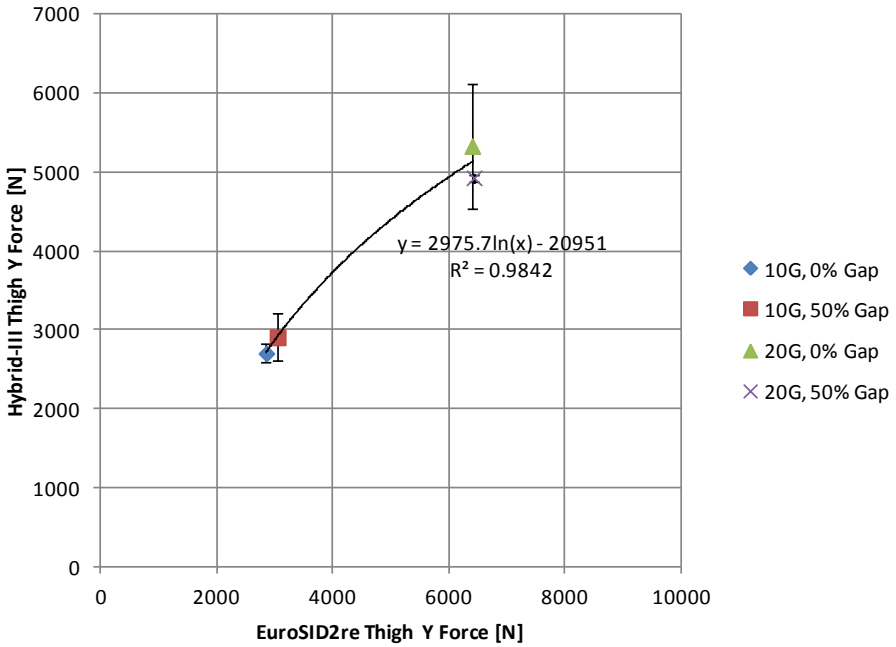

Figure 3.2-29. EuroSID/Hybrid III Thigh Support Lateral Force Comparison

3.2.4.2.5.5 Knee Lateral Force

Figure 3.2-30 shows the relationship of knee lateral forces between the EuroSID and Hybrid III dummies.

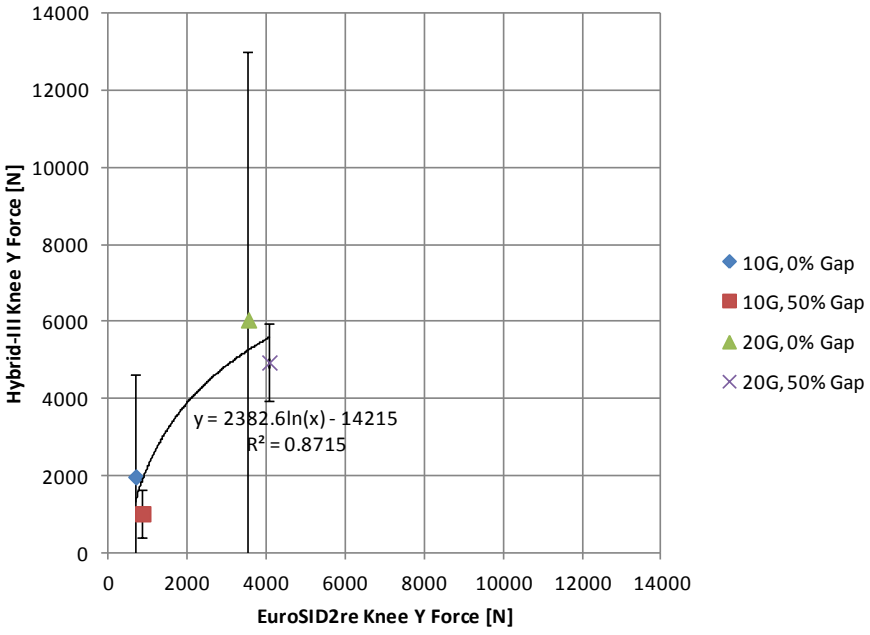

Figure 3.2-30. EuroSID/Hybrid III Knee Support Lateral Force Comparison

3.2.5 Conclusions and Recommendations

The sled test data collected in the AFRL HIA facility provides one of the most extensive databases for the Hybrid III ATD, including data for frontal, rearward, spinal, and lateral loading conditions. Detailed transient response data are provided in Appendix C. Appendix B provides a summary of the Sprague and Geers analysis obtained from the transient results, and Appendix D provides a comparison between the measured and predicted injury metrics. These data were used to assess four numerical models and their abilities to predict the ATD response for the four loading directions:

- LSTC Hybrid III
- FTSS Hybrid III
- MADYMO Hybrid III
- THUMS model

In general, none of the four numerical models generated results that correlated with the measured test data to within the desired 20-percent S&G magnitude criteria for the selected ATD response criteria, including the specific injury criteria specified in the HSIR document. This result is concerning since the assessment team would like to use numerical models to replace physical testing, especially for many of the vehicle-landing conditions where physical testing is not possible.

Overall, the FTSS Hybrid III model performed the best among the four numerical models, exhibiting the least deviation between numerical prediction and test results. This result was expected since the FTSS model has the longest development history and a long record of successful use for a wide variety of applications in the aerospace and automotive industries. The MADYMO model had less modeling capabilities than the FTSS and LSTC Hybrid III models since these models are FE-based, while the MADYMO ATD model consists of rigid links and the remainder of the structure was modeled with simple contact. The LSTC Hybrid III FEM is undergoing validation and improvements. The THUMS model is designed to replicate the human body and is not intended to directly replicate the Hybrid III ATD.

There are several possible causes of the lack of correlation between the models and the test data. First, there is test data variability. The repeat tests show this variability, and it is particularly evident for test cases where the results were expected to be symmetric and the test data were non-symmetric. This non-symmetry is the result of operational test conditions, such as response's sensitivity to initial conditions (e.g., ATD, belt positioning, and the nature of the test event).

The second cause of limited correlation is in the numerical models. While all of the models have been validated for specific loading conditions, the validation tests tend to be specific to ATD body regions (e.g., isolated ATD pendulum head drop to validate the head model) and do not capture the full interactions of the entire ATD in a realistic seated environment. The present tests are more complicated than the ATD validation tests so more discrepancies are expected with the computed response. Furthermore, the ATD numerical model was placed in a seat with a harness, adding additional uncertainties and challenges to the modeling effort.

Finally, there is the expertise of the individual modelers. For this study, independent modelers were used for each of the ATD numerical models. All of the modelers had extensive experience with ATD numerical modeling and come from industry and academic backgrounds. Even with this

expertise, it was apparent a significant cause of the difference between test and predictions was from the approach and techniques used by the modelers. While each modeler used identical sled-driving accelerations obtained from the test data, each modeler made their own assumptions in terms of ATD positioning, harness and seat characterizations, and preloads. All of these factors have been found to affect the ATD numerical response and are a cause of discrepancy between test and predictions.

For the present testing, the modelers had an opportunity to refine their models based on reviewing the test data and ATD response. Pre-test predictions before the models were refined and did not correlate with the test data. As a result, in situations where the models are to be used as a purely predictive tool, test data will not be available, which will lead to more uncertainty in the numerical predictions. The FAA requires numerical ATD models that will be used in place of testing to be validated for a physical environment (e.g., seat, constraints) and loading conditions similar to the test conditions that the model is to replace.

Before a numerical model is used to perform a final assessment of occupant injury, it is recommended that it be validated through physical testing. This testing should be conducted in a similar physical environment, including similar or identical seat, harness, helmet, and suit, and additional physical hardware components that interact with the occupant. Testing should be performed with various size ATDs. In addition, loading conditions for these physical modeling validation tests should be similar to the loading conditions that will ultimately be used for the occupant protection assessments.

3.3 BDR Model Refinements Summary

3.3.1 Introduction and Background

The primary objectives of this research effort were:

1. To develop biomechanical models to simulate the dynamic inertial response of the human body to Y-axis impact. These models were intended for the design and analysis of the performance of the Orion crew seat landing impact attenuation system. The dynamic models describe the whole body response and the distribution of forces to the side body support structures of the crew seat, especially the shoulder and hip supports.
2. To improve a biomechanical model(s) to evaluate the safety of the Orion crew seat occupants with restraint harnesses and seats with side body supports. The model is intended to provide insights regarding the causes of injuries to the seat occupant's shoulder that have been observed during high-speed racecar sideward impact. The model was intended to update the BDR model and exposure limits for Y-axis.

The first objective to simulate the dynamic inertial response of the human body to Y-axis impact was developed as a result of difficulties observed in simulations of the performance of the Orion impact attenuation system. The simulation included FEMs of the impact attenuators, seat support pallet, crew seats, and rigid masses representing the seat occupants. The CM impact caused the simulated assembly to resonate at high frequency with no evidence of significant damping. Furthermore, the impact attenuator stroke limit was exceeded at the extreme landing conditions.

The second objective was to develop a dynamic response model (DR_y) based upon sideward tests with volunteer subjects, where rigid side panels supported the subjects. The original DR_y natural frequency and damping coefficient were estimated on the basis of sideward impact tests where several frequencies were extracted using measurements of whole body force and impact velocity and an impedance computational method [ref. 21]. The natural frequency and damping coefficient

ratio was determined from tests without rigid side supports. The study described was intended to improve the BDR in the lateral, Y-direction by using data from an existing experimental study. While not simulating the side supports provided by the Orion crew seat, the data could be used to more accurately define the whole body, upper body, and lower body dynamic responses.

Based on prior experience with simulations of impact attenuator performance, a study was initiated to meet the first objective using data from impact tests with volunteers to develop simple lumped-parameter models of human impact inertial response to evaluate their influence on these simulations.

To evaluate the feasibility of developing such a model, Abbott [ref. 80] selected data from impact tests of several mid-size subjects from AFRL's Collaborative Biomechanics Data Network and evaluated the dynamic responses of the subjects using several linear analysis techniques, including a frequency domain transfer function analysis to identify the primary whole body natural frequency and associated damping coefficient ratio. From these analytical efforts (Figure 3.3-1), Abbott was able to develop simple models to represent the human body response for the +X-and +Z-axes. Figure 3.3-1 illustrates the results of Abbott's transfer function analysis of forces and accelerations measured during a +Z-axis impact testing. The model Abbott developed to duplicate the impedance computed from the tests data consisted of two masses connected by a spring and damper. Abbott's initial efforts to use the models demonstrated that the models eliminated the high-frequency ringing encountered in earlier simulations and demonstrated a potential to reduce impact attenuator stroke distance.

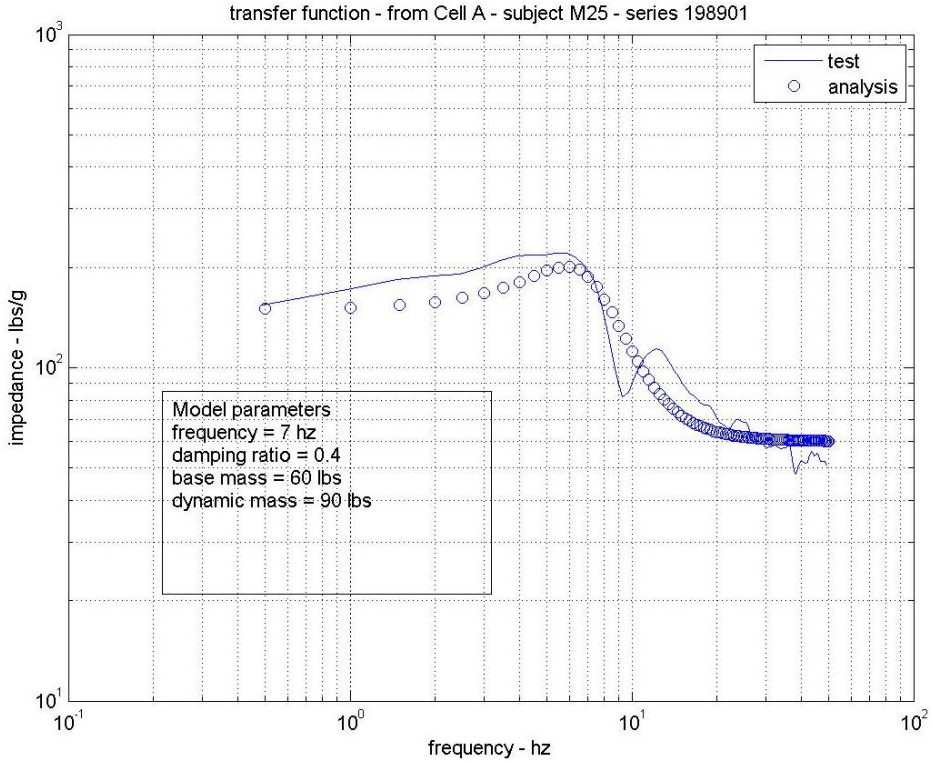

Figure 3.3-1. The Impedance Properties of a Volunteer Subject as a Function of Frequency

Using a similar frequency domain method to compute the transmissibility between the measurement of acceleration at the seat and the forces that were exerted by the subject as a result of the impact, existing data from Y-axis impact tests were analyzed to address the identified

objectives. Because of injuries to the shoulder complex observed as a result of NASCAR racecar sideward impacts, the effort was directed toward the establishment of a model that would be more representative of the forces acting through the test subject's shoulder. The injuries incurred were clavicular fractures and dislocations and a fracture of a driver's scapula. Although adverse cardiovascular responses had been identified as a potential injury mode in earlier experiments during the Apollo Program, these responses had been considered to be of no more than moderate risk and more recently have been proven to be minimized by preconditioning the crew prior to reentry [ref. 81]. Fracture or dislocation of the clavicle would prevent the crew from exiting the semi-supine crew seat and its restraint and disconnecting the pressure suit from the life support system without assistance. Medical attention would be required.

A significant number of concussions were noted during the analysis of the NASCAR racing accidents. Some of these accidents might only have resulted in stunning and a short period of disorientation, while other cases caused loss of consciousness (LOC). The injury predominately occurred during accidents where the highest impact occurred in the sideward direction. Only one concussion occurred from a rearward impact. This finding is consistent with clinical and experimental observations that sideward impact causes traumatic brain injury at lower impact levels than anterior-to-posterior or posterior-to-anterior impacts [ref. 82].

Current practice in the automotive industry is to use the HIC to evaluate the likelihood of head injury. Unfortunately, the HIC is intended to evaluate the skull fracture risk [ref. 83]. Although concussion may occur with skull fracture, the threshold for concussion is lower than the HIC would predict. Newman, Shewchenko, and Welbourne [ref. 84] used a laboratory-based reconstruction of football-helmeted head impacts using Hybrid III ATDs. The primary focus was to re-enact head-to-head collisions analyzed from game videos. The data were divided into injured and non-injured players. The HIC15 function for 24 cases of mild traumatic brain injury cases was computed using the resultant acceleration of the ATD head where the injury set was dominated by sideward head impacts. The corresponding injury risk curve, computed using a logistic regression, is shown in Figure 3.3-2.

The consideration of two modes of injury, concussion and injury of the shoulder complex, presents an issue that can be addressed using the BDR criteria. However, it is unknown if the BDR acceleration injury risk curves for the two injury modes will overlap. This issue could not be adequately addressed due to the cancellation of CxP and the Task 1 activities.

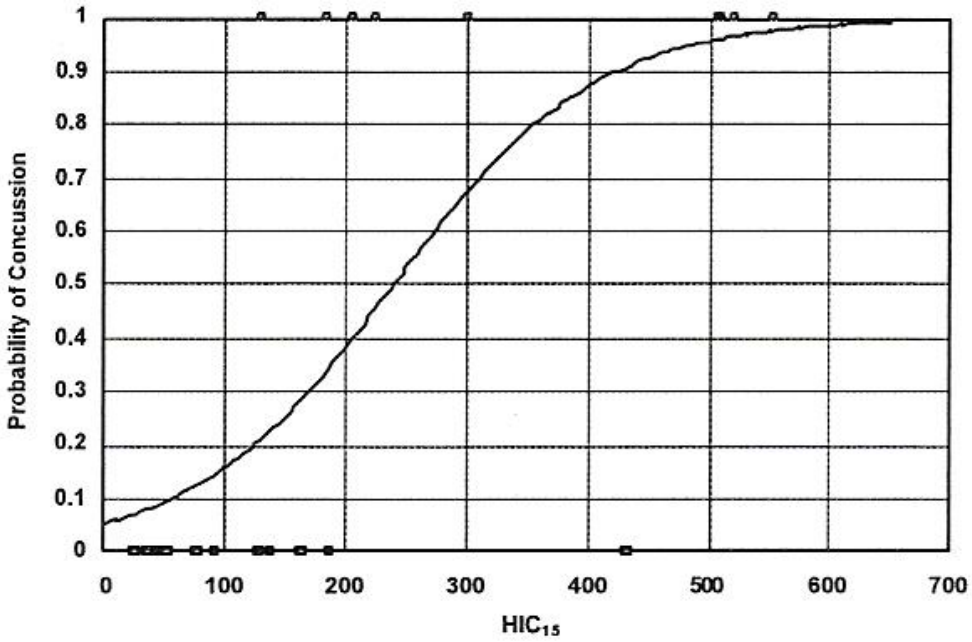

Figure 3.3-2. Probability of Concussion Based on the HIC

3.3.2 Methods

The impact test data that were used in the analysis were collected using a horizontal impact facility located within AFRL (Shaffer, August 1976) [ref. 85]. The tests were conducted to meet the joint research objectives of the USAF and the NHTSA that included:

- Comparison of ATD impact responses to test subjects.
- Measurement of the linear and angular motions of the head and neck using a head mounted nine-accelerometer array.
- Measurement of the supporting panel sideward impact forces exerted by the test subjects.

The tests were conducted at 3, 4.5, and 6 G; impact velocities were 8.6, 11.7, and 14 ft/sec; and pulse durations were 133, 118, and 110 msec, respectively. An example 6-G acceleration-time history is shown in Figure 3.3-3.

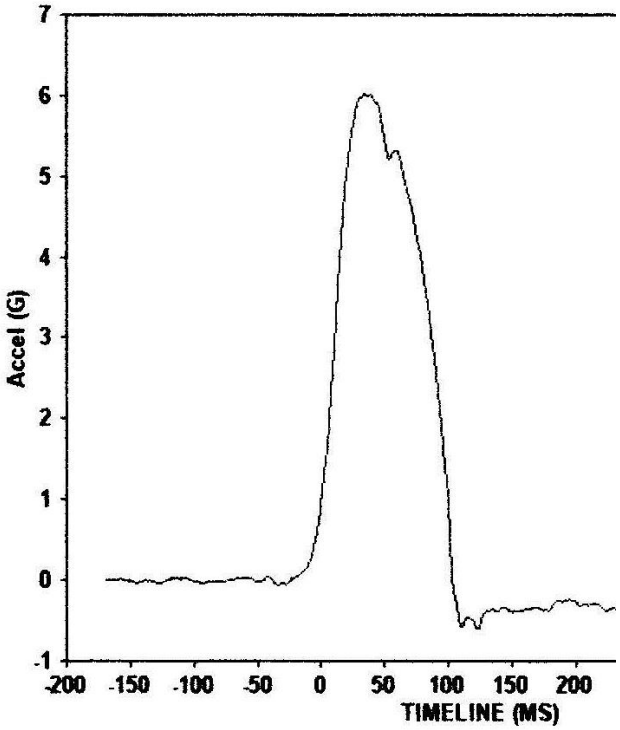

Figure 3.3-3. The Acceleration-time History at the 6-G Impact Level

Volunteer subjects were military officers and airmen. The subjects included 13 males and one female. Each subject was given a physical that included a radiographic examination of the cervical spine. Informed consent of all volunteers was obtained in accordance with USAF Regulation 169-3 [ref. 86].

A special-purpose test apparatus was designed to support and restrain the subject's body and extremities. Extra emphasis was given to ensuring that the frequency response of the test apparatus structure was above the anticipated measurements of the dummies and volunteer subjects. Impact tests were conducted to evaluate the structural adequacy of the test apparatus and to measure its frequency responses. The frequencies of the observed structural responses were 200 Hz or higher.

The body support and restraint system of the apparatus is shown in Figure 3.3-4 and Figure 3.3-5. Two instrumented side support panels were used. One supported the subject's upper body and extremities and the second supported the subject's lower body and legs. The dividing point between the two supports was at the iliac crest of the subject's pelvis to approximate the location of the test subject's center of gravity. Three Strainsert™ FLU1-25G force cells supported each panel. The upper body support panel force cells were positioned to support the shoulder, elbow, and wrist. The lower body force cells were positioned to support the hip, knee, and ankle. It is important to note that there was no gap between the subject and either of the side supports. This feature is important since the resulting injury criteria were based on test data collected for a configuration without gaps between the subject and side supports. For configurations with gaps, the resulting injury criteria will most likely be different.

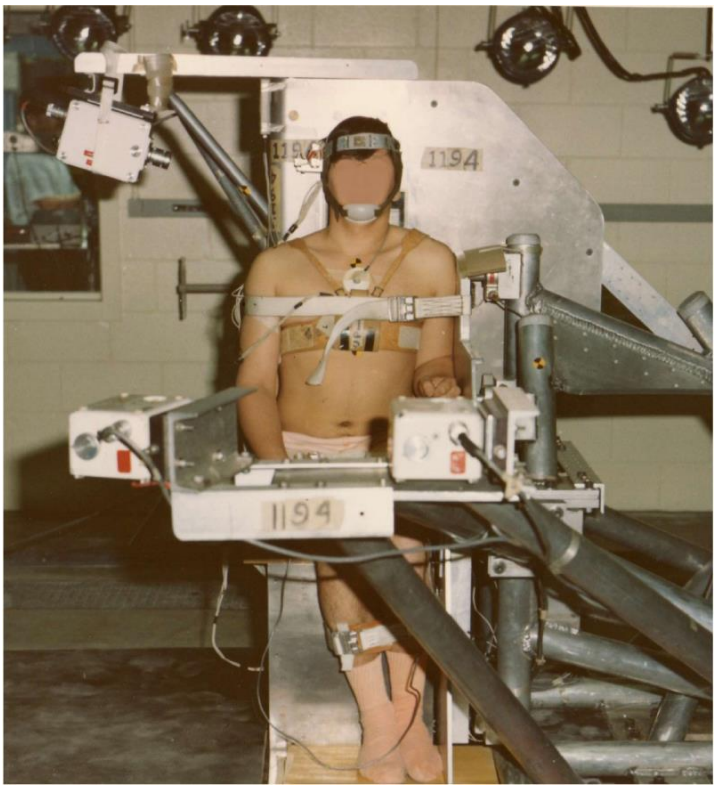

Figure 3.3-4. Sideward Impact Test Apparatus with Volunteer Subject

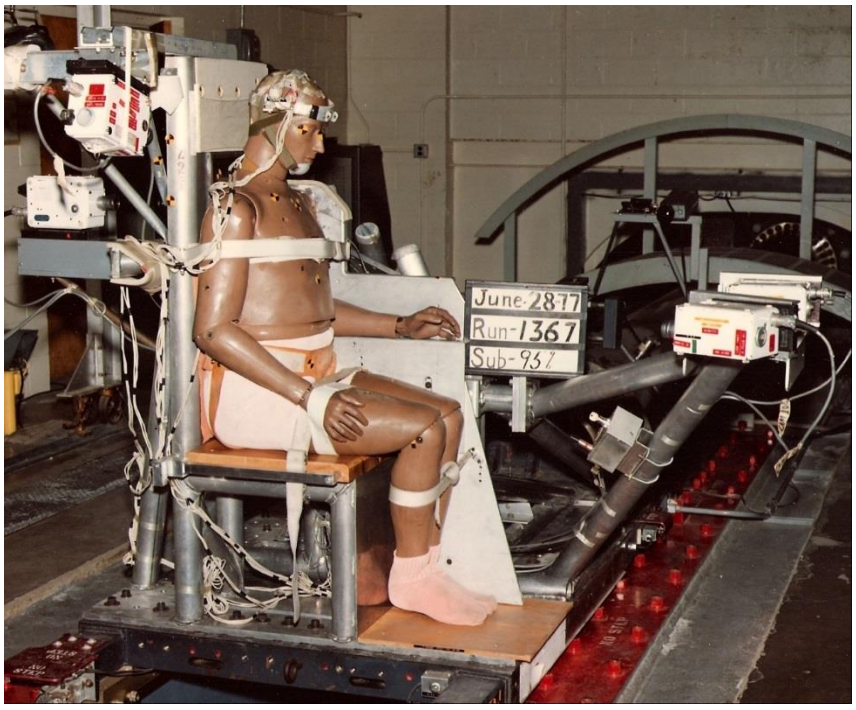

Figure 3.3-5. Side View of the Test Apparatus with a 95th-percentile ATD Subject

The force cells were located within a seat coordinate system. The origin (0) of this system was located at the intersection of the seat pan and seat back and centered at the seat back, sometimes referred to as the seat reference point. The force cell X-Z plane locations are defined in

Figure 3.3-6. The upper body panel was located 13.63 inches from the origin and the lower body panel was located 10.63 inches from the origin on the Y-axis.

The weight of the upper panel acting on the force cells was determined to be 6.6 lbs. The weight of the lower panel acting on the force cells was 16.8 lbs. During data processing, the force cell measurements were corrected for the tare weight of the panels.

The force and acceleration measurements were filtered using SAE class 60 filters with a 120-Hz corner frequency.

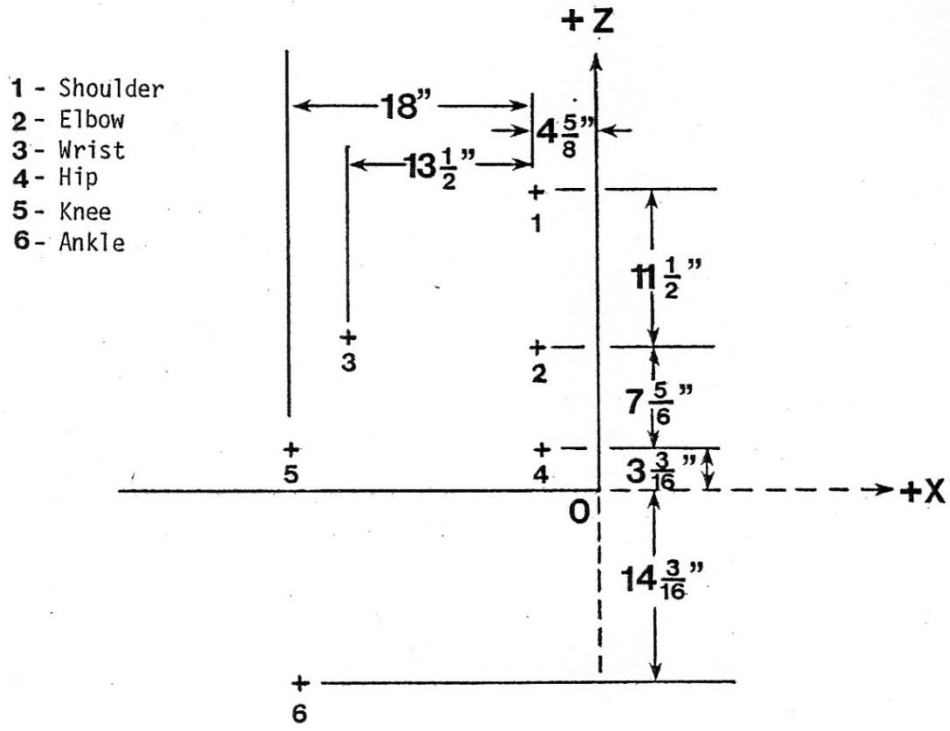

Figure 3.3-6. Positions of the Centers of the Force Cells are Defined with Respect to the Coordinate System Origin

Multiple tests were conducted using rigid 50-lb weights mounted to the upper and lower panels to evaluate the adequacy of the force-measuring system. The variance between the measured force cell outputs under acceleration was less than 0.5 lbf or 1 percent.

Triaxial linear acceleration and velocity of the impact sled were measured. Triaxial accelerometers were chest mounted. In some cases, the chest accelerations were not found to be reliable due to inadequate mounting and these accelerations were not used for analysis.

The first of the test program's original objectives was accomplished using a nine-accelerometer array attached to the test subject's and ATD's heads.

Data from 72 tests with volunteers were reprocessed from the original data files to use the tare-corrected upper body Y-axis forces, lower body Y-axis forces, and total body Y-axis forces.

Photometric reference targets were 1-inch-diameter quadrant-style targets mounted on the test subjects and the test apparatus. Four high-speed motion picture cameras mounted on the test apparatus and one on the side of the track recorded the movements of the subjects and the targets. The motion picture films were converted to video recordings. The application Visual Fusion™

was used to automatically track the positions of selected targets as a function of time. The positions of the targets were determined to be accurate to within 0.2 inches. In a few cases where the target contrast was not always adequate due to overexposure of the film or where the image of the target was momentarily lost, operator intervention was required.

Since they were of specific interest to this study, the displacement of the targets mounted over the manubrium and xiphoid processes of each subject was tracked as a function of time. Due to overexposure of the photographic images during the majority of the tests at 3 G and 4.5 G, these data were inadequate for analysis.

The targets mounted over the manubrium and video targets for 44 6-G tests, 5 4.5-G tests, and 1 3-G test were tracked to determine the maximum Y-axis manubrium displacement. The target over the manubrium was sometimes overexposed or in the shadow of the head and neck, which made it difficult to track it automatically in some cases. The anthropometric chest breadth measurement was used as the scaling factor for converting the video pixel to dimensional displacement. There was some variation is the computed scaling factors for each test so an average scaling factor was computed based on all of the 6-G tests. The maximum neck displacements from all of the tests were plotted as a function of the sled acceleration level.

Preliminary analysis was done using data from tests numbers 1194 and 1195 to determine the method to define model parameters to simulate the force-time histories measured by the force cells mounted to the two sideward support panels. The time domain and frequency domain methods were evaluated.

The impedance magnitude, impedance phase, and transmissibility magnitude were computed using the upper, lower, and total body Y-axis forces and the velocity as a function of time [ref. 87]. The natural frequency and damping ratio of the physical responses were calculated using the impedance analysis results.

The natural frequency and damping ratio of the upper body force, lower body force, total body forces, chest acceleration, and head acceleration were calculated for the two tests using a time domain approach. The LoadLsq computer program was used to conduct this analysis. The LoadLsq program uses a technique described by [ref. 88]. In this case, the program computed the natural frequency and damping coefficient ratio of a lumped parameter model that best fits the measured data by minimizing the least squared difference between impact parameters that are computed from the forces and the same parameters computed from the model. The four impact parameters used are the peak force level, impact start time, start time plus rise time, and end time. The program has the option to filter the data before finding the results. The natural frequency and damping coefficient ratio of the upper body, lower body, and whole body were computed for all 72 tests. A 50-Hz low pass filter was used except in a few cases where the signal was too irregular to obtain a good fit. In those cases, a 30-Hz low pass filter was used. Scatter plots with trend lines were created for the hip and shoulder forces as a function of the impact acceleration and the subject's weight, and for the hip and shoulder forces normalized by subject weight as a function of impact acceleration.

After a number of tests had been processed, it was determined that the time domain method was analyzing shoulder impact responses that were a composite of two frequencies; one of about 4 Hz and the other about 9.5 Hz. Analysis of the measured head accelerations indicated that the head and neck response was responsible for the lower frequency response and the shoulder complex was more likely to be the source of the higher frequency response. Additional

confirmation was obtained by study of the measured acceleration of the subject's chest. The analysis revealed that the response of the chest reflected a natural frequency of approximately 7 Hz. Therefore, the frequency domain method was selected since it was capable of defining the defining the amplitude of the responses at each frequency, and most importantly, identifying the model parameters for the model of the shoulder response.

3.3.3 Results

Figure 3.3-7 shows typical upper body forces and sled acceleration measured during the tests at the 6-G level. Note that the forces measured at the shoulder are dominant. The same relationship was observed in the measurements of the lower body forces. The forces measured at the subject's hip were larger than the forces measured at the knee and foot.

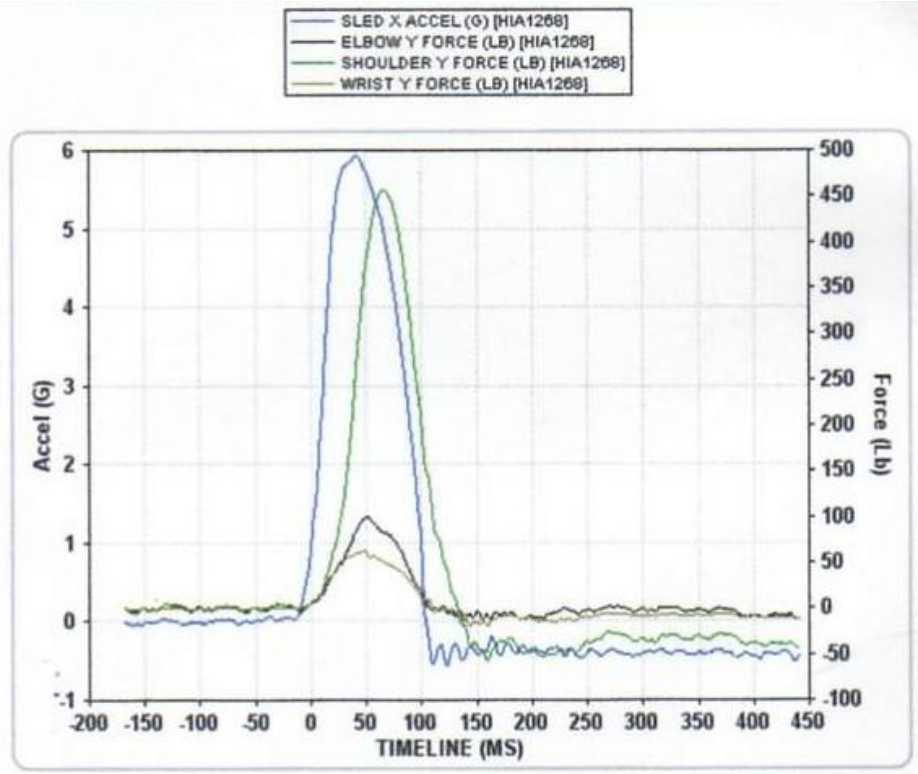

Figure 3.3-7. Sled Acceleration and Forces Measured by the Upper Body Support Panel

Scatter plots with trend lines were created for the hip and shoulder force as a function of impact acceleration and the subject weight, and for the hip and shoulder forces normalized by subject weight as a function of the impact acceleration. These plots are provided in Figure 3.3-8 and Figure 3.3-9.

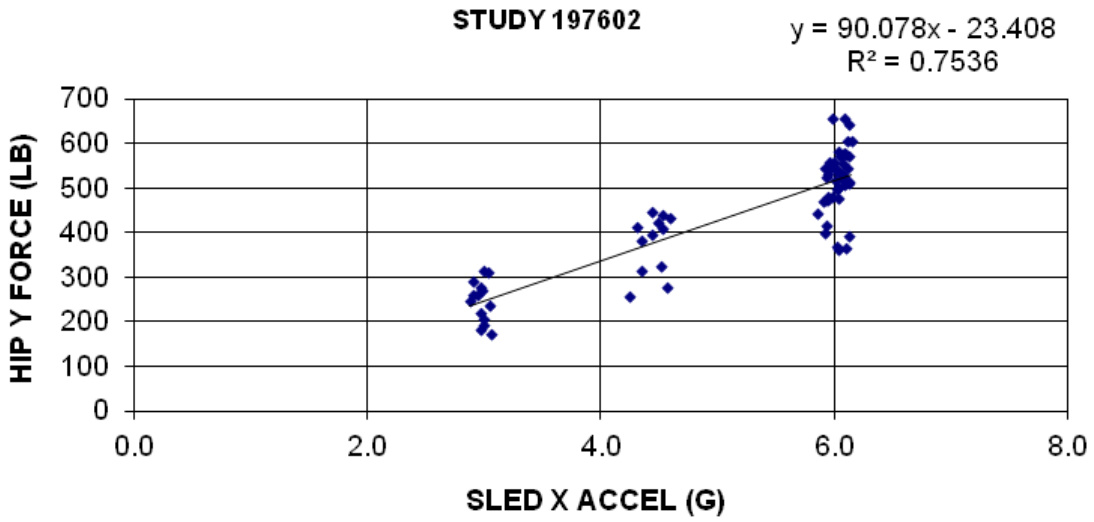

Figure 3.3-8. Y-Axis Force Measured at Each Subject's Hip as a Function of Sled Acceleration

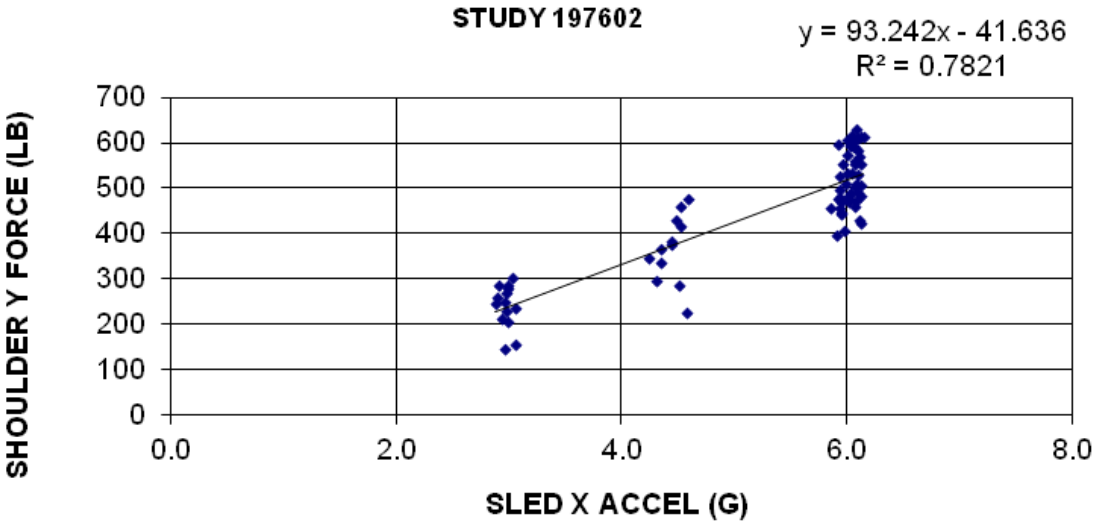

Figure 3.3-9. Y-Axis Force at Each Subject's Shoulder for Each Sled Acceleration Condition

Figure 3.3-10 shows the displacement of each subject's manubrium in the Y-axis. Unfortunately, due to over exposure of the motion picture films at most of the lower impact levels, these data were not available. The trend line that has been calculated is misleading. Its slope should lead to zero Y-axis displacement. At the 6-G level, the mean displacement of the manubrium was 2.36 inches (60.7 mm), standard deviation (std dev) = 0.37 inch (9.40 mm).

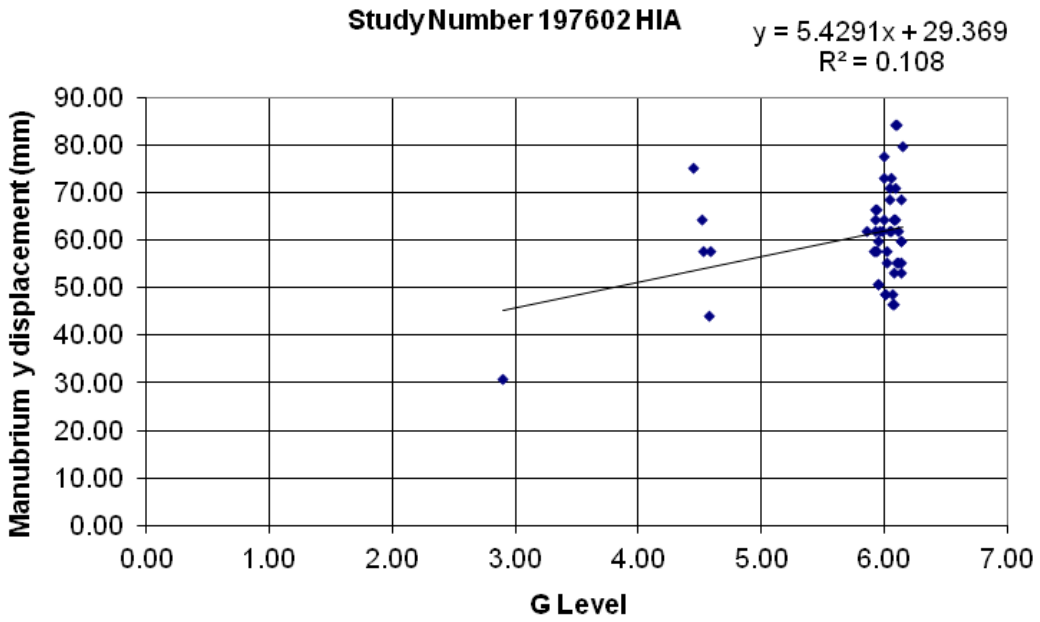

Figure 3.3-10. Maximum Displacement of the Target over Each Subject's Manubrium for Each Sled Acceleration Condition

The mean force measured at the force cell at the subjects' shoulder was 520 lbs (236 kg), std dev = 64.3 lbs (29.2 kg). The mean force measured at the elbow was 112 lbs (51 kg), std dev = 46 lbs (21.0 kg). The mean force measured at the wrist was 58 lbs (26 kg) with a standard deviation of 15.3 lbs (6.94). The mean of the total upper body force measured was 622 lbs (282 kg), std dev = 63.9 lbs (29.0 kg) n = 45.

The mean force measured at the hip was 520 lb (236 kg), std dev = 70.7 lbs (32.0 kg). The mean force measured at the knee was 354 lbs (161 kg), std dev = 69.3 (31.4 kg). The mean force measured at the subjects' ankle was 153 lbs (63.4 kg), std dev = 27.9 lbs (12.7 kg). The mean lower body force was 880 lbs (399 kg), std dev = 108 lbs (49.0 kg) n = 45.

The mean of the total whole body force was 1,430 lbs (649 kg), std dev = 162 lbs (73.5 kg) n = 45.

The upper body dynamic response model mean natural frequency was 5.13 Hz, std dev = 1.12. The mean damping coefficient was 0.50, std dev = 0.16. The mean natural frequency of the lower body dynamic model was 10.9 Hz, std dev = 1.86. The mean damping coefficient was 0.07, std dev = 0.07. The mean natural frequency of the whole body dynamic response model was 8.0 Hz, std dev = 1.26. The mean damping coefficient ratio was 0.31, std dev = 0.10.

The dynamic response model parameters for the shoulder force were calculated for each impact level as shown in Table 3.3-1.

Table 3.3-1. Dynamic Response Parameters for the Shoulder Impact Model

Impact Level (G)	Natural Frequency (Hz)	Damping Coefficient Ratio
3	9.8, std dev = 0.39	0.37, std dev = 0.08
4.5	11.5, std dev = 0.38	0.21, std dev = 0.06
6	12.9, std dev = 0.31	0.18, std dev = 0.05

Model stiffening is reflected in the increasing values of natural frequency as a function of G level. At these relatively low impact levels, this was not an unusual observation. The reduction in the damping coefficient is to be expected as the muscle tension of the subjects was overcome.

3.3.4 Discussion

Since tests with volunteers had not been planned as part of the technical efforts described within this report, the effort documented was limited to the use of data from an existing experimental study conducted by AFRL for a different purpose. However, the data were considered adequate to demonstrate the feasibility of meeting the two objectives of this technical effort. Furthermore, some of the findings may be used in the design of future crew seats and to analyze the interactions between an impact attenuation system, a crew seat, and the human body.

The notable differences between the test apparatus used in the experimental effort conducted by Killian and Boedecker [ref. 89] and potential designs of future crew seats and restraints include the use of full body support panels rather than sideward supports that may only support segment of the seat occupant's body, such as the helmeted head, shoulder, knees, and feet. The restraint system used in the experimental apparatus is different from a restraint that might be used in a future spacecraft crew seat, and could influence the results of this assessment.

Sideward impact studies that have been conducted to define impact exposure limits for the shoulder have been performed using PMHS. The tests have been performed using impact sleds to produce whole body impacts or by pendulum or pneumatically actuated rams that strike the shoulder area. Data from these tests have been used to specify impact exposure limits and protective padding. For the most part, the experimental efforts have been accomplished to support the efforts to reduce the injuries and fatalities associated with automotive highway accidents. The data resulting from these experimental efforts are used to specify sideward force limits or allowable impact pressures. Measured impact responses of specially designed automotive SID may be used to limit the likelihood of injury from sideward collisions.

The shoulder biodynamic response has not been extensively studied. The more recent studies conducted by Bolte, *et.al,* [ref. 90] and Koh, *et.al* [ref. 91] provide summaries of the previous research and their experimental efforts to define the response and injury thresholds of the shoulder complex to sideward and oblique impact. These recent studies have focused upon defining injury criteria in terms of shoulder impact force, deflection corridors, and the Y-axis motion of the first thoracic vertebra. The experimental efforts by Koh, *et al.* [ref. 91] supported a conclusion that a shoulder deflection of 40 mm for a 50^{th}-percentile male and a C_{max} of 20 percent (chest compression ratio) would result in a 50-percent risk of an abbreviated injury scale (AIS) code-2 shoulder injury. A shoulder deflection of 40 mm was exceeded in all but one of the impact tests conducted with volunteers reported in Figure 3.3-10. This difference could be based upon differences in the experimental methods, analytical methods, test conditions, or the use of PMHS versus healthy young, military volunteers.

Neither the current BDR acceleration exposure limits nor the Hybrid III ATD limit values specified in the HSIR document relate to the conclusions reached by Koh, *et al.* [ref. 91].

The current BDR acceleration exposure limits are shown in Figure 3.3-11; it presents the amplitude of half-sine impact pulses and the time to peak acceleration. Estimated risk levels were based upon the threshold of potentially adverse cardiovascular events (low risk) recorded during test with volunteers [refs. 21, 23, 24, and 92]. The high-risk threshold was defined on the basis of the

findings of Beeding and Mosley [ref. 92] and several accidents incurred during tests of escape systems (reports unavailable).

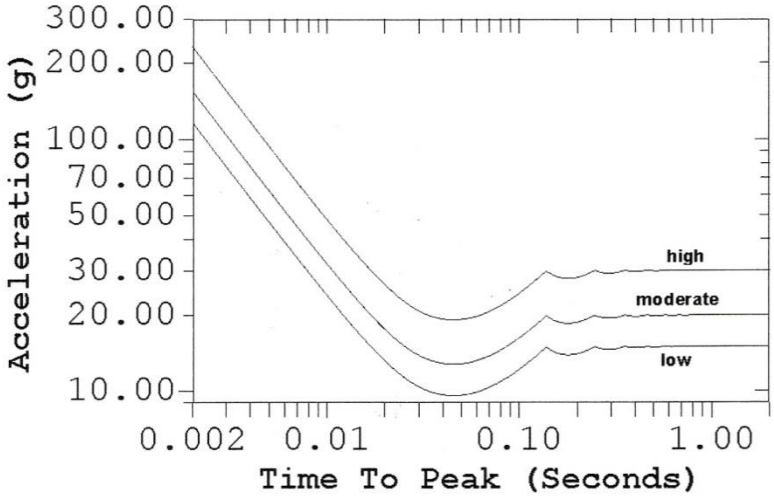

Figure 3.3-11. Current Dynamic Response Acceleration Exposure Limits for Sideward Half Sine Impacts

In Section 3.3.1, sideward impact injuries that were experienced during NASCAR racing accidents are reported. A logistic regression analysis of these injuries versus no injury cases revealed a low probability of injury (<0.5 percent) would correlate to a DR_y value of 21.9 G versus the existing DR_y low risk limit of 15 G. A moderate probability of injury threshold would correlate to a DR_y value of 31.3 G, whereas the existing moderate risk threshold is set at 20 G. A high risk probability of injury (>50 percent) would correlate to 48.9 G compared to 30 G using the current BDR model.

The model coefficients developed as a result of the tests of volunteers at an impact level of 6 G (see Table 3.3-1) were used to calculate the low, moderate, and high risk acceleration exposure limits for half-spine impact pulse as show in Figure 3.3-12.

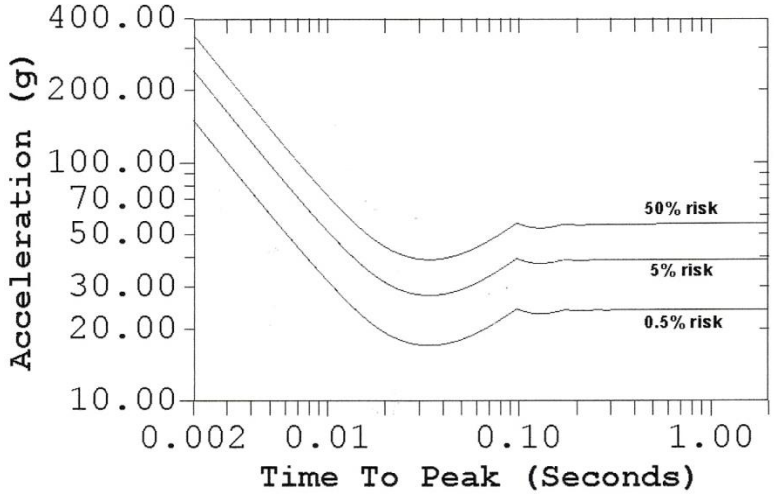

Figure 3.3-12. Dynamic Response Acceleration Exposure Limits Based on NASCAR Accidental Shoulder Complex Injuries

The most obvious reason for the difference is that the driver's seats of the NASCAR vehicles provide better protection than the rigid generic seats used in the laboratory tests. For example, the NASCAR seats have padding that surrounds the headrest and shoulders of the drivers.

Recent experiments conducted by the AFRL to study the responses of male and female sideward impacts with various helmets and headrest configurations have elicited strong complaints from the women. They have refused to participate in impact tests at levels above 6 G. Although no injuries of the cervical spine have been experienced, muscle pain and strains have been incurred. Lowering of the BDR acceleration exposure limits for the case where no side supports are provided should be considered after thorough analysis of these findings. Currently, the HSIR requirements implicitly require side supports as a result of the body movement requirements.

This section had two objectives; to develop biomechanical models to simulate the dynamic inertial response of the human body to Y-axis impact, and to update the BDR model and exposure limits for Y-axis. Progress towards meeting these objectives was made. However, the work is not complete, and no final recommendations were made.

3.4 THUMS Analyses

3.4.1 WPAFB Sled Test Analysis

The purpose of this study was to determine the similarity between the response of the THUMS model and the Hybrid III ATD given existing WPAFB sled tests. There were four tests selected for this comparison with frontal, spinal, rear, and lateral loading. The THUMS model was placed in a sled configuration that replicated the WPAFB configuration and the recorded seat acceleration for each test was applied to model seat. Once the modeling simulations were complete, they were compared to the WPAFB results using two methods. The first was a visual inspection of the sled test videos compared to the THUMS d3plot (3DPLOT[2]) files. This comparison resulted in an assessment of the overall kinematics of the two results. The other comparison was an assessment of the plotted data recorded for both tests. The metrics selected for comparison were seat acceleration, belt forces, and head and chest accelerations. These metrics were recorded in the WPAFB tests and were outputs of the THUMS model. Once the comparison of the THUMS to the WPAFB tests was complete, the THUMS model output was examined for possible injuries in these scenarios. These outputs included metrics for injury risk to the head, neck, thorax, lumbar spine, and lower extremities. The metrics to evaluate head response were peak head acceleration, HIC_{15}, and HIC_{36}. For the neck, N_{ij} was calculated. The thorax response was evaluated with peak chest acceleration, the combined thoracic index, sternal deflection, chest deflection, and chest acceleration 3-msec clip. The lumbar spine response was evaluated with lumbar spine force. Finally, the lower extremity response was evaluated by femur and tibia force. The results of the simulation comparisons indicate the THUMS model had a similar response to the Hybrid III ATD given the same input. The primary difference seen between the two was a more flexible response of the THUMS compared to the Hybrid III. This flexibility was most pronounced in the neck flexion, and shoulder and chest deflections. Due to the flexibility of the THUMS, the resulting head and chest accelerations tended to lag the Hybrid III acceleration trace and have a lower peak value. The results of the injury metric comparison identified possible injury trends between simulations. Risk of head injury was highest for the lateral simulations. The risk of chest injury

[2] Oasys D3PLOT is a 3D visualization and interrogation package for post-processing the results of LS-DYNA® analyses.

was highest for the rear impact. However, neck injury risk was approximately the same for all simulations. The injury metric value for lumbar spine force was highest for the spinal impact. The leg forces were highest for the rear and lateral impacts. The results of this comparison indicate the THUMS model performs in a similar manner as the Hybrid III ATD. The differences in the responses of model and the ATD are primarily due to the flexibility of the THUMS. This flexibility of the THUMS would be a more human like response. Based on the similarity between the two models, the THUMS should be used in testing to assess occupant injury risk.

Additional information regarding the study can be found in Appendix E.

4.0 Findings and NESC Recommendations

4.1 Findings

The following findings were identified:

F-1. The BDR model has the following limitations:

- Assumes basic seat geometry, restraint, and head protection and is therefore only an approximation for other seat designs and protection systems.
- Injury probability is not reduced with seat or restraint improvements.
- Injury risk cannot be lowered by improving the seated environment.
- Injury risk can only be lowered by reducing the driving loads into the seat.
- Injury risk is not reflected in gap distances between subject and seating support surface
- Estimates if an injury or adverse physiological response will occur, not the injury type or location.
- Valid for accelerations of less than 500 msec.
- Seat padding or cushions may not amplify transient linear accelerations transmitted to the occupant.
- +X-axis limits presume that the seat occupant's head is protected by a flight helmet with a liner meeting the test requirements of ANSI Z-90 (latest edition) or equivalent.
- Cannot predict injury caused by rigid suit elements (e.g., localized blunt trauma, localized point loading, and interference with restraints).

F-2. The most extensive collection of body region specific biodynamic injury criteria was developed for the automotive industry and are being used to ensure automotive safety.

F-3. There is limited direct science to extrapolate most biodynamic injury criteria to spacecraft landing.

F-4. Biodynamic injury criteria used by the automotive industry and FAA are designed for higher allowable probability of injuries than are acceptable for NASA and manned vehicle landings.

F-5. Utilizing biodynamic injury criteria developed for applications other than manned spacecraft requires extrapolation, interpretation, and SME judgment.

F-6. The currently available biodynamic criteria can only be used to approximate the HSIR required 0.5-percent probability of injuries.

F-7. Body movement requirements complement the biodynamic injury criteria by establishing requirements that limit relative body motions that could result in injury.

F-8. The BDR is only applicable to seat configurations with equivalent or improved lateral support and body movement constraints to the seat design used in its development.

F-9. HSIR occupant protection requirements can be quantified through numerical modeling and simulation, but requirements require physical testing for qualification.

F-10. Occupant biodynamic injury criteria are specific to the physical and numerical model.

F-11. The MADYMO model provided less modeling capabilities than the FTSS and LSTC Hybrid III models since these models are FE-based while the MADYMO ATD model consists of rigid links and the seated environment is modeled with simple contact.

F-12. The MADYMO and LSTC Hybrid II models did not perform well for correlating with sled test data.

F-13. The FTSS Hybrid III model performed best among the three ATD numerical models exhibiting the lesser amount of deviation between numerical prediction and test results, although they did not consistently produce correlation results to within the desired 20-percent of the test data.

F-14. The THUMS model is designed to replicate the human body and not intended to directly replicate the Hybrid III ATD.

F-15. The possible sources for the lack of correlation between the numerical models and the test data include: test data variability; ATD model limitations; and the absence of a standard model development methodology.

F-16. The Hybrid III ATD was primarily designed and validated for frontal impacts.

F-17. The THUMS model may provide an advantage over the Hybrid III numerical models for situations where it is desired to investigate specific regions or features of the human body.

F-18. It is more practical to utilize physical and numerical ATDs than the THUMS model to assess occupant injury.

F-19. HSIR requirements are qualification through analysis, which differs from the NHSTA and the FAA approach, which requires physical testing and analysis.

F-20. Crew exposure to microgravity has not been studied in the context of landing impact injury.

F-21. Limited information exists related to female tolerance of impact loads.

F-22. The influence of pressure suits and their design features cannot be evaluated until specific developmental designs are defined.

F-23. The FAA and NHTSA utilize standardized testing for commercial aircraft and automobile qualification for occupant safety. NASA does not provide for standardized testing and instead requires that occupant protection be assessed for all possible load conditions. Since all possible load conditions cannot be physically tested, qualification can only be performed through analysis.

4.2 NESC Recommendations

The following NESC recommendations were identified and directed toward CxP unless otherwise identified:

R-1. It is recommended that NASA perform actual human testing specific to the environment and loadings of the planned manned vehicles to anchor the occupant protection injury criteria with actual relevant test data. In the past, NASA deemed this type of testing

necessary and performed it for Apollo and similarly, the Russians performed this testing for Soyuz. Currently, there is no plan to obtain these data for Orion or for any other future planned manned vehicle. ***(F-3, F-5, F-6)***

R-2. Experts from the FAA and NHTSA have offered to review the current HSIR occupant protection requirements and to make suggestions for improvements. It is recommended that this offer be accepted. ***(F-3, F-4, F-5)***

R-3. Recent sled and VDT testing of the Hybrid III ATD in the Orion seat design has disclosed the difficulty with measuring all of the body movement requirements as specified in the HSIR. It is recommended these requirements be reviewed and possibly simplified. ***(F-7)***

R-4. The FAA requires that for numerical ATD models to be used in place of testing, the numerical model must be validated for a physical environment (e.g., seat, constraints, etc.) and loading conditions similar to the test conditions that the model is intended to replace. It is recommended that before any numerical model is used to perform a final assessment of occupant injury that the model be validated through physical testing. This testing should be performed in a similar physical environment, including similar or identical seat, harness, helmet, suit, and additional physical hardware components that interact with the occupant, and for different size crew representing both male and female crew. In addition, loading conditions for these physical modeling validation tests should be similar to the loading conditions that will ultimately be used for the occupant protection assessments. ***(F-12, F-13)***

R-5. It is recommended that additional human data be mined and analyzed to refine the injury criteria. ***(F-2 through F-6)***

R-6. Additional research is required to address landing impact injury tolerance and gender differences. ***(F-21)***

R-7. Additional research should be conducted to investigate the unique challenges of landing impact, such as crew deconditioning and suit-related trauma. Emphasis should be given to areas of the body that carry the highest impact loads during landing impact, such as hip, shoulder, and spinal column. ***(F-22)***

R-8. Consider the influence of specific design features of pressure suits, such as placement and design of suit bearings, on potential crew injuries due to blunt force trauma. ***(F-22)***

R-9. It is recommended that the qualification process be replaced or simplified through the use of sled or vertical drop tower (VDT) testing. (***F-23)***

5.0 Other Deliverables

No unique hardware, software, or data packages, outside those contained in this report, were disseminated to other parties outside this assessment.

6.0 Lessons Learned

This assessment was supported by a combination of contractors and civil servants at JSC and Glenn Research Center. In addition, several consultants were used to provide expertise that NASA did not have in-house in the area of occupant injury criteria and occupant protection. Utilization of these experts was critical for the success of this effort by providing the needed knowledge and for building a stronger in-house capability to work in the area of occupant protection in the future.

While there were many advantages to utilizing expert consultants, it was critical that the consultants provide written documentation on a regular basis so that items discussed verbally during meetings and teleconferences were captured in an efficient and timely manner. Waiting until the assessment is complete to write the final report is too late to capture all of the valuable discussions and insights. It is important that a regular reporting process be in place from the effort's inception so that the final report progresses instead of a last item to complete.

7.0 Definition of Terms

Finding	A conclusion based on facts established by the investigating authority.
Lessons Learned	Knowledge or understanding gained by experience. The experience may be positive, as in a successful test or mission, or negative, as in a mishap or failure. A lesson must be significant in that it has real or assumed impact on operations; valid in that it is factually and technically correct; and applicable in that it identifies a specific design, process, or decision that reduces or limits the potential for failures and mishaps, or reinforces a positive result.
Observation	A factor, event, or circumstance identified during the assessment that did not contribute to the problem, but if left uncorrected has the potential to cause a mishap, injury, or increase the severity should a mishap occur. Alternatively, an observation could be a positive acknowledgement of a Center/Program/Project/Organization's operational structure, tools, and/or support provided.
Problem	The subject of the independent technical assessment.
Recommendation	An action identified by the NESC to correct a root cause or deficiency identified during the investigation. The recommendations may be used by the responsible Center/Program/Project/Organization in the preparation of a corrective action plan.

8.0 References

1. NASA Constellation Program Human-Systems Integration Requirements (HSIR) Document, CxP 70024, Rev. D., 2009.
2. Jones, R. H., "Landing Impact Attenuation for Non-Surface-Planing Landers," NASA SP-8046, April 1970.
3. Air Force Systems Command, "Handbook of Instructions for Aircraft Designers (HIAD)," Vol. I, ARDCM 80-1, Air Research and Development Command, Wright-Patterson Air Force Base, Ohio, April 1960.

4. Eiband, M. A., "Human Tolerance to Rapidly Applied Accelerations: A Summary of the Literature," National Aeronautics and Space Administration, Washington D.C., June 1959.

5. Beeding, E. L., Jr., and Mosley, J. D., "Human Deceleration Tests," AFMDC-TR-60-2, Air Force Missile Development Center, Holloman Air Force Base, New Mexico, January 1960.

6. Kornhauser, M., "Impact Protection for the Human Structure," *Advances in Astronautical Sciences*, Paper 38, Vol. 3. Plenum, New York, 1958.

7. Headley, R. N., Brinkley, J. ,W., Lokatos, G. and Managan, R. F., "Human Factors Responses During Ground Impact," WADD Technical Report 60-590, Aero Medical Laboratory, Wright-Patterson Air November 1960.

8. Headley, R. N., Brinkley, J. W., Lokatos, G., and Managan, R. F., "Human Factors Responses During Ground Impact," *Aerospace Medicine*, 33(2):141-46, February 1962.

9. Brinkley, J. W., "Man Protection During Landing Impact of Aerospace Vehicles," Ballistic Missile and Space Technology, ed. LeGalley, D. P., Vol. I, Academic Press, New York, New York, 1960.

10. Brinkley, J. W, Headley, R. N. and Kaiser, K. K., "Abrupt Acceleration of Human Subjects in the Semi-Supine Position," Proceedings of the Symposium on Biomechanics of Body Restraint and Head Protection, Naval Air Material Center, Aircrew Equipment Laboratory, 14 June 1961. Also presented at the Aerospace Medical Association Meeting, May 1961.

11. Payne, P. R., "The Dynamics of Human Restraint Systems," *Impact Acceleration Stress*. Proceedings of the National Academy of Sciences–National Research Council Publication 977, November 1961.

12. Goldman, D. E., and von Gierke, H. E., "Effects of Shock and Vibration on Man," *Shock and Vibration Handbook*, Vol. 3, Ch. 44, pp 9-19, McGraw-Hill, New York, 1961.

13. NASA Defense Purchase Request T-9643(G), August 22, 1962.

14. Hershgold, E. J., "Roentgenographic Study of Human Subjects during Transverse Accelerations," *Aerospace Medicine*, 31:213:1960.

15. Stapp, J., Personal communication to James Brinkley, 1991.

16. Holcomb, G. A., "Human Experiments to Determine Human Tolerance to Landing Impact in Capsule Systems," *Ballistic Missile and Space Technology*, Ed. LeGalley, D. P., Vol. I, Academic Press, New York, New York, 1960.

17. Robinson, F. R., Hamlin, R. L., Wolfe, W. M., and Coermann, R. R., "Response of the Rhesus Monkey to Lateral Impact," *Aerospace Medicine*, 34(1), 56-62, 1963.

18. Schulman, M., Critz, G. T., Highly, F. M., and Hendler, E., "Determination of Human Tolerance to Negative Impact Acceleration," NAEC-ACEL-510, U. S. Naval Air Engineering Center, Philadelphia, Pennsylvania, November 1963.

19. Shaw, R. S., "Human Tolerance to Negative Acceleration of Short Duration," *Journal of Aviation Medicine*, 19:39, February 1948.

20. Clarke, N. P., Weis, E. B., Jr., Brinkley, J. W., and Temple, W. E., "Lateral Impact Tolerance Studies in Support of Apollo," AMRL Memorandum Report M-29, February 1963.

21. Weis, E. B., Jr., Clarke, N. P., and Brinkley, J. W., "Human Response to Several Impact Acceleration Orientations and Patterns," *Aerospace Medicine,* 34(12): 1122-1129, 1963.

22. Hixson, E. L., "Mechanical Impedance and Mobility," Harris, C. M., and Crede, C. E., Ed. Shock and Vibration Handbook, Vol. I, Ch. 10, McGraw-Hill, New York, 1961.

23. Stapp, J. P., and Taylor, E. R., "Space Cabin Landing Vector Effects on Human Physiology," *Aerospace Medicine,* 35(12): 1117-1132, 1964.

24. Brown, W. K., Rothsteiin, J. D. and Foster, P., "Human Response to Predicted Apollo Landing Impacts in Selected Body Orientations," *Aerospace Medicine,* 37(4), 394-398, 1966.

25. Klopfenstein, H. W., "Compression Fracture of the Seventh Thoracic Vertebrae Caused by Experimental Impact: A Case Report," Presented at the 40th Annual Meeting, Aerospace Medical Association, San Francisco, May 1969.

26. Payne, P. R., "Personnel Restraint and Support System Dynamics," AAMRL-TR-65-127, Aerospace Medical Research Laboratory, Wright-Patterson Air Force Base, Ohio, 1965.

27. Steck, E. L., and Payne, P. R., "Dynamic Models of the Human Body," AAMRL-TR-66-157, Aerospace Medical Research Laboratory, Wright-Patterson Air Force Base, Ohio, 1966.

28. Hearon, B. F., Brinkley, J. W., Luciani, R., and von Gierke, H. E., "F/FB-111 Ejection Experience (1967-1980) – Part I: Evaluation and Recommendations," AFAMRL-TR-81-113, November 1981.

29. Brinkley J. W., "Development of Aerospace Escape Systems," *Air University Review,* Vol. XIX, No. 5 (July-August 1968): 34-49.

30. Brinkley, J. W., and Shaffer, J. T., "Dynamic Simulation Techniques for the Design of Escape Systems: Current Applications and Future Air Force Requirements," Symposium on Biodynamic Models and Their Applications, 1971, AMRL-TR-71.-29, Aerospace Medical Research Laboratory, Wright-Patterson Air Force Base, Dayton, Ohio.

31. Mohr, G. C., Brinkley, J. W. and Kazarian, L. E., "Variations of Spinal Alignment in Egress Systems and Their Effect," *Aerospace Medicine,* 40(9):983-88, September 1969.

32. Brinkley, J. W. and Rock, J. C., "Advanced Concepts and Biotechnology for Future Escape Systems," *Medical Service Digest,* AFRP 160-1, Vol. XXXIV, No. 4, 1983.

33. Brinkley, J. W., "Personnel Protection Concepts for Advanced Escape System Design," *Human Factors Considerations in High Performance Aircraft,* AGARD Conference Proceedings No. 371, November 1984.

34. Shaw, R. S., "Human Tolerance to Negative Acceleration of Short Duration," *Journal of Aviation Medicine,* 19(1), 39, 1948.

35. Brinkley, J. W., Raddin, J. H., Jr., Hearon, B. F., McGowan, L. A., and Powers, J. M., "Evaluation of a Proposed Modified F/FB-111 Crew Seat and Restraint System," Aero Medical Research Laboratory, Wright-Patterson AFB, Ohio, November 1981. http://handle.dtic.mil/100.2/ADA110188

36. Zaborowski, A. V., "Lateral Impact Studies: Lap Belt Shoulder Harness Investigations, In: Proceedings," *9th Stapp Car Crash Conference*, Society of Automotive Engineers, Warrendale, Pennsylvania, pp 93-127, 1966.

37. Brinkley, J. W., "Acceleration Exposure Limits for Escape System Advanced Development," Proceedings of the 1984 SAFE Association Symposium, and also *SAFE Journal*, Vol. 15, No. 1, 1985.

38. Brinkley, J. W., Specker, L. J., and Mosher, S. E., "Development of Acceleration Exposure Limits for Advanced Escape Systems, Implications of Advanced Technologies for Air and Spacecraft Escape," NATO AGARD Proceedings, AGARD-CP-472, February 1990.

39. Specker, L. J., and Plaga, John A., "The K-36D Ejection Seat Foreign Comparative Testing (FCT) Program," May 1996. http://www.dtic.mil/docs/citations/ADA321294

40. Muellner, G. K., and Brinkley, J. W., "Peristroka Provides an Opportunity to Save US Lives," *The Combat Edge*, July 1998.

41. Strzelecki, J. P., "An Investigation with Human Subjects into the Potential for Dynamic Preloading of the Spinal Column to Improve Escape System Performance," AL/CF-TR-1993-0167, Armstrong Laboratory, Crew Systems Directorate, Wright-Patterson Air Force Base, Ohio, August 1993.

42. Allnutt, R. A., "Gender Effects in Traumatic Injury," *SAFE Journal*, Vol. 36, No. 1, 2008.

43. Morris, C. E., and Popper, S. E., "Gender and Effect of Impact Acceleration on Neck Motion," *Aviation, Space, and Environmental Medicine,* Vol. 70, 9, September 1999.

44. Buhrman, J. R., and Wilson, D. D., "Effects of Crewmember Gender and Size on Factors Leading to Increased Risk of Spinal Injury During Aircraft Ejection," Proceedings of the 40th Annual SAFE Symposium, 2002.

45. Perry, C. E., "The Effect of Helmet Inertial Properties on Male and Female Head Response During +Gz Impact Accelerations," *Safe Journal*, 28(1), 32-38, 1998.

46. Buhrman, J. R., Perry, C. E., and Mosher, S. E., "A Comparison of Male and Female Acceleration Responses During Laboratory Frontal –Gx Axis Impact Tests," AFRL-HE-WPTR-2001-0022, 2000.

47. Gallagher, H. L., Buhrman, J. R., Mosher, S. E., Perry, C. E., and Wilson, D. D., "A Comparison of Cervical Stress and BMD as Related to Gender and Size During +Gz Acceleration," Proceedings of the 44th SAFE Symposium, 2006.

48. Gallagher, H. L., Buhrman, J. R., Mosher, S. E., Perry, C. E., and Wilson, D. D., "An Analysis of Vertebral Stress and BMD During +Gz Impact Accelerations," AFRL-HE-TR-WP-TR-2007-0085, Human Effectiveness Directorate, Air Force Research Laboratory, Wright-Patterson Air Force Base, Ohio, 2007.

49. Buhrman, J. R., and Wilson, D. D., "Analysis of Vertebral Stress and BMD During +Gz Impact Accelerations as Related to Ejection Spinal Injury Risk for Varying Size Individuals," Proceedings of the 2003 RTO HSM Symposium, Koblenz, Germany, 2003.

50. Perry, C. E., Bontti, D. M., and Brinkley, J. W., "The Effect of Variable Seat Back Angles on Human Responses to +Gz Impact Accelerations," AL-TR-1991-0110, Crew Systems Directorate, Armstrong Laboratory, Wright-Patterson Air Force Base, May 1991.

51. Hearon, B. F., and Brinkley J. W., "Comparison of human impact response in restraint systems with and without a negative G strap," *Aviation, Space, and Environmental Medicine*, April 1986.

52. Hearon, B. F, Brinkley, J. W., and Raddin, J. H., "Vertical Impact Evaluation of the F/FB-111 Crew Restraint Configuration, Headrest Position, and Upper Extremity Bracing Technique," *Aviat Space Environ Med* 54(11):977-87 (1983) PMID 6651734.

53. Hearon, B. F., and Brinkley, J. W, "Effects of Seat Cushions on Human Response to +Gz Impact," *Aviat. Space Environ. Med.*, **57**:113 (1986).

54. Mertz, H. J., "Injury Risk Assessments Based on ATD Responses," *Accidental Injury—Biomechanics and Prevention*. 2nd Edition, Nahum, A. M. and Melvin, J. W., eds., Springer-Verlag, 2002.

55. Mertz, H. J., "A Procedure for Normalizing Impact Response Data," SAE Paper No. 840884, May 1984.

56. Mertz, H. J., Irwin, A. L., Melvin, J. W., Stalnaker, R. L., and Beebe, M. S., "Size, Weight and Biomechanical Impact Response Requirements for Adult Size Small Female and Large Male Dummies," SAE Paper No. 890756, March 1989.

57. Mertz, H. J., Prasad, P., and Irwin, A. L., "Injury Risk Curves for Children and Adults in Frontal and Rear Collisions," 41st Stapp Car Crash Conference Proceedings, SAE Paper No. 973318, November 1997.

58. Patrick, L. M., Lissner, H. R., and Gurdjian, E. S., "Survival by Design – Head Protection," 7th Stapp Car Crash Conference Proceedings, Charles C. Thomas, Springfield, Illinois, 1965

59. Gadd, C. W., "Use of a Weighted –Impulse Criterion for Estimating Injury Hazard," *10th Stapp Car Crash Conference Proceedings*, SAE Paper No. 660793, November 1966.

60. Versace, J., "A Review of the Severity Index," *15th Stapp Car Crash Conference Proceedings*, SAE Paper No. 710881, November 1971.

61. Hodgson, V. R, and Thomas, L. M., "Effect of Long-Duration Impact on Head," *16th Stapp Car Crash Conference Proceedings*, SAE Paper No. 720956, November 1972.

62. Begeman, P., and Melvin, J., "Mathematical Modeling of Crash-Induced Dynamic Loads on Race Car Drivers," *Proceedings of the 2002 Motorsports Engineering Conference* (P-382), pp. 195-230, SAE Technical Paper No. 2002-01-3305, Society of Automotive Engineers, Warrendale, Pennsylvania, 2002.

63. Mertz, H. J., and Patrick, L. M., "Strength and Response of the Human Neck," *15th Stapp Car Crash Conference Proceedings*, SAE Paper No. 710855, November 1971.

64. Patrick, L. M., and Chou, C. C., "Response of the Human Neck in Flexion, Extension and Lateral Flexion," SAE Vehicle Research Institute Report No. VRI 7.3, April 16, 1976.

65. McElhaney, J. H., Nightingale, R. W., Winkelstein, B. A., Chancey, V. C., and Myers, B. S. "Biomechanical Aspects of Cervical Trauma," *Accidental Injury—Biomechanics and Prevention*, 2nd Edition, Nahum, A. M. and Melvin, J. W., eds., Springer-Verlag, 2002.

66. Mertz, H. J., "Anthropomorphic Test Devices," *Accidental Injury—Biomechanics and Prevention*, 2nd Edition, Nahum, A. M. and Melvin, J. W., eds., Springer-Verlag, 2002.

67. SFI Foundation, Inc., Specification SFI 38.1, Poway, California, 2009.

68. Cavanaugh, J. M., "Biomechanics of Thoracic Trauma," *Accidental Injury—Biomechanics and Prevention*, 2nd Edition, Nahum, A. M. and Melvin, J. W., eds., Springer-Verlag, 2002.

69. Safety Test Instrumentation Standards Committee, "SAE International. Instrumentation for Impact Test - Part 1 - Electronic Instrumentation," Troy, Michigan, July 27, 2007.

70. Cragg, C., "Orion Crew Seat Attenuation Peer Review of the LS-DYNA™ Model" (Tasks 1 & 2), NESC TI-08-00469, 2009.

71. TNO Automotive Safety Solutions, "MADYMO Model Manual," Release 6.4, Delft, Netherlands, 2007.

72. TNO Automotive Safety Solutions. "MADYMO Theory Manual," Release 6.4.1. Delft, The Netherlands 2007

73. Iwamoto, M., Kisanuki, Y., Watanabe, I., Furusu, K., Miki, K., and Hasegawa, J., "Development of a Finite Element Model of the Total Human Model for Safety (THUMS) and Application to Injury Reconstruction," Pp. 31–42, Proceedings of the 2002 IRCOBI International Conference on the Biomechanics of Impact, Bron, France: IRCOBI Secretariat, 2002.

74. Takhounts A. G., Eppinger R. H., Campbell J., Tannous R. E., Power E. D., Shook L. S,. "On the Development of the SIMon Finite Element Head Model," *Stapp Car Crash Journal*, 47:107-133, October 2003.

75. Takhounts, E. G., Ridella, S. A., Hasija, V., Tannous, R. E., Campbell, J. Q., Malone, D., Danelson, K., Stitzel, J., Rowson, S., and Duma, S., "Investigation of Traumatic Brain Injuries Using the Next Generation of Simulated Injury Monitor (SIMon) Finite Element Head Model," *Stapp Car Crash Journal,* Vol. 52, November 2008.

76. Vander Vorst, M., Stuhmiller, J., Ho, K., Yoganandan, N., and Pintar, F., "Statistically and biomechanically based criterion for impact-induced skull fracture," *Association for the Advancement of Automotive Medicine*, 47:363-81, 2003.

77. Guha, S., Bhalsod, D., and Krebs, J., "LSTC Hybrid III Dummies: Positioning & Post-Processing," Livermore, California, 2008.

78. Kang, S., and Xiao, P., "Comparison of Hybrid III Rigid Body ATD Models," Paper presented at: *10th International LS-DYNA® Users Conference*, 2008.

79. Moorcroft, D., "Selection of Validation Metrics for Aviation Seat Models," Presented at the *Fifth Triennial International Aviation Fire and Cabin Safety Research Conference* October 29–November 1, 2007.

80. Abbott, P. W., Personal communication, Lockheed Martin Space Systems Company, Littleton, Colorado. April 2008.

81. Johnston, S. L., and Jones, J. A,, Personal communication regarding cardiovascular deconditioning countermeasure, 2008.

82. Goldsmith, W., and Ommaya, A. K., "Head and Neck Injury Criteria and Tolerance Levels," Aldman, B., and Chapon, A., (eds.), The Biomechanics of Impact Trauma, Elsevier Science Publishers, Amsterdam, 1984.

83. Prasad, P., and Mertz, Harold J., "The Position of the United States Delegation to the ISO Working Group 6 on the Use of HIC in the Automotive Environment," *SAE International*, 1985. http://papers.sae.org/851246/

84. Newman, J. A., Shewchenko, N., Welbourne, E., "A Proposed New Biomechanical Head Injury Assessment Function – The Maximum Power Index," *44th Stapp Car Crash Conference*, The Stapp Association, 2000.

85. Shaffer, J. T., "The Impulse Accelerator: An Impact Sled Facility for Human Research and Safety Systems Testing," AMRL-TR-76-8, Aero Medical Research Laboratory, Wright-Patterson AFB, Ohio, August 1976.

86. United States Air Force, "Use of Human Subjects in Research, Development, Tests, and Evaluation," Air Force Regulation 169-3, February 12, 1979.

87. Vierck, R. K., "Vibration Analysis," Thomas J. Crowell Co., Harper and Row Publishers, New York, pp. 120-128, 1979.

88. Buhrman, J. R., and Perry, C. E., "A Comparison of Male and Female Acceleration Responses During Laboratory Frontal -Gx Axis Impact Tests," Air Force Research Lab Wright-Patterson AFB Ohio, Human Effectiveness Directorate, December 2000. http://handle.dtic.mil/100.2/ADA387802

89. Killian, J., and Boedecker, H. F., "Whole Body Response - Lateral: Comparison Between Human and ATD Subjects Utilizing a Nine Transducer Accelerometer Package," Unpublished experimental study report #197602, Aerospace Medical Research Laboratory, Wright-Patterson Air Force Base, Ohio, January 1981.

90. Bolte, J. H., Hines, M. H., Herriott, R. G., McFadden, J. D., and Donnelly, B.R., "Shoulder Impact Response and Injury Due to Lateral and Oblique Loading," *Stapp Car Crash Journal*, Vol. 47, 2003.

91. Koh, S-W., Cavanaugh, J. M., Mason, M. J., Peterson, S. A., Marth, D. R., Rouhana, S. W., and Bolte, J. H., "Shoulder Injury and Response Due to Lateral Glenohumeral Joint Impact: An Analysis of Combined Data," *Stapp Car Crash Journal*, Vol. 49, 2005.

92. Beeding, E. L., Jr., and Mosely, J. D., "Human Tolerance to Ultra High G Forces," AFMDC-TN-60-2, Holloman Air Force Base, NM: Aeromedical Field Laboratory, Air Force Missile Development Center, 1960.

93. National Aeronautics and Space Administration, "Constellation Program System Requirements for the Orion System," CxP 72000 Revision B, Houston, Texas, 2008.

94. AAAM, "AIS 2005: The Injury Scale," (Eds. Gennarelli, T., and Wodzin, E.), *Association of Advancement of Automotive Medicine*, 2004.

95. National Aeronautics and Space Administration, "Constellation Architecture Requirements Document (CARD), CxP 70000 Revision D," Houston, Texas, 2009.

REPORT DOCUMENTATION PAGE

Form Approved
OMB No. 0704-0188

1. REPORT DATE *(DD-MM-YYYY)*	2. REPORT TYPE	3. DATES COVERED *(From - To)*
01- 09 - 2016	Technical Memorandum	

4. TITLE AND SUBTITLE
Crew Exploration Vehicle (CEV) (Orion) Occupant Protection

5a. CONTRACT NUMBER

5b. GRANT NUMBER

5c. PROGRAM ELEMENT NUMBER

6. AUTHOR(S)
Currie-Gregg, Nancy J.; Gernhardt, Michael L.; Lawrence, Charles; Somers, Jeffrey T.

5d. PROJECT NUMBER

5e. TASK NUMBER

5f. WORK UNIT NUMBER
869021.01.05.01.03

7. PERFORMING ORGANIZATION NAME(S) AND ADDRESS(ES)
NASA Langley Research Center
Hampton, VA 23681-2199

8. PERFORMING ORGANIZATION REPORT NUMBER
L-20751

9. SPONSORING/MONITORING AGENCY NAME(S) AND ADDRESS(ES)
National Aeronautics and Space Administration
Washington, DC 20546-0001

10. SPONSOR/MONITOR'S ACRONYM(S)
NASA

11. SPONSOR/MONITOR'S REPORT NUMBER(S)
NASA/TM-2016-219337/Volume I

12. DISTRIBUTION/AVAILABILITY STATEMENT
Unclassified - Unlimited
Subject Category 16-Space Transportation and Safety
Availability: NASA STI Program (757) 864-9658

13. SUPPLEMENTARY NOTES

14. ABSTRACT
Dr. Nancy J. Currie, of the NASA Engineering and Safety Center (NESC), Chief Engineer at Johnson Space Center (JSC), requested an assessment of the Crew Exploration Vehicle (CEV) occupant protection as a result of issues identified by the Constellation Program and Orion Project. The NESC, in collaboration with the Human Research Program (HRP), investigated new methods associated with occupant protection for the Crew Exploration Vehicle (CEV), known as Orion. The primary objective of this assessment was to investigate new methods associated with occupant protection for the CEV, known as Orion, that would ensure the design provided minimal risk to the crew during nominal and contingency landings in an acceptable set of environmental and spacecraft failure conditions. This documents contains the outcome of the NESC assessment. NASA/TM-2013-217380, "Application of the Brinkley Dynamic Response Criterion to Spacecraft Transient Dynamic Events." supercedes this document.

15. SUBJECT TERMS
NASA Engineering and Safety Center; Crew Exploration Vehicle; Human Research Program; Crew Module; Brinkley Dynamic Response; Anthropomorphic Test Devices

16. SECURITY CLASSIFICATION OF:			17. LIMITATION OF ABSTRACT	18. NUMBER OF PAGES	19a. NAME OF RESPONSIBLE PERSON
a. REPORT	b. ABSTRACT	c. THIS PAGE			STI Help Desk (email: help@sti.nasa.gov)
					19b. TELEPHONE NUMBER *(Include area code)*
U	U	U	UU	117	(443) 757-5802